October 2021

POLYMER-BASED STRATEGIES FOR THERAPEUTIC DELIVERY TO BACTERIAL BIOFILMS

Cheng-Hsuan Li
University of Massachusetts Amherst

POLYMER-BASED STRATEGIES FOR THERAPEUTIC DELIVERY TO BACTERIAL BIOFILMS

A Dissertation Presented

by

CHENG-HSUAN LI

Submitted to the Graduate School of the
University of Massachusetts Amherst in partial fulfillment
of the requirements for the degree of

DOCTOR OF PHILOSOPHY

September 2021

Chemistry

POLYMER-BASED STRATEGIES FOR THERAPEUTIC DELIVERY TO BACTERIAL BIOFILMS

A Dissertation Presented

by

CHENG-HSUAN LI

Approved as to style and content by:

_____
Vincent M. Rotello, Chair

_____
Michelle E. Farkas, Member

_____
Michael J. Knapp, Member

_____
M. Sloan Siegrist, Member

_____
Ricardo Metz, Department Head
Department of Chemistry

DEDICATION

To my mother Mei-Chueh, my father Yen-Lung, my sister Hsing-Chen, and my fiancée Ying-Hsuan Chen; all the work is for you and would not have been possible without your love.

ACKNOWLEDGMENTS

I would like to express my sincerest gratitude to my research advisor, Professor Vincent M. Rotello. He is knowledgeable, resourceful, and willing to support me over the years. The way he conducts himself and his writing style benefit me not just throughout my staying at Amherst. I would also like to thank him for understanding the difficulties of the international students during the pandemic and giving me full support to my graduation. I am grateful for the opportunities he has provided me in my time working in his laboratory and I wish him the best of luck in the future.

I would also like to thank my committee members, Professor Michelle E. Farkas, Professor Michael J. Knapp, and Professor M. Sloan Siegrist for their advice and support. Without their help, I would not pass the qualifying examinations. I would also like to thank Dr. James Chambers for the assistances in confocal microscopy.

I would like to express my appreciation for the co-workers including Dr. Ryan F. Landis, Dr. Akash Gupta, Dr. Li-Sheng Wang, Dr. Yi-Wei Lee, Dr. Yingying Geng, and Rui Huang. Especially thank to “Avengerms”, Jessa Marie V. Makabenta, Ahmed Nabawy, and Jungmi Park, who is brilliant and with strong work ethic.

I am thankful to staffs of the Chemistry department. I would like to express my appreciation to Carol Green, JMS, Robert Sabola, Ryan Feyrer, and Deirdre McDaniel. I would also like to thank Dennis Glick at the stockroom.

I would like to thank Dr. Chien-Wei Hsu, who was my senior in National Tsing Hua University. Dr. Chien-Wei Hsu inspired and encouraged me to study a Ph.D. program abroad. I consider him as the start of my Ph.D. journey. I would also like to

thank my friends in Amherst and Taiwan, who helped me get through all the difficulties these several years.

Finally, I would like to express my sincere love and appreciation of my family. I would like to especially thank my mother, Mei-Chueh Li, who is extraordinary tough, with a tender heart, and always backing me up. I would also like to thank my fiancée, Ying-Hsuan Chen, who has consistently loved and supported me through my entire Ph.D. grogram.

ABSTRACT

POLYMER-BASED STRATEGIES FOR THERAPEUTIC DELIVERY TO BACTERIAL BIOFILMS

SEPTEMBER 2021

CHENG-HSUAN LI

B.S., CHUNG YUAN CHRISTIAN UNIVERSITY

M.S., NATIONAL TSING HUA UNIVERSITY

Ph.D., UNIVERSITY OF MASSACHUSETTS AMHERST

Directed by: Professor Vincent M. Rotello

Bacterial infections are emerging threat to public health. Antibiotics once provided front-line treatments to bacterial infections; however, bacteria adapted to resist antibiotics through drug resistance mechanisms and biofilm formation. In this dissertation, I describe polymer-based strategies for therapeutic delivery as treatments of bacterial biofilm infections. Initially, I developed a functional polymer for delivering hydrophobic carvacrol (the primary constituent of oregano oil) to the bacterial biofilms. This strategy incorporates a cross-linking strategy to fabricate a robust yet biodegradable nanoemulsion, improving antimicrobial activity of carvacrol and overcoming antimicrobial resistance development. Next, I demonstrated that this functional polymer-based emulsion platform provides a general and flexible strategy that improves the antimicrobial activity of a library of phytochemicals including eugenol, linalool, methyl eugenol, *p*-cymene, (+)-limonene, and *α*-pinene against the bacterial biofilms. In this follow up study, I also showed that encapsulating low log P phytochemicals effectively eliminates biofilms while demonstrating low cytotoxicity against mammalian fibroblast cells. In a related system, I worked with an antimicrobial nanoemulsion composed of all

nature-derived materials. This antimicrobial platform uses gelatin stabilized by photocrosslinking with riboflavin (vitamin B_2) as a photocatalyst, and carvacrol as the active antimicrobial. The engineered nanoemulsions demonstrate broad-spectrum antimicrobial activity towards drug-resistant bacterial biofilms and significantly expedite wound healing *in vivo*. Additionally, these nanoemulsions are particularly suitable to probe the interaction between nanomaterials and bacteria within the biofilm matrix. I have generated penetration profiles of nanoemulsions with varied surface charges to a bacteria biofilm using synthetic polymers and quantitative techniques. Finally, this dissertation includes a preliminary study of polymer encapsulation of bacteriophages for the treatment of bacterial biofilms. I have demonstrated that the polymer-bacteriophage nanoassembly improves antimicrobial activity of the bacteriophage against biofilms. In summary, this dissertation provides evidence that our polymer delivery strategy improves the antimicrobial efficacy of encapsulated therapeutics against bacterial biofilms.

TABLE OF CONTENTS

Page

LIST OF TABLES

Table Page

LIST OF FIGURES

CHAPTER 1

1. NANOTHERAPEUTICS FOR ANTIBIOTIC-RESISTANT BACTERIAL AND BIOFILM INFECTIONS

Portions of this chapter included material from: Makabenta, J. M. V.; Nabawy, A.; Li, C.-H.; Schmidt-Malan, S.; Patel, R.; Rotello, V. M. Nanomaterial-Based Therapeutics for Antibiotic-Resistant Bacterial Infections. *Nat. Rev. Microbiol.* **2021**, *19*, 23–36., Springer Nature

1.1 Introduction

The emergence of antibiotic resistance in bacteria has resulted in the challenge of recalcitrant infections.[1,2] Multidrug-resistant (MDR) bacteria are a global crisis, increasing morbidity and mortality of infected individuals and negatively impacting the clinical outcome of a wide range of groups, including those in intensive care units or undergoing surgery, transplantation or cancer treatment.[2] A 2017 report from the WHO Global Antimicrobial Surveillance System highlighted antibiotic resistance as a worldwide challenge. The estimated cost of treating antibiotic-resistant infections is substantial (~US$50,000 per individual), with an estimated US$20 billion societal cost annually.[3] The use, and in some situations misuse, of antibiotics, combined with the scarcity of new therapeutics entering the antibiotic pipeline, further exacerbates this public health threat.[4]

Planktonic (free-floating) bacteria are central players in multiple health threats, including sepsis. Infections associated with planktonic bacteria present acute threats and are rapidly becoming more challenging to treat owing to rising rates of acquired antibiotic resistance. This challenge is amplified when bacteria form biofilms, which are associated with recurring and chronic bacterial infections.[5] The ability of bacteria to protect themselves within biofilms complicates treatment of numerous infection types,

including chronic wounds, osteomyelitis and infective endocarditis.[6] Antibiotic resistance associated with the biofilm state is distinct from acquired resistance, but can compound and exacerbate therapeutic challenges.[7] Bacterial cells produce extracellular polymeric substances (EPS), which may serve as a barrier against host immune responses and some conventional antimicrobial agents.[5,7] More importantly, biofilms exhibit a diversity of altered phenotypes, including slow growth rates, the presence of persister cells and spatial and chemical heterogeneities that contribute to resistance to many available antibiotics.[8,9]

Antibiotics are currently the main therapeutic strategy for treating both planktonic and biofilm infections.[10] They target processes necessary for growth and/or survival of bacteria, including cell wall and cell membrane synthesis or maintenance, or the production of DNA, RNA or essential proteins. Many antibiotics are derived from products that have been deployed by microorganisms to combat one another for billions of years. The offensive molecules that have evolved throughout this warfare have generated defence responses; bacteria have developed the intrinsic ability to escape the activity of many traditional antibiotics.[11] Eradicating MDR bacteria may require multiple or high dosages of antibiotic agents or the use of 'last-resort' antibiotics.[10] Adding to the therapeutic challenge, when bacteria are present in biofilms, biofilm-associated resistance becomes a compounding factor, often requiring physical removal of the biofilm through aggressive debridement, for example, accompanied by high doses of antibiotics.[12,13] These strategies can result in long and expensive treatments, with the possibility of adverse effects and uncertain outcomes.

Nanomaterials access antimicrobial modalities that are novel to bacteria and thus are not in their natural defensive arsenal (Figure 1. 1). Recent advances in nanomaterial-

based systems provide new opportunities to address MDR planktonic as well as biofilm infections, acting either as inherent therapeutics or as nanocarriers for antimicrobial agents.[14] The unique physico-chemical properties of nanomaterials, such as size, shape and surface chemistry, influence their therapeutic activity.[15] The sizes and shapes of different nanomaterials are similar to those of bacterial biomolecules, affording a variety of interactions that can be regulated through surface functionalization. High surface-to-volume ratios and multivalent interactions are important for creating antibacterial nanomaterials.[14,15] Nanomaterials can evade existing resistance mechanisms and may be less prone to select for resistance than conventional antibiotics.[16] Moreover, nanomaterials have the ability to eradicate bacteria in biofilms.[15] From the aforementioned points taken together, nanotechnology provides a new toolkit for the creation of treatment strategies for MDR infections.

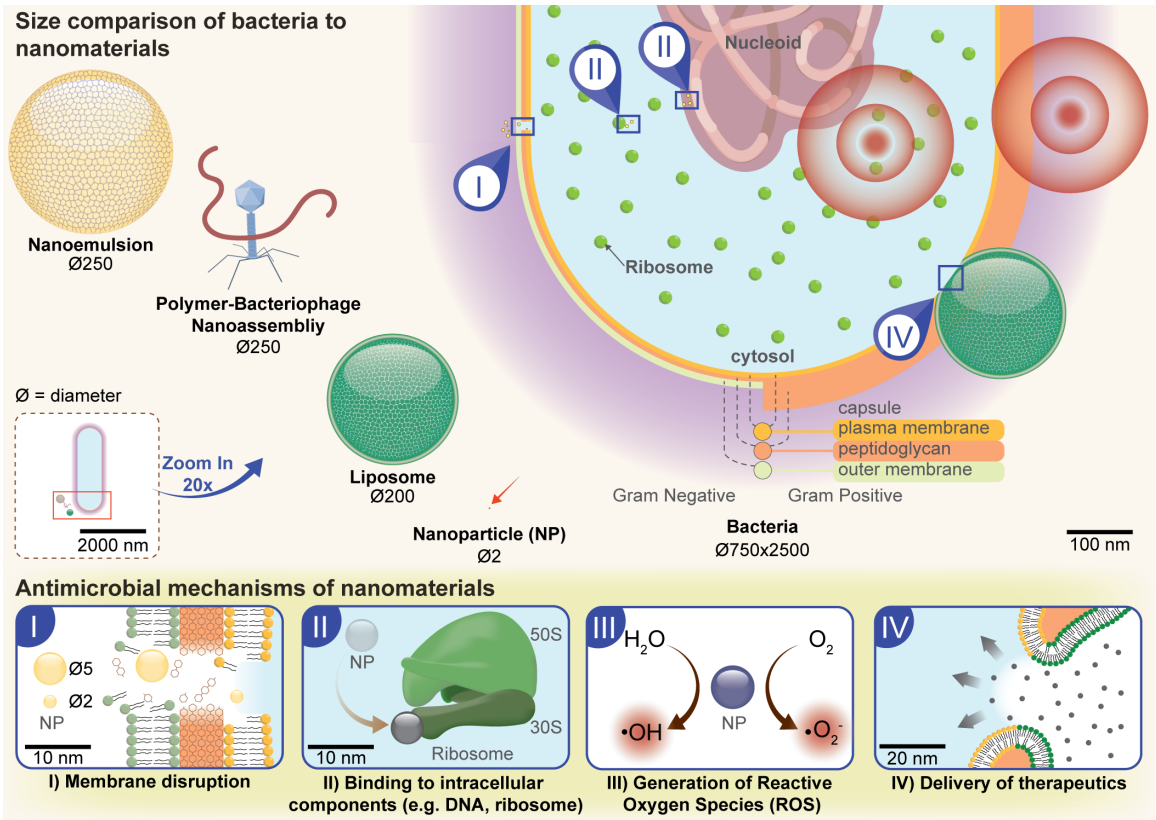

Figure 1. 1. Bacteria typically have diameters ranging from 0.2 to 10 µm. Different nanomaterials and preparation methods provide a wide range of particle sizes (2 - 500 nm) that facilitate maximal contact and strong interactions with bacterial membranes. Nanomaterials display a variety of bactericidal mechanisms. Electrostatic interactions of nanomaterials with the negatively charged groups present on bacterial surfaces result in membrane damage and cytoplasmic leakage. Nanomaterials can bind various intracellular components, such as ribosomes, proteins and/or DNA, disrupting their functions. Nanomaterials with catalytic activities increase the production of reactive oxygen species (ROS), such as hydroxyl radicals and superoxides, causing oxidative cellular stress. Nanomaterials can also be used for delivery of therapeutic agents; some nanomaterials readily enter bacterial cells through membrane fusion, facilitating delivery of their cargo. NP, nanoparticle.

Polymeric nanomaterials provide promising strategies to combating MDR and biofilm infections, as polymers are stable, biocompatible, and even biodegradable *in vitro* as well as *in vivo*.[17] Modern polymer chemistry allows control of the bulk properties of target polymers including polydispersity index, polymer length, hydrophobicity/hydrophilicity, and backbone rigidity.[18,19] Engineered polymers have been used to mimic the activity of antimicrobial peptides,[20,21] and to deliver antibiotics to

increase drug solubility, stability and efficacy, and improve the pharmacokinetic profiles of drugs.[22]

1.2 Overview and contributions

In this dissertation, I illustrate how polymers could be used to deliver therapeutics to combat bacterial biofilm infections. In the Chapter 2, I describe the synthesis of a polymer for stabilizing an antimicrobial oil in aqueous solution. This research uses a synthetic polymer and cross-linking strategy that provides a stable yet biodegradable nanoemulsion for combating bacterial biofilms. Chapter 3 is a follow-up study of the material in Chapter 2, exploring the use of the synthetic polymer to deliver a library of antimicrobial oils to bacterial biofilms. The cytotoxicity of this synthetic polymer-based nanoemulsion is also evaluated in this Chapter. Chapter 4 demonstrates a related nanoemulsion system using only naturally-derived materials. The use of biopolymers can ameliorate safety concerns and improve acceptance by the public. The antimicrobial activity and wound healing of this all-natural therapeutic *in vivo* is also studied. Chapter 5 discusses the use of the synthetic nanoemulsion system to explore the relationship between surface charge and biofilm penetration profiles. These results can provide guideline for designing synthetic polymers for antimicrobial nanoemulsions. In Chapter 6, I describe a preliminary study about the delivery of bacteriophages into bacterial biofilms using polymers. The promising results shown indicate the potential of the polymer-bacteriophage nanoassemblies for treating bacterial biofilm infections. Finally, in the last Chapter, I conclude this dissertation and discuss possible future directions for these works.

1.3 References

1 Ventola, C. L. The Antibiotic Resistance Crisis Part 1 : Causes and Threats. *Pharm. Ther.* **2015**, *40*, 277–283.

2 Michael, C. A.; Dominey-Howes, D.; Labbate, M. The Antimicrobial Resistance Crisis: Causes, Consequences, and Management. *Frontiers in Public Health*, **2014**, *2*, 145.

3 Naylor, N. R.; Atun, R.; Zhu, N.; Kulasabanathan, K.; Silva, S.; Chatterjee, A.; Knight, G. M.; Robotham, J. V. Estimating the Burden of Antimicrobial Resistance: A Systematic Literature Review. *Antimicrob. Resist. Infect. Control* **2018**, *7*, 58.

4 Willyard, C. The Drug-Resistant Bacteria That Pose the Greatest Health Threats. *Nature* **2017**, *543*, 15.

5 Lebeaux, D.; Chauhan, A.; Rendueles, O.; Beloin, C. From in Vitro to in Vivo Models of Bacterial Biofilm-Related Infections. *Pathogens* **2013**, *2*, 288–356.

6 Lebeaux, D.; Ghigo, J.-M.; Beloin, C. Biofilm-Related Infections: Bridging the Gap between Clinical Management and Fundamental Aspects of Recalcitrance toward Antibiotics. *Microbiol. Mol. Biol. Rev.* **2014**, *78*, 510–543.

7 Bjarnsholt, T. The Role of Bacterial Biofilms in Chronic Infections. *APMIS* **2013**, *121*, 1–58.

8 Van Acker, H.; Van Dijck, P.; Coenye, T. Molecular Mechanisms of Antimicrobial Tolerance and Resistance in Bacterial and Fungal Biofilms. *Trends Microbiol.* **2014**, *22*, 326–333.

9 Flemming, H.; Wingender, J. The Biofilm Matrix. *Nat. Rev. Microbiol.* **2010**, *8*, 623–633.

10 Ventola, C. L. The Antibiotic Resistance Crisis Part 2 : Management Strategies and New Agents. *Pharm. Ther.* **2015**, *40*, 344–352.

11 Aminov, R. A Brief History of the Antibiotic Era: Lessons Learned and Challenges for the Future. *Front. Microbiol.* **2010**, *1*, 134.

12 Arciola, C. R.; Campoccia, D.; Montanaro, L. Implant Infections: Adhesion, Biofilm Formation and Immune Evasion. *Nat. Rev. Microbiol.* **2018**, *16*, 397–409.

13 Wu, Y.-K.; Cheng, N.-C.; Cheng, C.-M. Biofilms in Chronic Wounds: Pathogenesis and Diagnosis. *Trends Biotechnol.* **2019**, *37*, 505–517.

14 Wang, L. S.; Gupta, A.; Rotello, V. M. Nanomaterials for the Treatment of Bacterial Biofilms. *ACS Infect. Dis.* **2016**, *2*, 3–4.

15 Gupta, A.; Landis, R. F.; Rotello, V. M. Nanoparticle-Based Antimicrobials: Surface Functionality Is Critical. *F1000Research* **2016**, *5*, 364.

16 Pelgrift, R. Y.; Friedman, A. J. Nanotechnology as a Therapeutic Tool to Combat Microbial Resistance. *Adv. Drug Deliv. Rev.* **2013**, *65*, 1803–1815.

17 Xiong, M. H.; Bao, Y.; Yang, X. Z.; Zhu, Y. H.; Wang, J. Delivery of Antibiotics with Polymeric Particles. *Adv. Drug Deliv. Rev.* **2014**, *78*, 63–76.

18 Nomura, K.; Abdellatif, M. M. Precise Synthesis of Polymers Containing Functional End Groups by Living Ring-Opening Metathesis Polymerization (ROMP): Efficient Tools for Synthesis of Block/Graft Copolymers. *Polymer (Guildf).* **2010**, *51*, 1861–1881.

19 Das, D.; Srinivasan, S.; Kelly, A. M.; Chiu, D. Y.; Daugherty, B. K.; Ratner, D. M.; Stayton, P. S.; Convertine, A. J. RAFT Polymerization of Ciprofloxacin Prodrug Monomers for the Controlled Intracellular Delivery of Antibiotics. *Polym. Chem.* **2016**, *7*, 826–837.

20 Palermo, E. F.; Kuroda, K. Structural Determinants of Antimicrobial Activity in Polymers Which Mimic Host Defense Peptides. *Appl. Microbiol. Biotechnol.* **2010**, *87*, 1605–1615.

21 Song, J.; Jang, J. Antimicrobial Polymer Nanostructures: Synthetic Route, Mechanism of Action and Perspective. *Adv. Colloid Interface Sci.* **2014**, *203*, 37–50.

22 Landis, R. F.; Gupta, A.; Lee, Y.-W.; Wang, L.-S.; Golba, B.; Couillaud, B.; Ridolfo, R.; Das, R.; Rotello, V. M. Cross-Linked Polymer-Stabilized Nanocomposites for the Treatment of Bacterial Biofilms. *ACS Nano* **2017**, *11*, 946–952.

CHAPTER 2

2. BIODEGRADABLE NANOCOMPOSITE ANTIMICROBIALS FOR THE ERADICATION OF MULTIDRUG-RESISTANT BACTERIAL BIOFILMS WITHOUT ACCUMULATED RESISTENCE

* indicates equal contribution

2.1 Introduction

Multidrug-resistant (MDR) bacteria infect more than two million people annually in the U.S., resulting in significant loss of life and limb, with treatment requiring prolonged and costly therapeutic regimens.[1-3] These dangerous pathogens, including *Pseudomonas aeruginosa* and *Staphylococcus aureus*, further frustrate treatment by their innate ability to micro-colonize into biofilms.[4-6] Bacterial biofilm infections are challenging to treat on wounds and indwelling medical devices, as the extracellular polymeric substances (EPS) in these biofilms both inhibit antibiotic penetration and aid bacteria to evade host immune response.[7-9] Furthermore, the slow growth rate of bacteria and the biofilm microenvironment act together to facilitate the development of antibiotic resistance.[10-12] The emerging threat of antibiotic resistant biofilm infections has triggered an international push to develop alternative therapeutic platforms capable of eliminating these infections.[13,14]

Plant-derived phytochemicals have emerged as an alternative to traditional antibiotic paradigms to combat MDR bacteria,[15-19] providing a potential strategy for

avoiding antibiotic tolerance and horizontal gene transfer that dramatically accelerate acquisition of drug resistance.[20,21] Phytochemicals feature low cost,[22] biocompatibility,[23] and can be effective towards bacterial infections.[24] However, the poor solubility of these hydrophobic oils in aqueous media limit their practical application as antimicrobial agents.[25] Surfactant, nanoparticle, and polymer additives aid in phytochemical delivery by forming oil-in-water emulsions.[26-29] Furthermore, crosslinking of these emulsions have demonstrated phytochemical stability in even complex media such as serum.[30] However, such crosslinking strategies are non-biodegradable and may persist and accumulate within the body, causing unwanted side effects, such as inflammation and carcinogenesis.[31-33]

Here, we report crosslinked poly(oxanorborneneimide)-stabilized oil-in-water nanocomposites (**X-BNCs**) engineered to be biodegradable in the presence of endogenous biomolecules such as glutathione and esterase enzymes (Figure 2. 1). These 'nanosponges' incorporate disulfide[34] and ester[35,36] crosslinkers that provide long-term stability in aqueous environments while facilitating nanocomposite degradation in biological milieus. We demonstrate the loading of these **X-BNCs** with carvacrol to provide therapeutics that eradicate Gram negative/positive bacteria including MDR strains. These nanocomposites are stable in serum-containing media, however, degrade rapidly in the presence of glutathione or esterase proteins. The potential of **X-BNCs** as a wound healing therapeutic was demonstrated in an *in vitro* coculture with biofilms grown on top of mammalian 3T3 fibroblast cells. A 4-log reduction in bacterial colonies was observed with no change in fibroblast cells viability. In stark contrast to antibiotics, **X-BNCs** do not evoke resistance in bacteria, maintaining their potency against pathogenic

Escherichia coli (CD-2) in a 20-cycle serial passage study. Taken together, the efficacy, biodegradability, and stability of these anti-biofilm agents coupled with their lack of resistance accumulation make them a promising therapeutic platform to combat the rising dangers of MDR bacterial infections.

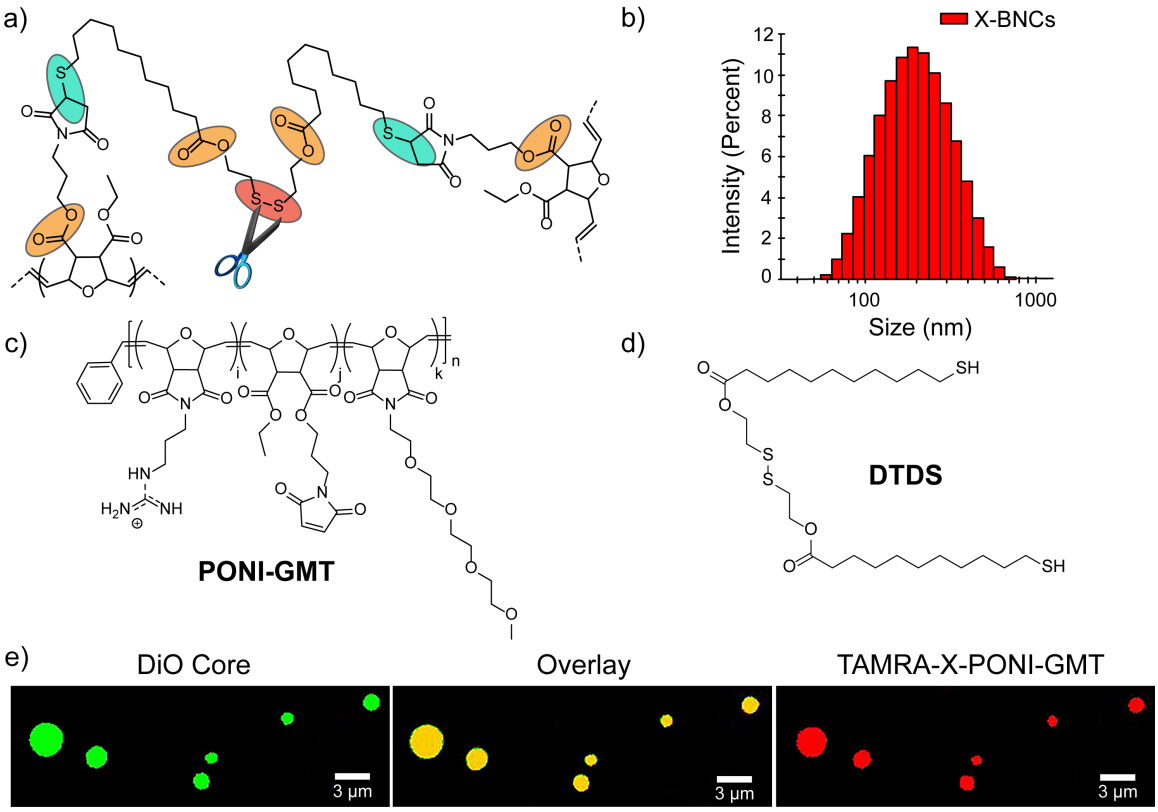

Figure 2. 1. (a) Crosslinked **PONI-GMT-DTDS** structure showing linkage points reactive to endogenous biomolecules. (b) DLS histogram of crosslinked **PONI-GMT-DTDS** nanosponges loaded with carvacrol in phosphate buffer saline (150 mM). (c) Chemical structures of **PONI-GMT** and (d) **DTDS**. (e) Confocal micrograph of crosslinked micron-sized biodegradable composites. **PONI-GMT** labeled with TAMRA-X (red fluorescence), and the oil core is loaded with DiO (green fluorescence). A composite morphology is indicated by co-distribution of **PONI-GMT** with the hydrophobic oil core. Scale bar is 3µm.

2.2 Results and Discussion

2.2.1 Generation and Characterization of Nanocomposites

The X-BNC platform uses a poly(oxanorborneneimide) scaffold bearing guanidine, maleimide, and tetraethyleneglycol monomethyl ether groups (**PONI-GMT**) and provides a well-controlled and scalable platform.[30] Biodegradability was imparted through use of a dithiol-disulfide (**DTDS**) crosslinker that is stable > 2 years in storage. An additional degradation modality was provided using ester-linked maleimide groups to enable thiols of **DTDS** to crosslink rapidly once the polymers assemble at the oil-water interface.[37] Copolymerization of monomers bearing guanidine, maleimido, and tetreaethylene glycol monomethyl ether units at a 40:10:50 monomer ratio respectively provided the precursor polymer **PONI-GMT**. The maleimido monomer ratio was kept low to ensure adequate solubility of **PONI-GMT** in aqueous conditions, necessary for efficient nanocomposite formation.

Nanocomposites were fabricated by emulsifying carvacrol oil loaded with DTDS or carvacrol only (non-crosslinked control, **NX-NC**) into water. Upon emulsification, **PONI-GMT** assembles and initially stabilizes the oil-water interface. In the presence of **DTDS**, with crosslinking further stabilizing the oil droplets in water. **PONI-GMT** and **DTDS** generated nanocomposites **(X-BNCs**) with a diameter of ~220 nm as shown by dynamic light scattering (DLS). We hypothesized the overall charge of **X-BNCs** would be reversed yielding a positively charged surface. The measured zeta (ζ) potential supported this prediction, reporting a cationic nanocomposite (Figure 2. 2), attributed to guanidine units at or beyond the oil-water interface. Significantly, DLS experiments on

stock solutions of **X-BNCs** that were stored on the bench for one year indicated the composites maintained stability with a minimal change in size (Figure 2. 3).

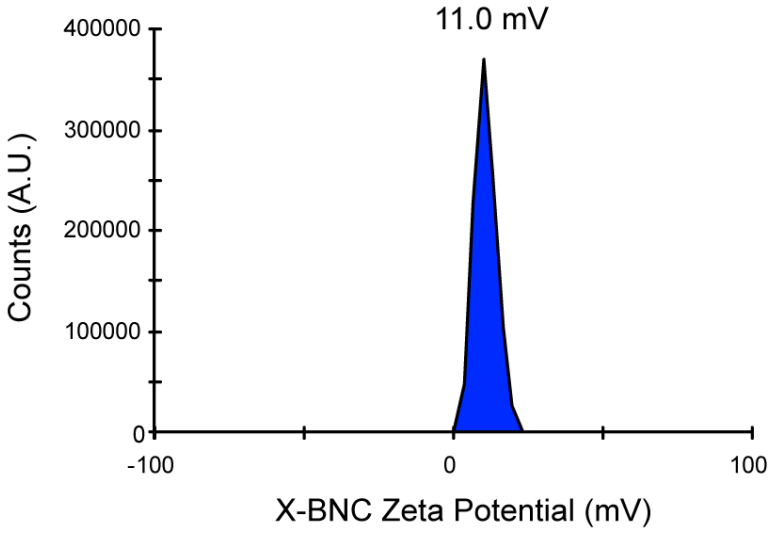

Figure 2. 2. Zeta potential of **X-BNCs**. The cationic charge is derived from guanidine moieties found on **PONI-GMT** and is expected to be located at the oil-water interface and throughout the emulsion, given the architecture is a composite morphology.

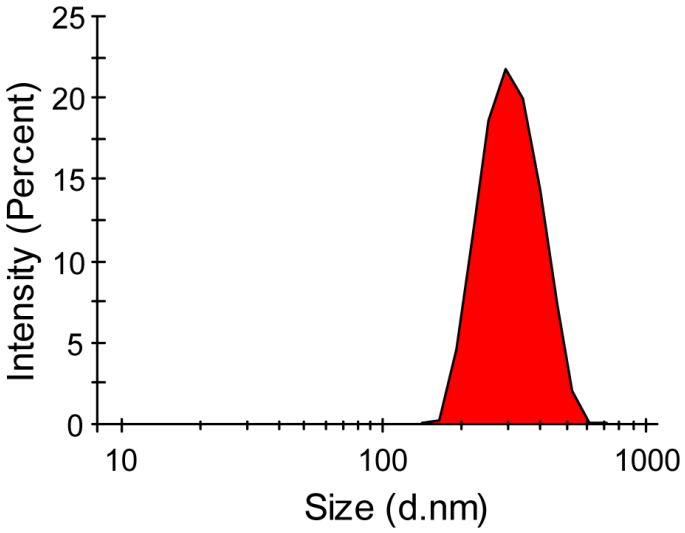

Figure 2. 3. Size distribution of **X-BNCs** stock solution in PBS after 1 year of storage. The average size of **X-BNCs** increased to ~ 310 nm indicating that the crosslinking scaffold of **X-BNCs** slows the onset of flocculation.

Next, the morphology (core-shell versus nanocomposites) of **X-BNCs** was established through confocal microscopy of larger micron-sized analogs of the **X-BNC**

nanoemulsions. TAMRA-X (red fluorescence) was conjugated to **PONI-GMT**, while 3,3-dioctadecyloxacarbocyanine (DiO, green fluorescence) was loaded within the oil. As shown in Figure 2. 1e, both green and red fluorescence were co-distributed across the microparticle, indicating the morphology adopts a composite "sponge" architecture. Given that previous reports have observed norbornene-based polymers (Mn's ~ 100,000 g/mol) adopt length scales of ~ 40 nanometers,[38] it is reasonable to suggest that **PONI-GMT** would exist in a composite morphology in the **X-BNCs** nanoemulsions. This notion is further supported in literature as carvacrol and other phytochemicals are miscible with glycols,[39] such as the high density of tetraethylene glycol units found on **PONI-GMT**.

2.2.2 Stability and Degradability of X-BNC

Macromolecular vehicles need to be stable to deliver therapeutic payloads yet degrade to avoid vehicle accumulation over time.[40] After characterizing the morphology of **X-BNCs**, we next probed the colloidal stability of the composites via monitoring particle size by dynamic light scattering (DLS).[41] As shown in Figure 2. 4a, when **X-BNCs** were incubated with 10% serum media for 2 hours, an increase in **X-BNCs** size (~25 nm) was observed, suggesting negatively charged serum proteins adsorb onto the positively charged **X-BNCs** surface. Notably, no evidence of **X-BNC** destabilization/aggregation was observed even at longer incubation times (e.g. 6 hours). However, as a control, non-crosslinked analogues using the same formulation minus **DTDS** showed essentially no stability in serum (Figure 2. 5).

We next explored the degradability of X-BNCs in the presence of glutathione (GSH) and the ester-hydrolyzing enzyme porcine liver esterase (**PLE**). Using

physiologically relevant concentrations of both biomolecules, **X-BNCs** were incubated for 24 hours with either 10 mM **GSH** or 35 µM **PLE** (1 U/µL) with PBS as a control. Figure 2. 4b shows the size of X-BNCs remained the same after 24 hours in PBS, however the size increased significantly in **GSH**/**PLE** solutions, indicating degradation of the nanocomposites structure with concomitant generation of agglomerated structures through an Ostwald ripening-like process. Taken together, the results indicate the crosslinked composite framework within **X-BNCs** are robust in serum yet biodegrade in the presence of chosen biological environments.

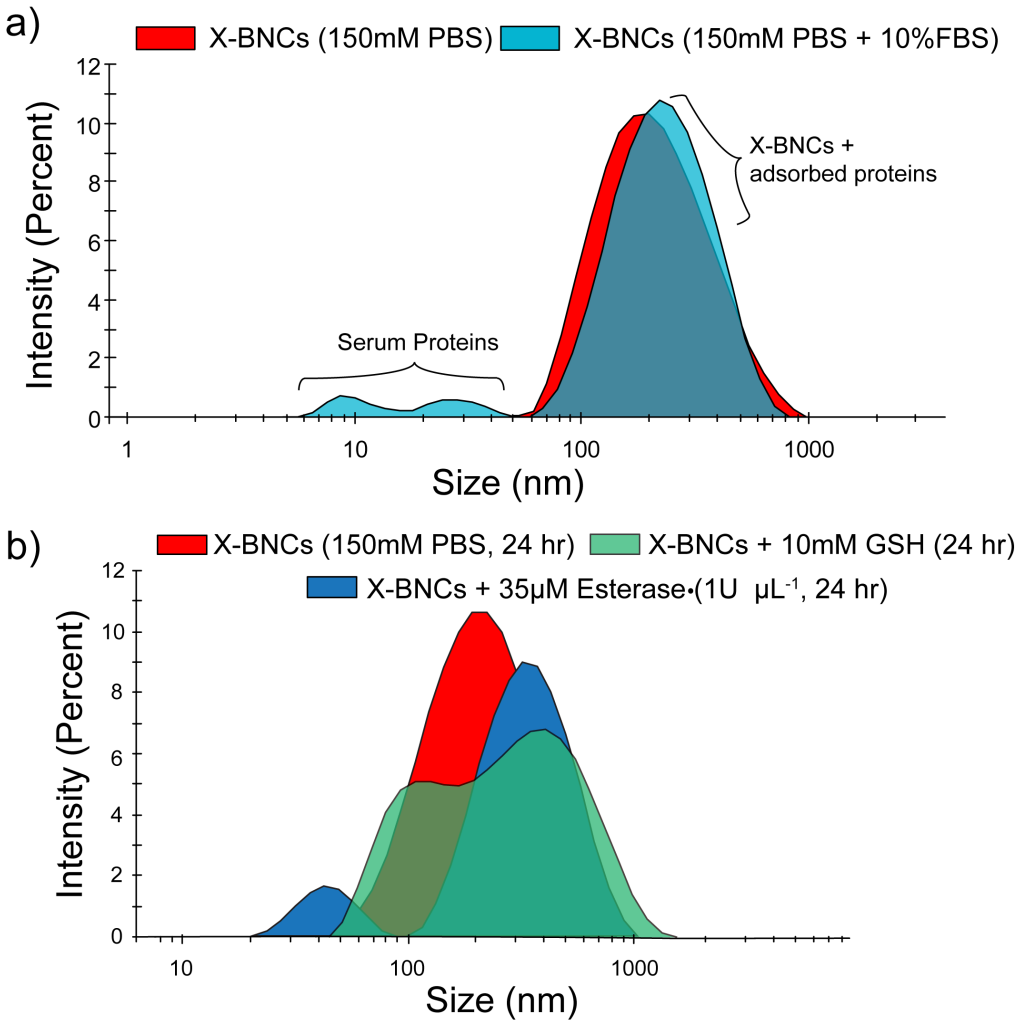

Figure 2. 4. Stability and degradability of **X-BNCs**. DLS size distribution changes of X-BNCs when incubated with (a) 10% FBS media for two hours or (b) physiologically relevant biomolecules (glutathione and lipase) in PBS, showing degradation from disulfide cleavage and hydrolysis.

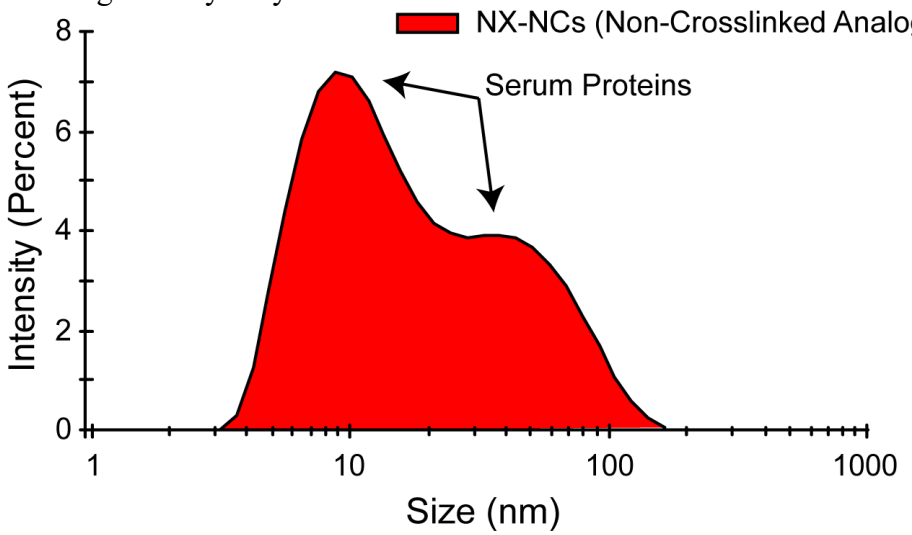

Figure 2. 5. Size distribution of non-crosslinked analogs of **X-BNCs** (**NX-NCs**) after two hours in 10% fetal bovine serum using dynamic light scattering (DLS) measurements. **NX-NCs** show no stability in serum-containing conditions with the DLS results indicating only serum proteins present.

2.2.3 Antimicrobial Activity of X-BNCs Against Biofilms

We focused our antimicrobial efforts on highly refractory biofilms, where the efficacy of traditional antibiotic therapy is significantly compromised relative to planktonic pathogens.[42] We investigated the ability of **X-BNCs** to penetrate EPS followed by quantitative analysis of their therapeutic efficacy towards enclosed pathogenic bacteria. **X-BNC** penetration into biofilms formed by red fluorescent protein (RFP)-expressing *E. coli* was tracked by loading 3,3-dioctadecyloxacarbocyanine (DiO, green fluorescence) within the oil core. As shown in Figure 2. 6, **X-BNCs** readily penetrate and diffuse throughout the biofilm, with fluorescence colocalizing with enclosed bacteria. The data demonstrates **X-BNCs** deliver their payload efficiently, reaching enclosed pathogens deep within the films' matrix.

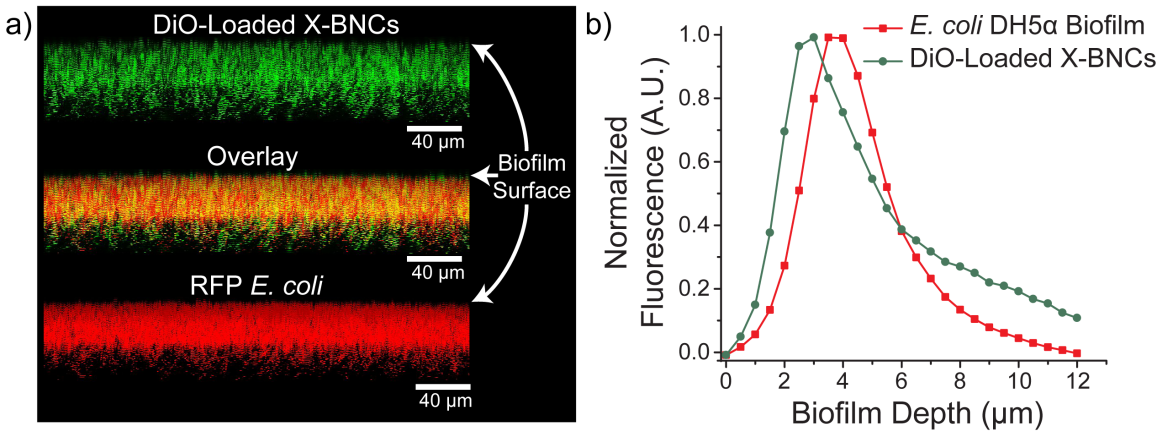

Figure 2. 6. Confocal image stacks and penetration profile of *E. coli* DH5α biofilm after 1-hour treatment with X-BNCs loaded with DiO. Scale bars are 40 μm and are not representative of the biofilm depth. Each projected z-stack image (a) is spaced by 1.3 μm at a 5° angle from the biofilm's x-plane. Both the overlay and biofilm depth fluorescence graph (b) indicates X-BNCs completely penetrate the biofilm, colocalizing with bacteria that expresses red fluorescent protein.

Next, the antimicrobial activity of **X-BNCs** against multiple pathogenic Gram-negative and Gram-positive biofilms were evaluated. Four pathogenic bacterial strains of clinical isolates, *Staphylococcus aureus* (CD-489, a methicillin-resistant strain), *Pseudomonas aeruginosa* (CD-1006), *Escherichia coli* (CD-2), and *Enterobacter cloacae* (CD-1412) complex were chosen to be tested as their associated infections are typically common in hospital-related settings.[43,44] As shown in Figure 2. 7, **X-BNCs** effectively eliminated bacterial cells in all four-biofilm species within 3 hours. Notably, both Gram positive (*S. aureus*) and Gram negative (*P. aeruginosa*, *E. coli*, and *E. cloacae* complex) bacteria can be treated with **X-BNCs**, highlighting their broad-spectrum activity even in a biofilm matrix setting.

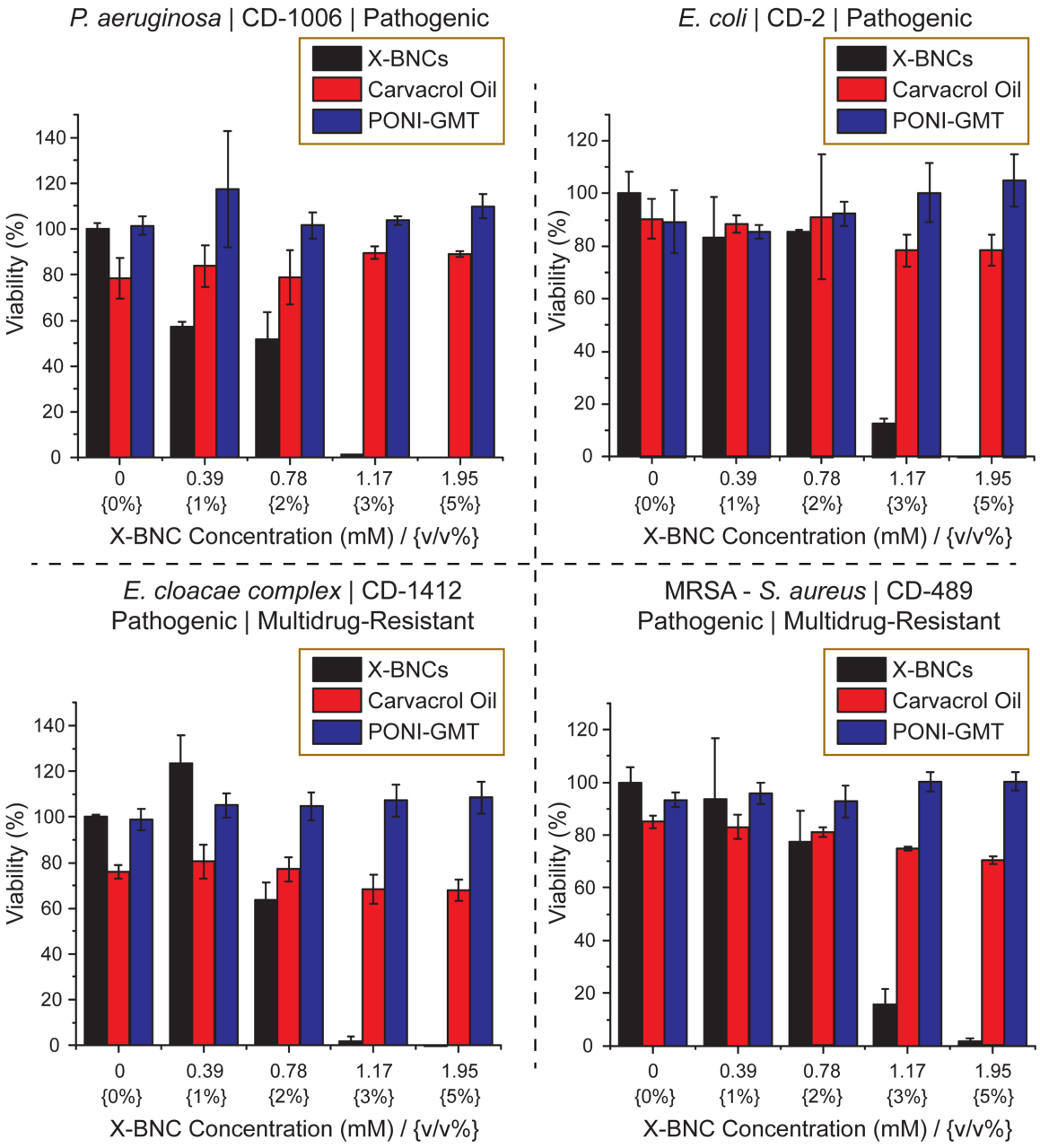

Figure 2. 7. Viability of one-day-old Gram negative/positive biofilms after a three-hour treatment with **X-BNCs** and the individual components as controls at different emulsion concentrations (Displayed as mM and v/v % of emulsion). The results shown are averaged triplicates, and the error bars indicate the standard deviation.

2.2.4 Selective Killing of Biofilms in a Coculture Model

Beyond treating biofilms on surfaces, eliminating these bacterial infections on human tissue and organs is a greater challenge and more relevant to patients who suffer

from skin ulcers, burn injuries, or wound trauma. A fundamental issue associated with these infections is their ability to interfere with the host's tissue regeneration process. We evaluated the efficacy of **X-BNCs** as a topical treatment by using an *in vitro* co-culture model comprised of a biofilm grown on top of mammalian fibroblasts. *P. aeruginosa* and NIH 3T3 fibroblast cells were selected to build this co-culture model, since *P. aeruginosa* is widely associated with skin infections and fibroblast cells are critical during wound healing.[45-47] The co-cultures were treated with X-BNCs for 3 hours, washed, and the viabilities of bacteria and fibroblast cells were determined. As shown in Figure 2. 8, a 4-fold log reduction (~99.5%) in biofilm colonies was observed at a **X-BNCs** concentration of 16 v/v %, while 3T3 fibroblast viability remained uncompromised. Significantly, little change in fibroblast viability was observed at 32 v/v %, where a 6 *log unit* reduction in bacteria was observed. This selective toxicity to biofilm bacteria makes the X-BNC platform promising for addressing wound biofilms.

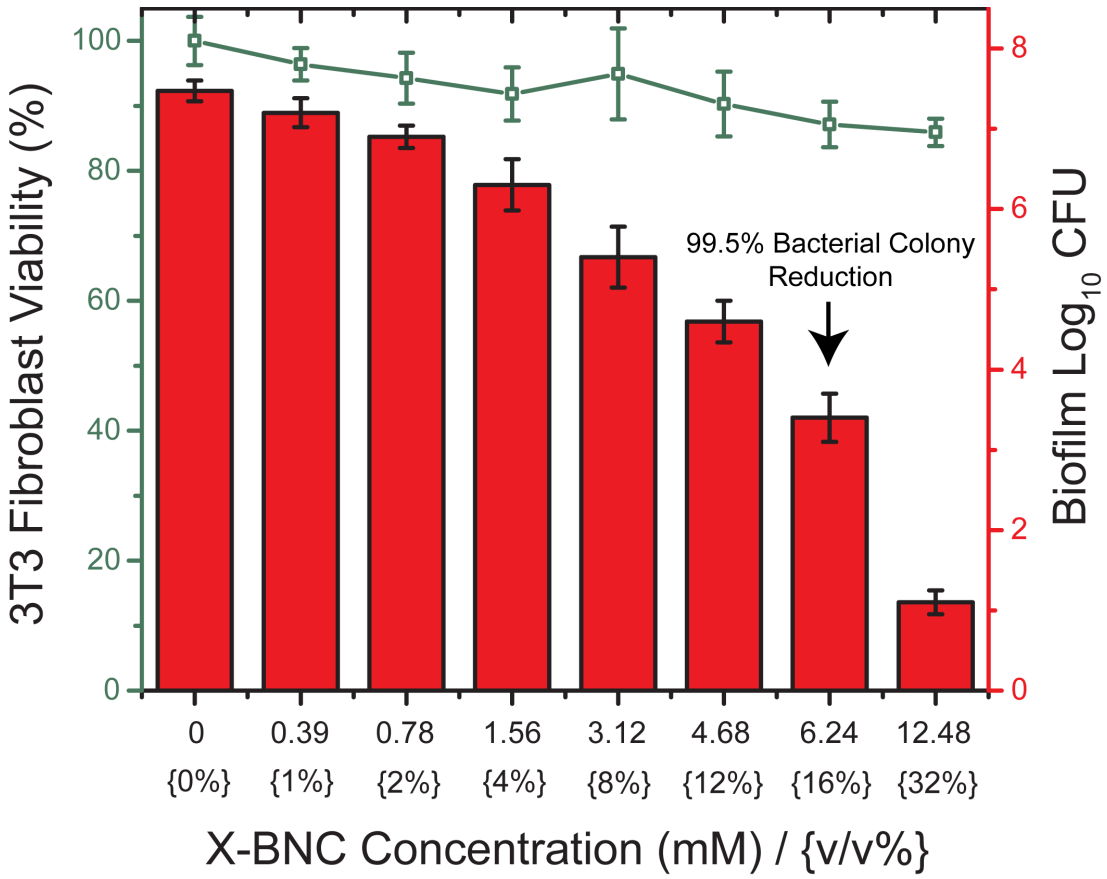

Figure 2. 8. Viability of 3T3 fibroblast cells and *P. aeruginosa* biofilms in the coculture model after treating **X-BNCs** at different emulsion concentrations for three hours. 3T3 fibroblast cell viabilities are shown as a line. Bar plots represent $\log_{10}$ of colony-forming bacteria units in biofilms. Each result is an average of three experiments, and the error bars designate the standard deviations.

2.2.5 Bacterial Resistance Towards Antibiotics Vs. X-BNCs

The number of antibiotic-resistant bacteria and their associated infections is increasing globally, leading to cases where infections have become untreatable. Although efforts to discover novel antibiotic classes to slow the progression of antibiotic resistance is ongoing,[48] developing alternative therapeutic platforms where bacteria cannot develop resistance towards must take precedence. We hypothesized that the membrane disruption induced by the antimicrobial phytochemical payload of **X-BNCs** would sidestep normal bacterial defense adaptations, preventing accumulated resistance. We tested this

hypothesis by subjecting planktonic bacteria to X-BNCs and a negative control antibiotic (ciprofloxacin, enzyme inhibitor) in the presence of propidium iodide (Figure 2. 9). PI is not permeant to live bacterial cells, however, easily diffuses through membrane-compromised cells, generating fluorescence upon intercalating with DNA. X-BNC treatment quickly generated PI fluorescence, indicating its action mechanism compromises bacterial membrane integrity. Ciprofloxacin is an enzyme inhibitor antibiotic and therefore does not act on bacterial membranes, generating no observed fluorescence.

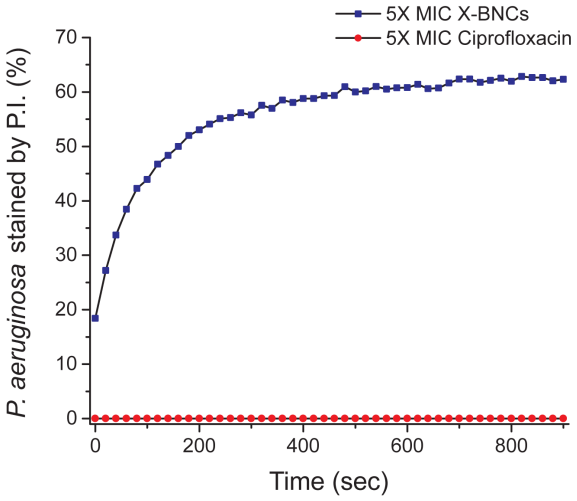

Figure 2. 9. Percentage of *P. aeruginosa* stained by propidium iodide (PI) following treatment with **X-BNCs** or ciprofloxacin. **X-BNCs** quickly disrupted cell membrane, therefore PI could bind to nucleic acids and generate red fluorescence. However, no fluorescence was observed with ciprofloxacin as its action mechanism towards bacteria involves enzyme inhibition and not membrane disruption. The remaining percent of *P. aeruginosa* that were not stained is likely due to the large concentration of bacteria used (OD_{600} = 0.5) along with a complete consumption of X-BNC composites during the study.

Next, pathogenic *E. coli* (CD-2) was passaged in the presence of **X-BNCs**, or three commercially available antibiotics, ciprofloxacin (quinolone class), ceftazidime (β-lactam class), and tetracycline (tetracycline class). Briefly, we subjected the bacteria to

the sub-minimum inhibitory concentrations (66% of MIC) of the antimicrobial agent. The resulting bacterial populations for each individual therapeutic was defined as the first passage, harvested, and their respective MICs evaluated. The subsequent passage was derived by exposing the previous passage with the 66% MIC of each respective therapeutic dosage. As shown in Figure 2. 10a, no resistance was generated towards **X-BNCs** even after *20* serial passages (~1,300 bacterial generations). Meanwhile, *E. coli* rapidly developed resistance towards each of the antibiotics, with respective MIC increases of 33,000, 4,200, and 256-fold where the drugs reached their solubility limit in media. Going further, biofilms were grown with the 20th serial passage and subjected to X-BNCs for 3 hours, where CD-2 *E. coli* was still susceptible to nanoemulsion treatment (Figure 5b). These results indicate the mechanism of **X-BNCs** mitigates the onset of resistance in both planktonic and biofilm settings.

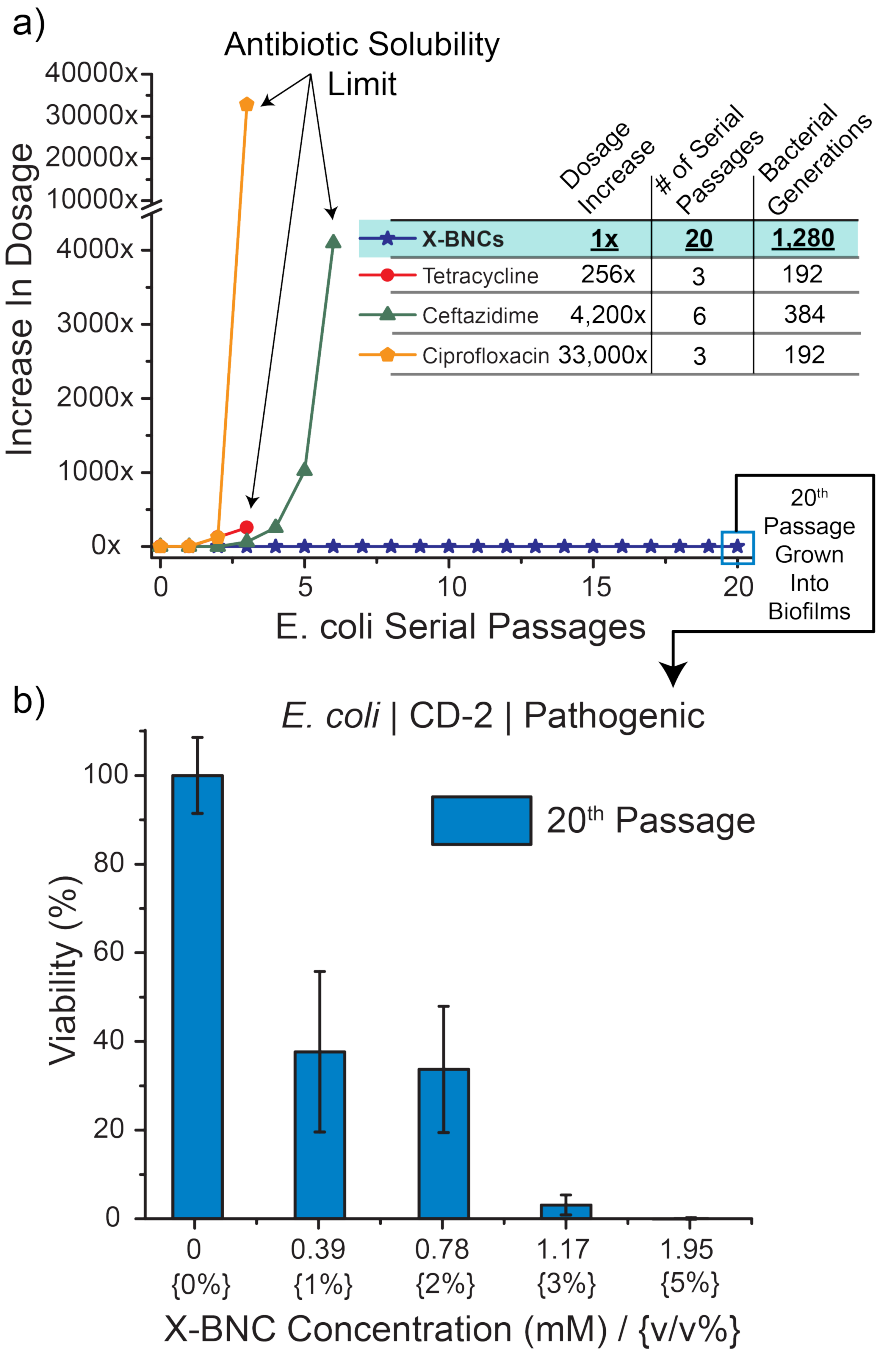

Figure 2. 10. Accumulated resistance of pathogenic *E. coli* (CD-2) in both plankton and biofilm settings. (a) Resistance development of planktonic species during serial passaging in the presence of sub-MIC dosing's of antimicrobials. The y-axis indicates the increase in dosage as compared to the initial bacterial cells (0^{th} passage) and the figure is representative of three independent experiments. (b) Derived *E. coli* cells from 20 serial passages of sub-MIC X-BNCs dosing was grown into a biofilm and subjected to a three-hour treatment of X-BNCs at different emulsion concentrations. The results indicate that evolved pathogenic *E. coli* remain susceptible to X-BNCs.

2.3 Conclusion

In summary, we report the construction, characterization, and antimicrobial potential of a biodegradable crosslinked polymer-stabilized oil-in-water nanocomposite. These nanoemulsions maintain stability in serum yet degrade in the presence of selected biomolecules, a necessary attribute to avoid vehicle accumulation over time. Furthermore, the nanocomposites are highly effective against both Gram negative and positive bacteria biofilms, with no observed toxicity to mammalian fibroblast cells. In stark contrast to traditional antibiotics, bacteria were unable to accumulate resistance towards our nanoemulsions whether the bacteria were planktonic or in biofilms. The therapeutic polymer-based phytochemical nanoemulsion we present is a highly promising antimicrobial platform with the potential to impact treatment of wound biofilms and other difficult bacterial infections.

2.4 Experimental Section

2.4.1 Materials and Methods

All reagents and materials were purchased from Fisher Scientific and used as received. NIH-3T3 cells (ATCC CRL-1658) were purchased from ATCC. Dulbecco's Modified Eagle's Medium (DMEM) (DMEM; ATCC 30-2002) and fetal bovine serum (Fisher Scientific, SH3007103) were used in cell culture. Pierce LDH Cytotoxicity Assay Kit was purchased from Fisher Scientific.

2.4.2 Preparation of Nanocomposites

Stock nanocomposite solutions were prepared in 0.6 ml Eppendorf tubes. To prepare the stock **X-BNC** emulsions, 3 μL of carvacrol oil (containing 3 wt% **DTDS**)

was added to 497 μL of Milli-Q H_2O containing 6 μM of **PONI-GMT** and emulsified in an amalgamator for 50 s. The non-crosslinked analogs were generated in the same fashion however without **DTDS** dissolved in carvacrol. The emulsions were allowed to rest overnight prior to use.

2.4.3 Biofilm Formation

Bacteria were inoculated in LB broth at 37°C until stationary phase. The cultures were then harvested by centrifugation and washed with 0.85% sodium chloride solution three times. Concentrations of resuspended bacterial solution were determined by optical density measured at 600 nm. Seeding solutions were then made in M9 to reach OD_{600} of 0.1. 100 μL of the seeding solutions were added to each well of the microplate. M9 medium without bacteria was used as a negative control. The plates were covered and incubated at room temperature under static conditions for a desired period. Planktonic bacteria were removed by washing with PB saline three times.

Varied v/v % of X-NCs, made in M9 medium, were incubated with the biofilms for 3 h. Biofilms were washed with phosphate buffer saline (PBS) three times and viability was determined using an Alamar Blue assay. M9 medium without bacteria was used as a negative control.

2.4.4 Biofilm-3T3 Fibroblast Cell Co-culture

A total of 20,000 NIH 3T3 (ATCC CRL-1658) cells were cultured in Dulbecco's modified Eagle medium (DMEM; ATCC 30-2002) with 10% bovine calf serum and 1% antibiotics at 37^{o}C in a humidified atmosphere of 5% CO_2. Cells were kept for 24 hours to reach a confluent monolayer. Bacteria (*P. aeruginosa*) were inoculated and harvested.

Afterwards, seeding solutions were made in buffered DMEM supplemented with glucose to reach an OD_{600} of 0.1. Old medium was removed from 3T3 cells followed by addition of 100 μL of seeding solution. The co-cultures were then stored in a box with damp paper towels at 37°C overnight without shaking. Testing solutions at different concentrations were made by diluting nanocomposites into DMEM prior to use. Media was removed from co-culture, replaced with testing solutions, and incubated for 3 hours at 37°C. Co-cultures were then analyzed using a LDH cytotoxicity assay to determine mammalian cell viability. To determine the bacteria viability in biofilms, the testing solutions were removed, and co-cultures were washed with PBS. Fresh PBS was then added to disperse remaining bacteria from biofilms in co-culture by sonication for 20 min and mixing with pipet. The solutions containing dispersed bacteria were then plated onto agar plates and colony forming units were counted after incubation at 37°C overnight.

2.4.5 Membrane Disruption Study via PI Staining

P. aeruginosa was cultured in LB medium at 37°C and 275 rpm until the stationary phase was reached. The cultures were centrifuged then resuspended in 70% isopropyl alcohol for obtaining dead bacteria or resuspended in 0.85% sodium chloride solution for live bacteria. Both bacteria were incubated for 1 hour at room temperature and then washed with 0.85% sodium chloride solution again. The O.D. of these solutions were determined and adjusted to 1.

100 μL of live bacteria were added to the wells of a black 96-well plate. 5 uL of 1 mg/L propidum iodide (PI) was then added. Fluorescence intensities were measured immediately after adding 100 μL of PBS containing 10X MIC of X-BNCs

(Excitation/Emission: 535 nm/ 617 nm). Live bacteria were also treated with PI and ciprofloxacin as negative control. Dead bacteria were treated with PI as positive control.

2.4.6 Synthesis of DTDS (3)

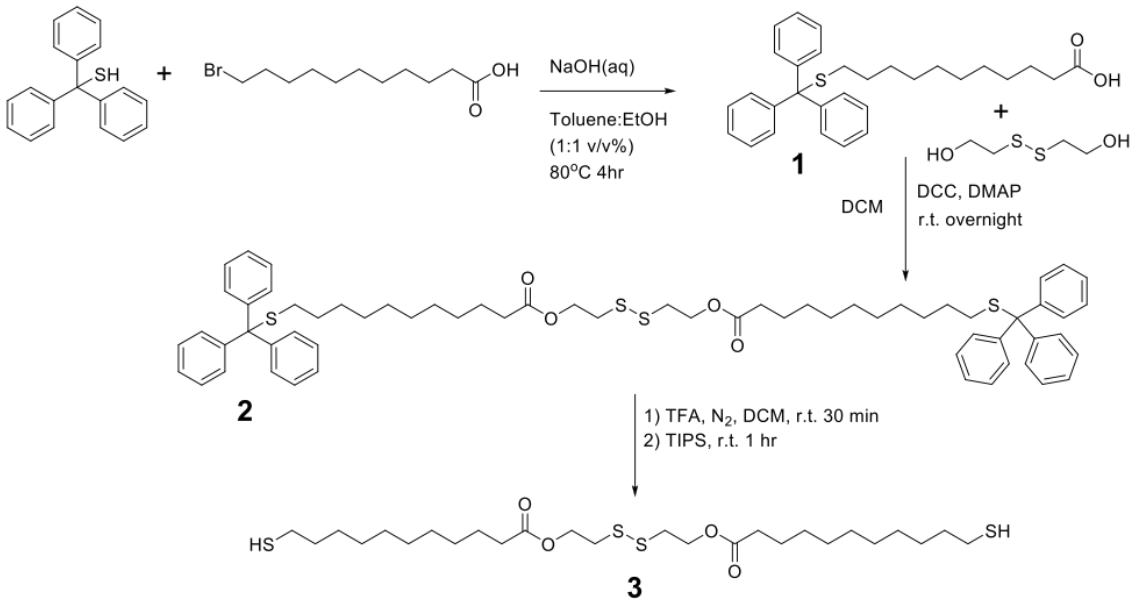

Figure 2. 11 Synthetic scheme of DTDS

2.4.6.1 Synthesis of 1

To a 250ml round bottom flask equipped with a stir-bar was added triphenylmethylmercaptan (5.0 g, 18.09 mmol, 1.0 eq), 11-bromoundecanoic acid (4.80 g, 18.09 mmol, 1.0 eq), and 75 mL of both toluene and ethanol. The mixture was allowed to stir to completely dissolve the reagents. Meanwhile, sodium hydroxide (1.60 g, 39.80 mmol, 2.2 eq) was dissolved in a minimal amount of water and then added to the reaction flask. The flask was heated to 80 ºC for 4 hours, cooled to room temperature, and the solvents rotovaped. Water was then added, and the mixture acidified with 1M HCl. The aqueous mixture was extracted with ethyl acetate three times. The combined organic

layers were washed with brine, dried with sodium sulfate, filtered, and rotovaped to yield an off-white solid that was purified through column chromatography to yield **1** (White solid, yield = 92%). (^{1}H NMR, $CDCl_3$, 400 MHz) 11.2 (br, 1H), 7.45 (d, 6H), 7.3 (t, 6H), 7.21 (t, 3H), 2.35 (t, 2H), 2.15 (t, 2H), 1.65 (m, 2H), 1.4 (m, 2H), 1.25 (m, 12H).

2.4.6.2 Synthesis of 2

To a 250 mL round bottom flask equipped with a stir-bar was added **1** (4.71 g, 10.22 mmol, 2.0 eq), 2-hydroxyethyl disulfide (0.63 mL, 5.11 mmol, 1.0 eq), 4-dimethylaminopyridine (0.31 g, 2.55 mmol, 0.5 eq), and 100 mL of dichloromethane. The reaction flask was stirred and finally N,N'-dicyclohexylcarbodiimide (2.22 g, 10.74 mmol, 2.1 eq) was added and allowed to stir at room temperature overnight. Afterwards, the solvent was evaporated and diethyl ether (150 mL) was added to the reaction residue, sonicated, and placed in a freezer for 1 hour to precipitate most of the DCU biproduct. The reaction mixture was filtered and washed with cold diethyl ether. The filtrate was rotovaped and the product was purified with column chromatography to yield **2** (light yellow solid, yield = 90%). (^{1}H NMR, $CDCl_3$, 400 Mhz) 7.41 (d, 12H), 7.28 (t, 12H), 7.21 (t, 6H), 4.35 (t, 4H), 2.92 (t, 4H), 2.32 (t, 4H), 2.15 (t, 4H), 1.63 (m, 4H), 1.4 (m, 4H), 1.25 (m, 24).

2.4.6.3 Synthesis of 3 (DTDS)

To a 250 mL round bottom flask equipped with a stir-bar, was added **2** (2.6 g, 2.50 mmol, 1.0 eq). Next, nitrogen was bubbled through 100 mL of dichloromethane for 5 minutes and added to the reaction flask. The flask was sealed with a septum and a continuous flow of nitrogen was introduce to the reaction flask until after trifluoroacetic

acid (7.66 mL, 100.04 mmol, 40.0 eq) was added. The reaction mixture color immediately changed to yellow and was allowed to stir for 30 minutes to completely form the triphenylmethyl carbocation. After 30 minutes, triisopropylsilane (1.1 mL, 5.25 mmol, 2.1 eq) was added to the reaction flask and allowed to stir for 1 hour. During this time the color changed back to nearly colorless. Afterwards, excess trifluoroacetic acid was removed by rotovaping the reaction 4 times with 100 mL of dichloromethane. The obtained residue was easily purified and isolated using column chromatography with no degradation or rearrangement of **3 (DTDS,** off-white solid, yield = 85%). (^{1}H NMR, $CDCl_3$, 400 MHz) 4.31 (t, 4H), 2.91 (t, 4H), 2.5 (q, 4H), 2.31 (t, 4H), 1.61 (m, 8H), 1.31 (m, 24H).

2.4.7 Storage Stability of DTDS

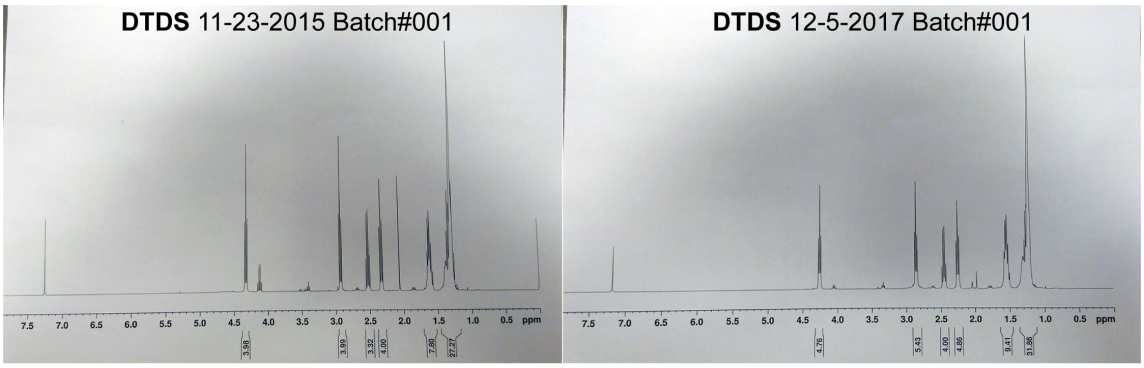

Figure 2. 12. DTDS was stored in a nitrogen purged 20ml scintillation vial, covered with aluminum foil and kept in a -4°C freezer for over two years. ^{1}H NMR analysis of **DTDS** two years later revealed no degradation or rearrangement of its initial structure. It is hypothesized that **DTDSs** stability is attributed to its solid physical properties.

2.4.8 Synthesis of Maleimide Monomer (8)

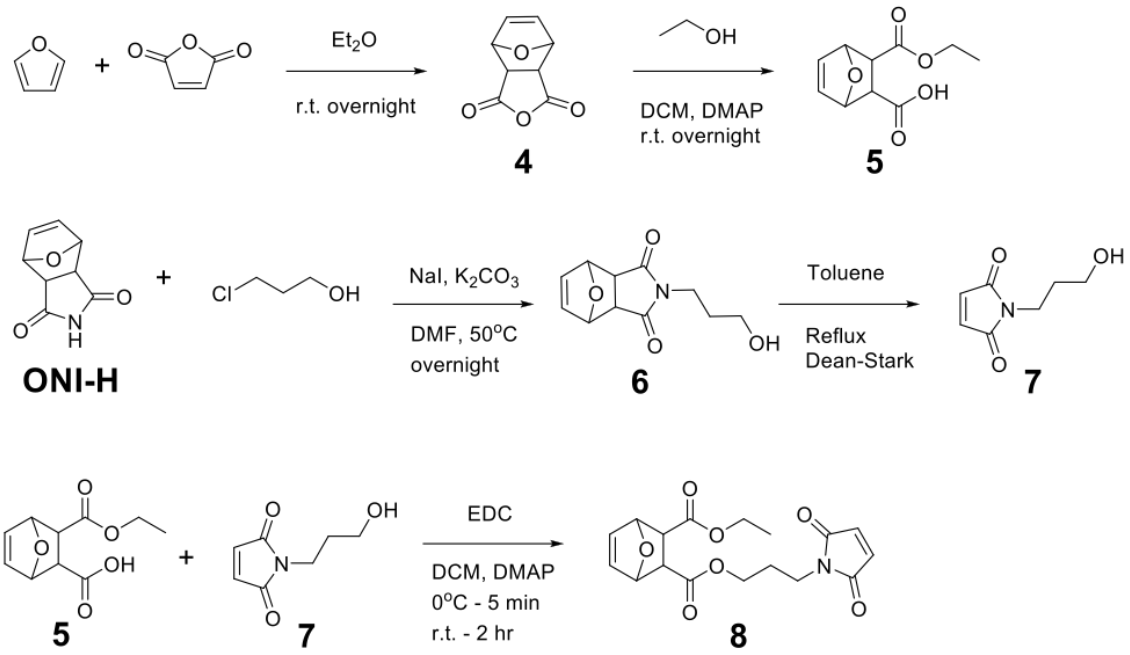

Figure 2. 13. Synthetic scheme of Maleimide Monomer

2.4.8.1 Synthesis of 4

To a 250 mL round bottom flask equipped with a stir-bar, was added furan (18.5 mL, 255.0 mmol, 5.0 eq) and 100 mL of diethyl ether. Maleic anhydride (5.0 g, 51.0 mmol, 1.0 eq) was added to the flask and the reaction was stirred at room temperature overnight. Afterwards, the formed precipitate in the reaction flask was filtered and washed with copious amounts of diethyl ether to afford **4** (white solid, yield = 88%). (^{1}H NMR, DMSO-D_6, 400 MHz) 6.55 (s, 2H), 5.31 (s, 2H), 3.3 (s, 2H).

2.4.8.2 Synthesis of 5

To a 250 mL round bottom flask equipped with a stir-bar, was added **4** (7.5 g, 45.22 mmol, 1.0 eq), 4-dimethylaminopyridine (0.55 g, 4.52 mmol, 0.1 eq), and 100 mL of dichloromethane. Anhydrous ethanol (3.17 mL, 54.26 mmol, 1.2 eq) was added and

the reaction was stirred at room temperature overnight. Afterwards the solvent was evaporated, and the product was purified with column chromatography to yield **5** (White solid, yield = 82%). (^{1}H NMR, $CDCl_3$, 400 MHz) 10.2 (br, 1H), 6.45 (q, 2H), 5.28 (s, 1H), 5.21 (s, 1H), 4.15 (q, 2H), 2.81 (q, 2H), 1.21 (t, 3H).

2.4.8.3 Synthesis of 6

To a 250 mL round bottom flask equipped with a stir-bar, was added **ONI-H** (7.0 g, 42.40 mmol, 1.0 eq) and 50 mL of N,N-dimethylformamide. Then, potassium carbonate (23.40 g, 169.55 mmol, 4.0 eq) was added and the reaction flask was stirred at 50°C for 5 minutes. Afterwards, sodium iodide (1.27 g, 8.48 mmol, 0.2 eq) was added followed by 3-chloropropanol (3.72 mL, 44.51 mmol, 1.05 eq) and the reaction flask was stirred overnight at 50°C. Afterwards, the reaction flask was cooled to room temperature and water was added. The reaction mixture was transferred to a separatory funnel and extracted with ethyl acetate three times. The organic layers were combined and washed with saturated sodium bicarbonate, 1M HCl, and brine. The organic layer was dried with sodium sulfate, filtered and rotovaped to yield a solid residue that was purified using column chromatography to afford **6** (White solid, yield = 86%). (^{1}H NMR, $CDCl_3$, 400 MHz) 6.49 (s, 2H), 5.21 (s, 2H), 3.58 (t, 2H), 3.49 (q, 2H), 2.81 (s, 2H), 2.65 (br, 1H), 1.73 (m, 2H).

2.4.8.4 Synthesis of 7

To a 250 mL round bottom flask equipped with a stir-bar, was added **6** (7.0 g, 31.36 mmol, 1.0 eq) and 150 mL of toluene. A dean-stark trap was added to the reaction flask and the reaction was stirred under reflux overnight. Afterwards, the solvent was

rotovaped and purified using column chromatography to afford **7** (White solid, yield = 88%). (^{1}H NMR, $CDCl_3$, 400 MHz) 6.65 (s, 2H), 3.6 (t, 2H), 3.51 (t, 2H), 2.65 (br, 1H), 1.73 (m, 2H).

2.4.8.5 Synthesis of 8

To a 250 mL round bottom flask equipped with a stir-bar, was added **7** (1.6 g, 10.31 mmol, 1.0 eq), **5** (2.20 g, 10.31 mmol, 1.0 eq), 4-dimethylaminopyridine (0.13 g, 1.03 mmol, 0.1 eq), and 100 mL of dichloromethane. The reaction flask was cooled to 0°C and 1-Ethyl-3-(3-dimethylaminopropyl)carbodiimide (2.17 g, 11.34 mmol, 1.1 eq) was added and stirred at 0°C for 10 minutes, followed by at room temperature for 2 hours. **Note: It is critical to only allow the reaction to proceed for 2 hours and not overnight. Leaving the reaction overnight will result in complete degradation of the product** Afterwards, the solvent was rotovaped and the residue was purified using column chromatography to afford **8** (light yellow oil, yield = 75%). (^{1}H NMR, $CDCl_3$, 400 MHz) 6.69 (s, 2H), 6.45 (s, 2H), 5.29 (s, 1H), 5.23 (s, 1H), 4.13 (t, 2h), 4.1 (m, 2H), 3.61 (t, 2H), 2.8 (s, 2H), 1.92 (m, 2H), 1.25 (t, 3H).

2.4.9 Synthesis of PONI-GMT (12)

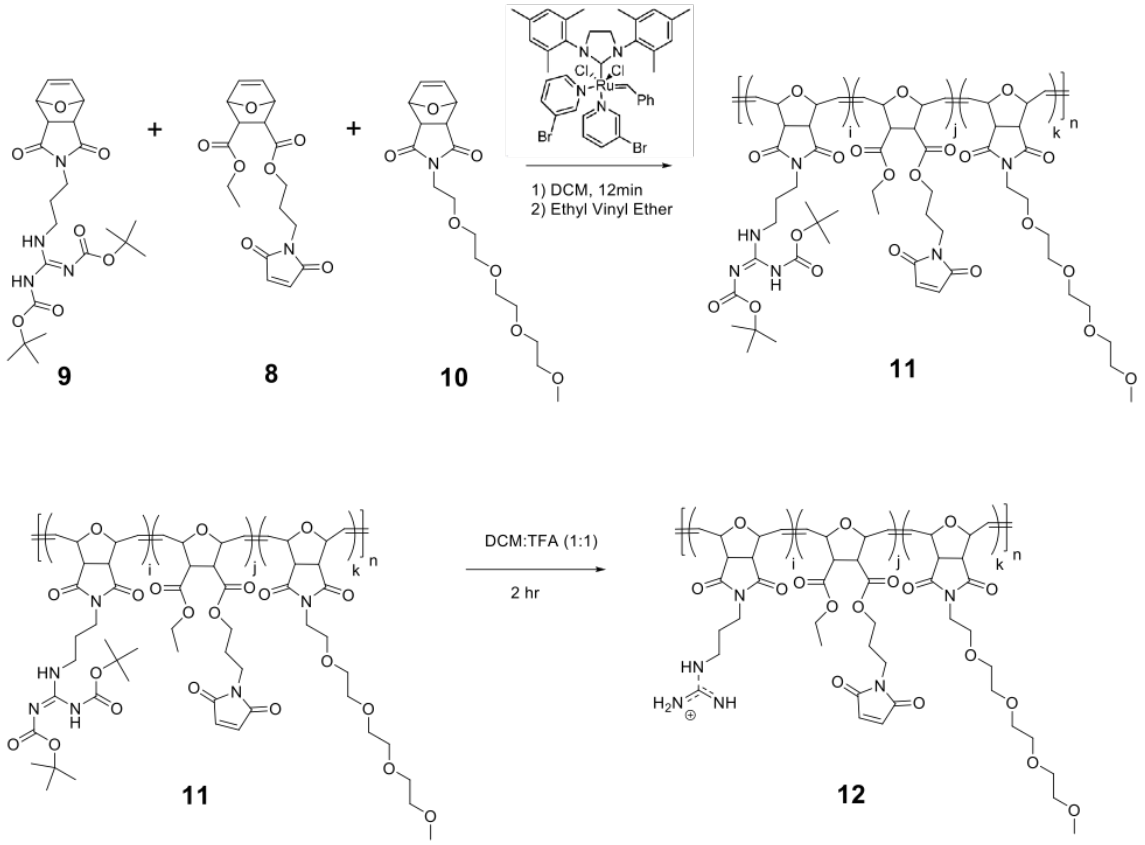

Figure 2. 14. Synthetic Scheme of PONI-GMT

2.4.9.1 Synthesis of 11

To a 10 mL pear-shaped air-free flask equipped with a stir-bar was added **9** (0.27 g, 0.57 mmol, 0.4 eq), **10** (0.25 g, 0.72 mmol, 0.5 eq), **8** (0.05 g, 0.14 mmol, 0.1 eq), and 4 mL of dichloromethane. In a separate 10 mL pear-shaped air-free flask was added Grubbs 3rd generation catalyst (0.015 g, 0.017 mmol, 0.012 eq) and 1mL of dichloromethane. Both flasks were sealed with septa and attached to a schlenk nitrogen/vacuum line. Both flasks were freeze-pump-thawed three times. After thawing, Grubbs 3rd generation catalyst solution was measured and dispensed via syringe to the flask containing the monomers and allowed to react for 12 minutes. After the allotted

time, ethyl vinyl ether (200 µL) was added and allowed to stir for 15 minutes. The reaction mixture was then diluted to two times the volume and precipitated into a heavily stirred solution of ether: hexane (150 mL, 1: 1 volume ratio) to yield Polymer **11**. MW = 46,157, PDI = 1.45, as determined by THF GPC using a polystyrene calibration curve). ^{1}H NMR (500MHz, $CDCl_3$) 11.49 (s, 2H), 8.45 (br, 2H), 6.71 (br, 0.8H), 6.09 (br, 4H), 5.8 (br, 6H), 5.05 (br, 6H), 4.5 (br, 4H), 3.65 (br, 52H), 3.45 (br, 2H), 3.35 (s, 7H), 3.33 (br, 2H), 1.89 (br, 4H), 1.8 (br, 4H), 1.49 (s, 20H), 1.2 (br, 2H).

2.4.9.2 Synthesis of PONI-GMT (12)

To a 50 mL round bottom flask equipped with a stir-bar was added Polymer **11** (400 mg). Dichloromethane was purged with nitrogen for five minutes and 12 mL was added to the flask, sealed with a septum and purged with nitrogen for five minutes. The main nitrogen line was left in the septum and the nitrogen pressure was reduced to a steady stream. 12 mL of trifluoroacetic acid (excess) was added and the reaction was stirred for two hours. Afterwards, excess TFA was removed by rotovaping with dichloromethane, three times. The reaction residue was dissolved in a minimal amount of water, filtered through a polyethersulfone (PES) syringe filter and lyophilized to yield polymer **12** as a white solid which readily dissolves in water. MW ~ 33,157, as determined using GPC. ^{1}H NMR (400MHz, D_2O) 6.7 (br, 0.4H), 5.94 (br, 4H), 5.74 (br, 4H), 4.82 (br, 4H), 4.45 (br, 4H), 3.5 (br, 40H), 3.2 (s, 6H), 3.02 (br, 4H), 1.7 (br, 4H), 1.05 (br, 2H).

2.4.10 Synthesis of TAMRA-PONI-GMT

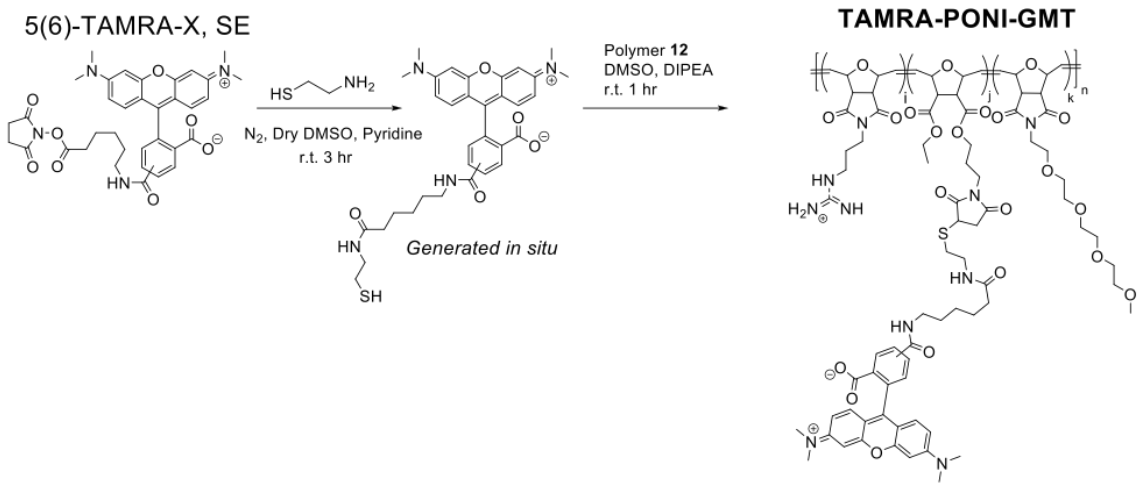

Figure 2. 15. Synthetic Scheme of TAMRA-PONI-GMT

To a 7 mL scintillation vial equipped with a stir-bar, was added 5(6)-TAMRA-X, SE (0.001 g, 0.0016 mmol, 1.0 eq), pyridine (0.14 mL, 0.0017 mmol, 1.1 eq), and 1 mL of anhydrous DMSO (previously purged with nitrogen). A blanket of nitrogen was introduced to the vial, cysteamine (0.00012 g, 0.0016 mmol, 1.0 eq) was added, the vial was sealed, covered with aluminum foil, and was stirred at room temperature for 3 hours. Meanwhile, in a 20 mL scintillation vial equipped with a stir-bar, was added Polymer **12** (0.08 g), N,N-diisopropylethylamine (0.1 mL), and 2 mL of anhydrous DMSO. After three hours, the terminal thiol-TAMRA that was generated *in situ* was added to the stirred vial containing Polymer **12**, covered with aluminum foil, sealed with a blanket of nitrogen, and stirred at room temperature overnight. Afterwards, the reaction vial was diluted with water and acidified using 1M HCl as to avoid a turbid solution. The reaction solution was completely homogenous at this time and was transferred to a 10,000 MWCO dialysis snake skin tubing. The dialysis tube was stirred in a 5 L bucket for three days, changing the water every two hours the first day, and periodically for the remaining

two days. Afterwards, the reaction solution was filtered through a PES syringe filter and lyophilized to afford **TAMRA-PONI-GMT** (Red-crystalline solid). TLC analysis (Mobile phase = ethyl acetate) of **TAMRA-PONI-GMT** against the *in situ* generated terminal thiol indicated that TAMRA was successfully conjugated to **12** in addition to any free TAMRA dye being removed during dialysis.

2.5 References

1. Nathwani, D.; Raman, G.; Sulham, K.; Gavaghan, M.; Menon, V. Clinical and Economic Consequences of Hospital-Acquired Resistant and Multidrug-Resistant Pseudomonas Aeruginosa Infections: A Systematic Review and Meta-Analysis. *Antimicrob. Resist. Infect. Control* **2014**, *3*, 32–47.

2. Morales, E.; Cots, F.; Sala, M.; Comas, M.; Belvis, F.; Riu, M.; Salvadó, M.; Grau, S.; Horcajada, J. P.; Montero, M. M.; *et al.* Hospital Costs of Nosocomial Multi-Drug Resistant Pseudomonas Aeruginosa Acquisition. *BMC Health Serv. Res.* **2012**, *12*, 122–129.

3. Tam, V. H.; Rogers, C. A.; Chang, K.-T.; Weston, J. S.; Caeiro, J.-P.; Garey, K. W. Impact of Multidrug-Resistant Pseudomonas Aeruginosa Bacteremia on Patient Outcomes. *Antimicrob. Agents Chemother.* **2010**, *54*, 3717–3722.

4. Drenkard, E.; Ausubel, F. M. Pseudomonas Biofilm Formation and Antibiotic Resistance Are Linked to Phenotypic Variation. *Nature* **2002**, *416*, 740–743.

5. Schierle, C. F.; De la Garza, M.; Mustoe, T. A.; Galiano, R. D. Staphylococcal Biofilms Impair Wound Healing by Delaying Reepithelialization in a Murine Cutaneous Wound Model. *Wound Repair Regen*. **2009**, *17*, 354–359.

6. Sanchez, C. J.; Mende, K.; Beckius, M. L.; Akers, K. S.; Romano, D. R.; Wenke, J. C.; Murray, C. K. Biofilm Formation by Clinical Isolates and the Implications in Chronic Infections. *BMC Infect. Dis.* **2013**, *13*, 47–58.

7. Wu, H.; Moser, C.; Wang, H.-Z.; Hoiby, N.; Song, Z.-J. Strategies for Combating Bacterial Biofilm Infections. *J. Oral. Sci.* **2015**, *7*, 1–7.

8. Anderl, J. N.; Franklin, M. J.; Stewart, P. S. Role of Antibiotic Penetration Limitation in Klebsiella Pneumoniae Biofilm Resistance to Ampicillin and Ciprofloxacin. *Antimicrob. Agents Chemother.* **2000**, *44*, 1818–1824.

9. Tseng, B. S.; Zhang, W.; Harrison, J. J.; Quach, T. P.; Song, J. L.; Penterman, J.; Singh, P. K.; Chopp, D. L.; Packman, A. I.; Parsek, M. R. The Extracellular Matrix Protects Pseudomonas Aeruginosa Biofilms by Limiting the Penetration of Tobramycin. *Environ. Microbiol.* **2013**, *15*, 2865–2878.

10. Szomolay, B.; Klapper, I.; Dockery, J.; Stewart, P. S. Adaptive Responses to Antimicrobial Agents in Biofilms. *Environ. Microbiol*. **2005**, *7*, 1186–1191.

11. Walters, M. C.; Roe, F.; Bugnicourt, A.; Franklin, M. J.; Stewart, P. S. Contributions of Antibiotic Penetration, Oxygen Limitation, and Low Metabolic Activity to Tolerance of Pseudomonas Aeruginosa Biofilms to Ciprofloxacin and Tobramycin. *Antimicrob. Agents Chemother.* **2003**, *47*, 317–323.

12. Olsen, I. Biofilm-Specific Antibiotic Tolerance and Resistance. *Eur. J. Clin. Microbiol. Infect. Dis.* **2015**, *34*, 877–886.

13. Stewart, P. S.; William Costerton, J. Antibiotic Resistance of Bacteria in Biofilms. *Lancet* **2001**, *358*, 135–138.

14. del Pozo, J. L.; Patel, R. The Challenge of Treating Biofilm-Associated Bacterial Infections. *Clin. Pharmacol. Ther.* **2007**, *82*, 204–209.

15. Cowan, M. M. Plant Products as Antimicrobial Agents. *Clin. Microbiol. Rev.* **1999**, *12*, 564–582.

16. Djeussi, D. E.; Noumedem, J. A. K.; Seukep, J. A.; Fankam, A. G.; Voukeng, I. K.; Tankeo, S. B.; Nkuete, A. H. L.; Kuete, V. Antibacterial Activities of Selected Edible Plants Extracts against Multidrug-Resistant Gram-Negative Bacteria. *BMC Complement. Altern. Med.* **2013**, *13*, 164–171.

17. Monte, J.; Abreu, C. A.; Borges, A.; Simões, C. L.; Simões, M. Antimicrobial Activity of Selected Phytochemicals against Escherichia Coli and Staphylococcus Aureus and Their Biofilms. *Pathogens* **2014**, *3*, 473–498.

18. Ahmad, I.; Beg, A. Z. Antimicrobial and Phytochemical Studies on 45 Indian Medicinal Plants against Multi-Drug Resistant Human Pathogens. *J. Ethnopharmacol.* **2001**, *74*, 113–123.

19. Simões, M.; Bennett, R. N.; Rosa, E. A. S. Understanding Antimicrobial Activities of Phytochemicals against Multidrug Resistant Bacteria and Biofilms. *Nat. Prod. Rep.* **2009**, *26*, 746–757.

20. O'Connell, K. M. G.; Hodgkinson, J. T.; Sore, H. F.; Welch, M.; Salmond, G. P. C.; Spring, D. R. Combating Multidrug-Resistant Bacteria: Current Strategies for the Discovery of Novel Antibacterials. *Angew. Chemie Int. Ed.* **2013**, *52*, 10706–10733.

21. Madsen, J. S.; Burmølle, M.; Hansen, L. H.; Sørensen, S. J. The Interconnection between Biofilm Formation and Horizontal Gene Transfer. *FEMS Immunol. Med. Microbiol.* **2012**, *65*, 183–195.

22. Maia, M. F.; Moore, S. J. Plant-Based Insect Repellents: A Review of Their Efficacy, Development and Testing. *Malar. J.* **2011**, *10*, S11.

23. Freire Rocha Caldas, G.; Araújo, A. V.; Albuquerque, G. S.; Silva-Neto, J. D. C.; Costa-Silva, J. H.; De Menezes, I. R. A.; Leite, A. C. L.; Da Costa, J. G. M.; Wanderley, A. G.; Caldas, G. F. R.; *et al.* Repeated-Doses Toxicity Study of the Essential Oil of Hyptis Martiusii Benth. (Lamiaceae) in Swiss Mice. *Evidence-Based Complement. Altern. Med.* **2013**, *2013*, No. 856168.

24. Nazzaro, F.; Fratianni, F.; De Martino, L.; Coppola, R.; De Feo, V. Effect of Essential Oils on Pathogenic Bacteria. *Pharmaceuticals* **2013**, *6*, 1451–1474.

25. Chen, H.; Davidson, P. M.; Zhong, Q. Impacts of Sample Preparation Methods on Solubility and Antilisterial Characteristics of Essential Oil Components in Milk. *Appl. Environ. Microbiol.* **2013**, *80*, 907–916.

26. Chang, Y.; McLandsborough, L.; McClements, D. J. Physicochemical Properties and Antimicrobial Efficacy of Carvacrol Nanoemulsions Formed by Spontaneous Emulsification. *J. Agric. Food Chem.* **2013**, *61*, 8906–8913.

27. Anwer, M. K.; Jamil, S.; Ibnouf, E. O.; Shakeel, F. Enhanced Antibacterial Effects of Clove Essential Oil by Nanoemulsion. *J. Oleo Sci.* **2014**, *63*, 347–354.

28. Duncan, B.; Li, X.; Landis, R. F.; Kim, S. T.; Gupta, A.; Wang, L. S.; Ramanathan, R.; Tang, R.; Boerth, J. A.; Rotello, V. M. Nanoparticle-Stabilized Capsules for the Treatment of Bacterial Biofilms. *ACS Nano* **2015**, *9*, 7775–7782.

29. Donsì, F.; Annunziata, M.; Vincensi, M.; Ferrari, G. Design of Nanoemulsion-Based Delivery Systems of Natural Antimicrobials: Effect of the Emulsifier. *J. Biotechnol.* **2012**, *159*, 342–350.

30. Landis, R. F.; Gupta, A.; Lee, Y.-W.; Wang, L.-S.; Golba, B.; Couillaud, B.; Ridolfo, R.; Das, R.; Rotello, V. M. Cross-Linked Polymer-Stabilized Nanocomposites for the Treatment of Bacterial Biofilms. *ACS Nano* **2017**, *11*, 946–952.

31. Chandra Sekhara Rao, G.; Satish Kumar, M.; Mathivanan, N.; Bhanoji Rao, M. E. Nanosuspensions as the Most Promising Approach in Nanoparticulate Drug Delivery Systems. *Pharmazie* **2004**, *59*, 5–9.

32. Kamaly, N.; Yameen, B.; Wu, J.; Farokhzad, O. C. Degradable Controlled-Release Polymers and Polymeric Nanoparticles: Mechanisms of Controlling Drug Release. *Chem. Rev.* **2016**, *116*, 2602–2663.

33. Simone, E. A.; Dziubla, T. D.; Muzykantov, V. R. Polymeric Carriers: Role of Geometry in Drug Delivery. *Expert Opin. Drug Deliv.* **2008**, *5*, 1283–1300.

34. Cheng, R.; Feng, F.; Meng, F.; Deng, C.; Feijen, J.; Zhong, Z. Glutathione-Responsive Nano-Vehicles as a Promising Platform for Targeted Intracellular Drug and Gene Delivery. *J. Control. Release* **2011**, *152*, 2–12.

35. Sanson, C.; Schatz, C.; Le Meins, J.-F.; Brûlet, A.; Soum, A.; Lecommandoux, S. Biocompatible and Biodegradable Poly(Trimethylene Carbonate)-b-Poly(l-Glutamic Acid) Polymersomes: Size Control and Stability. *Langmuir* **2010**, *26*, 2751–2760.

36. Yang, J.; Liu, F.; Yang, L.; Li, S. Hydrolytic and Enzymatic Degradation of Poly(Trimethylene Carbonate-Co-d,l-Lactide) Random Copolymers with Shape Memory Behavior. *Eur. Polym. J.* **2010**, *46*, 783–791.

37. Pounder, R. J.; Stanford, M. J.; Brooks, P.; Richards, S. P.; Dove, A. P. Metal Free Thiol-Maleimide “Click” Reaction as a Mild Functionalisation Strategy for Degradable Polymers. *Chem. Commun.* **2008**, 5158–5160.

38. Sukegawa, T.; Masuko, I.; Oyaizu, K.; Nishide, H. Expanding the Dimensionality of Polymers Populated with Organic Robust Radicals toward Flow Cell Application:

Synthesis of TEMPO-Crowded Bottlebrush Polymers Using Anionic Polymerization and ROMP. *Macromolecules* **2014**, *47*, 8611–8617.

39. Levic, J.; Cabarkapa, I.; Todorovic, G.; Pavkoc, S.; Sredanovic, S.; Coghill-Galonja, T.; Kostadinovic, L. In Vitro Antibacterial Activity of Essential Oils from Plant Family Lamiaceae. *Rom. Biotechnol. Lett.* **2011**, *16*, 6034–6041.

40. Kataoka, K.; Harada, A.; Nagasaki, Y. Block Copolymer Micelles for Drug Delivery: Design, Characterization and Biological Significance. *Adv. Drug Deliv. Rev.* **2001**, *47*, 113–131.

41. Gèze, A.; Putaux, J.-L.; Choisnard, L.; Jéhan, P.; Wouessidjewe, D. Long-Term Shelf Stability of Amphiphilicβ-Cyclodextrin Nanosphere Suspensions Monitored by Dynamic Light Scattering and Cryo-Transmission Electron Microscopy. *J. Microencapsul.* **2004**, *21*, 607–613.

42. Flemming, H.-C.; Wingender, J.; Szewzyk, U.; Steinberg, P.; Rice, S. A.; Kjelleberg, S. Biofilms: An Emergent Form of Bacterial Life. *Nat. Rev. Microbiol.* **2016**, *14*, 563–575.

43. Richards, M. J.; Edwards, J. R.; Culver, D. H.; Gaynes, R. P. Nosocomial Infections in Combined Medical-Surgical Intensive Care Units in the United States. *Infect. Control. Hosp. Epidemiol.* **2000**, *21*, 510–515.

44. Jarvis, W. R.; Martone, W. J. Predominant Pathogens in Hospital Infections. *J. Antimicrob. Chemother.* **1992**, *29*, 19–24.

45. Serra, R.; Grande, R.; Butrico, L.; Rossi, A.; Settimio, U. F.; Caroleo, B.; Amato, B.; Gallelli, L.; de Franciscis, S. Chronic Wound Infections: The Role of Pseudomonas Aeruginosa and Staphylococcus Aureus. *Expert Rev. Anti. Infect. Ther.* **2015**, *13*, 605–613.

46. Fazli, M.; Bjarnsholt, T.; Kirketerp-Møller, K.; Jørgensen, B.; Andersen, A. S.; Krogfelt, K. A.; Givskov, M.; Tolker-Nielsen, T. Nonrandom Distribution of Pseudomonas Aeruginosa and Staphylococcus Aureus in Chronic Wounds. *J. Clin. Microbiol.* **2009**, *47*, 4084–4089.

47. Sun, B. K.; Siprashvili, Z.; Khavari, P. A. Advances in Skin Grafting and Treatment of Cutaneous Wounds. *Science* **2014**, *346*, 941–945.

48. Ling, L. L.; Schneider, T.; Peoples, A. J.; Spoering, A. L.; Engels, I.; Conlon, B. P.; Mueller, A.; Schaberle, T. F.; Hughes, D. E.; Epstein, S.; *et al.* A New Antibiotic Kills Pathogens without Detectable Resistance. *Nature* **2015**, *517*, 455–459.

CHAPTER 3

3. PHYTOCHEMICAL-BASED NANOCOMPOSITES FOR THE TREATMENT OF BACTERIAL BIOFILMS

Reprinted (adapted) with permission from "Li, C.-H.*; Chen, X.*; Landis, R. F.; Geng, Y.; Makabenta, J. M.; Lemnios, W.; Gupta, A.; Rotello, V. M. Phytochemical-Based Nanocomposites for the Treatment of Bacterial Biofilms. *ACS Infect. Dis.* **2019**, *5*, 1590-1596." Copyright (2019) American Chemical Society

* indicates equal contribution

3.1 Introduction

Bacterial infection is a serious threat to public health with 2 million cases occurring each year in the US alone. Among these infections, at least 65% are associated with biofilm formation,[1] often occurring on medical implants, mucus, or tissues, leading to chronic wounds.[2-4] Biofilms are microcolonies of bacteria residing in an extracellular polymeric substances (EPS) matrix.[5] The EPS serves as a physical barrier, preventing the interaction between antimicrobial agents and bacterial cells. The charged polymeric components and embedded enzymes deactivate antibiotics and retard their penetration throughout the matrix. Moreover, dormant bacteria inside biofilms possess more antibiotic-tolerance and/or resistance than regular bacteria.[6-9] These mechanisms may act simultaneously, ending in failure of standard antibiotic treatments. Currently, chemical antibiofilm treatments include long-term use of high dosages of antibiotics, or combinations of antibiotics with different killing mechanisms.[10] However, these strategies are costly and still inefficient.[11]

Phytochemicals are plant-derived oils that have emerged as a promising alternative to current employed antimicrobial agents.[12,13] Phytochemicals are secondary metabolites and are key components in the self-defense mechanism of plants against

pathogenic microorganisms.[14] They can be effective against both planktonic and biofilm multidrug-resistant bacteria.[15,16] However, poor solubility of phytochemicals in aqueous media limits their medical applications. This limitation can be addressed using delivery vehicles such as surfactants, nanoparticles, or polymers.[17-19] While these strategies improve the solubility of the phytochemicals, the resulting engineered materials often have hemolytic activity and/or limited stability.

Recently, we reported a polymer-stabilized carvacrol-in-water nanocomposite (NCs) as a therapeutic against bacterial biofilm.[20] However, although carvacrol is generally recognized as safe (GRAS), it demonstrates cytotoxicity toward mammalian cells.[21] We hypothesized that the toxicity and hence therapeutic effects of NCs could be tuned by changing the encapsulated phytochemicals. Herein, we report the antimicrobial properties and cytotoxicity of NCs loaded with different active phytochemical ingredients. These NCs demonstrated improved antimicrobial activity against planktonic bacteria, with at least 4-fold decrease in minimum inhibitory concentrations (MICs). In addition, we found that NCs loaded with less hydrophobic phytochemicals demonstrated more potent antibiofilm efficacy. Finally, we evaluated the cytotoxicity of NCs toward 3T3 fibroblast cells to test their potential as a wound infection therapeutic agent. The results revealed that NCs encapsulating phytochemicals with lower log P and no phenolic hydroxyl groups provide a viable treatment strategy for wound biofilm infections.

3.2 Results and Discussion

3.2.1 Generation and Characterization of Nanocomposites

We recently reported that incorporating carvacrol into cross-linked poly(oxanorbornenimide) polymers (PONIs) improves emulsion stability and enhances antimicrobial properties. Briefly, PONI polymers were modified with guanidinium, maleimide, and tetraethyleneglycol monomethyl ether moieties (**PONI-GMT**). Tetraethyleneglycol monomethyl ether increased amphiphilicity of the polymers so that PONIs and hydrophobic carvacrol would self-assemble into NCs. The cationic guanidinium group was used to increase interaction with the negatively charged bacterial membranes and EPS.[22] Finally, maleimide moieties on PONIs were used to stabilize the nanocomposites. These moieties can form cross-linked structure via maleimide-Michael addition reactions with the biodegradable crosslinker, dithiol-disulfide (DTDS), in carvacrol (Figure 3. 1).[23]

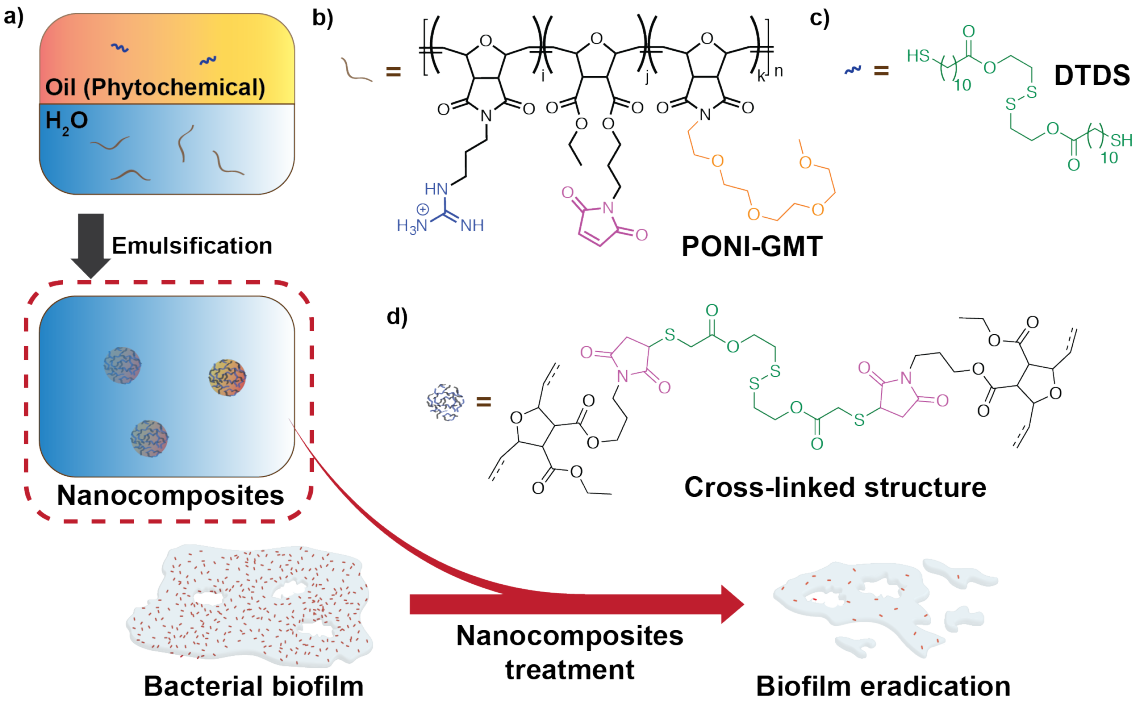

Figure 3. 1. a) Preparation of NCs loaded with different phytochemicals. DTDS, the biodegradable crosslinker, was dissolved in the selected phytochemical. This resulting oil solution was then emulsified into water in the presence of PONI-GMT to form cross-linked polymer-stabilized nanocomposites. This delivery strategy demonstrated improved antimicrobial activity against bacterial biofilms; b) Chemical structure of PONI-GMT; c) Chemical structure of DTDS; d) Cross-linked structure of NCs.

We postulated that other phytochemicals could be stabilized in aqueous media using the NC platform. We chose eugenol,[24] methyl eugenol,[25] carvacrol,[26] linalool,[27] (+)-limonene,[28] *p*-cymene,[29] and *α*-pinene[30] for this study as they are liquid phytochemicals at room temperature and reported to demonstrate antimicrobial activity. These oils were first mixed with DTDS. Subsequently, the oil solution was emulsified into Milli-Q water containing PONI-GMT. During emulsification, PONI-GMT and the oil self-assemble, forming the NCs. These emulsions were defined as 100 v/v% and found to have sizes ranging from ~180 to ~530 nm (Table 3. 1).

Table 3. 1. Chemical structures of the selected phytochemicals, their log P values, their particle sizes, and their polydispersity indexes (noted as PDI) after emulsification.

	Eugenol	Linalool	Methyl eugenol	Carvacrol	*p*-Cymene	(+)-Limonene	*α*-pinene
Structure	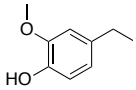	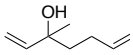	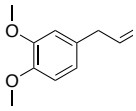	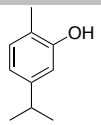	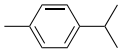	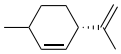	
log P	2.49	2.97	3.03	3.49	4.1	4.57	4.83
Size (nm)	270	290	370	180	180	530	220
PDI	0.13	0.01	0.02	0.25	0.28	0.13	0.12

3.2.2 Antimicrobial Activity of NCs against Gram-negative Planktonic Bacteria

We first evaluated the antimicrobial activity of these NCs against planktonic bacteria using clinical isolates of pathogenic Gram-negative bacterial strains including *Escherichia coli* (CD2), *Pseudomonas aeruginosa* (CD1006), and *Enterobacter cloacae*

complex (CD1412). All NCs demonstrated inhibition of bacterial growth with MICs ranging from 2 – 8 v/v% (Table 3. 2). In contrast, their bulk oil counterparts demonstrated less or no antibacterial activity, even though those solutions were prepared in 5 v/v% dimethyl sulfoxide (DMSO) aqueous solution. MICs of eugenol and carvacrol against all three Gram-negative bacteria were 4-fold or 8-fold higher than the nanocomposite counterpart, whereas limonene showed less antimicrobial activity towards all the strains we tested. None of the other oils showed inhibition of bacterial growth at the highest concentration used in this study (Table 3. 2). These results indicated that incorporating oils into cross-linked NCs improved their antimicrobial activity, even with oils lacking antimicrobial phenolic hydroxyl groups.[31] This improvement may be attributed to electrostatic interaction between positively charged NCs and negatively charged bacterial membranes.[32,33]

Table 3. 2. MICs (v/v%) against CD2, CD1006, and CD1412. These bacteria were treated with phytochemical dissolved in 5 v/v% DMSO aqueous solution or NCs. Colistin was used as control. MIC experiments were performed in M9 minimal medium.

Treatment	**Phytochemical**			**Nanocomposites (NCs)**		
	CD2	CD1006	CD1412	CD2	CD1006	CD1412
	E. coli	*P. aeruginosa*	*E. cloacae* complex	*E. coli*	*P. aeruginosa*	*E. cloacae* complex
Eugenol	16	16	16	4	4	4
Linalool	>32	>32	>32	2	8	8
Methyl eugenol	>32	>32	>32	4	2	4
Carvacrol	16	16	16	4	4	2
p-cymene	>32	>32	>32	4	4	4
(+)-limonene	32	32	>32	2	2	8
α-pinene	>32	>32	>32	2	4	4
Colistin	1 mg/L	1 mg/L	1 mg/L	--	--	--

3.2.3 Antimicrobial Activity of Nanocomposites against Gram-negative Bacterial Biofilms

Next, we investigated the antimicrobial activity of these NCs toward more refractory bacterial biofilms. As shown in Figure 3. 2, these nanocomposites eradicated 90% of bacteria in the biofilms at concentrations ranging from 2 to 43 v/v%. We found that using amphiphilic polymers to deliver phytochemicals containing phenyl hydroxyl groups, such as eugenol and carvacrol, provided especially promising bacteria-combating capability against biofilms. Furthermore, we observed a trend that phytochemicals with lower log P demonstrated more potent antimicrobial activity against biofilms. Specifically, NCs loaded with eugenol (log P: 2.49) were able to kill 90% of bacteria in the biofilms at about 12 v/v%. Linalool (log P: 2.97) NCs demonstrated similar antimicrobial activity using higher concentrations, 26 or 30 v/v%. NCs encapsulating phytochemicals with even higher log P, such as *p*-cymene (log P: 4.1) and *α*-pinene (log P: 4.83), were incapable of eradicating 90% of bacteria in CD2 and CD1006 biofilms, even with the highest concentration used in this study. Moreover, we performed crystal violet (CV) biofilm assays to evaluate NCs' capability to reduce biofilm biomass. CD2, CD1006, and CD1412 biofilms were treated with NCs at $MBEC_{90}$ (minimum biofilm eradication concentration for eradication of 90% of bacteria in the biofilm) or 48 v/v%. In general, NCs loaded with low log P oils were capable of removing biofilm biomass up to 70% (Figure 3. 3). In contrast, incorporating high log P oils into NCs were less effective in biofilm dispersal. In some cases, such as *α*-pinene NCs against CD1006 and CD2, these NCs even promoted the production of biomass. Similar hormetic-like responses were also observed in the treatments with 10 × MIC of colistin against CD1006 and CD2 biofilms.

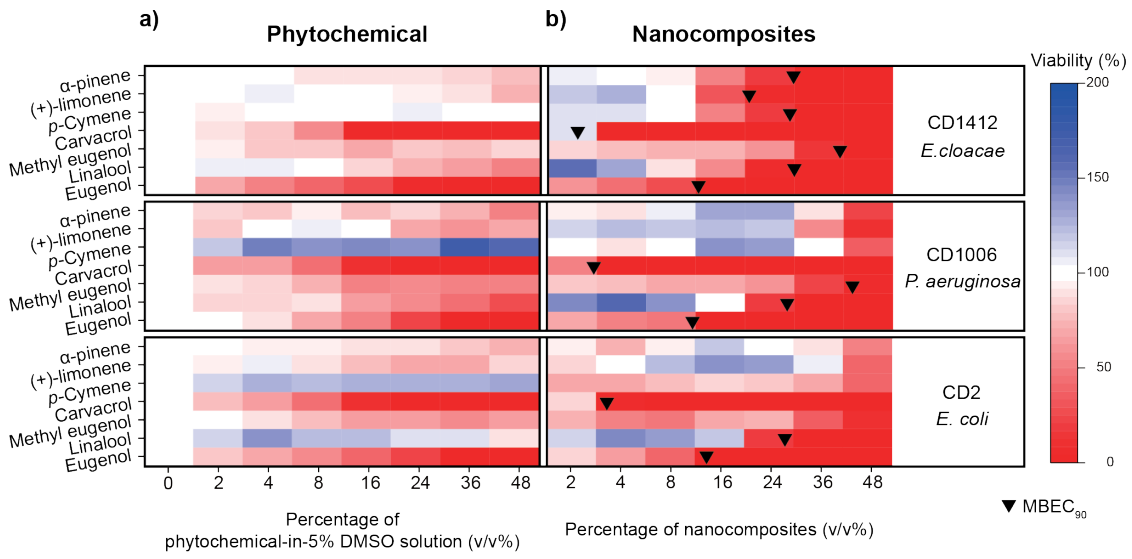

Figure 3. 2. Viabilities of CD2, CD1006, and CD1412 biofilms after a three-hour treatment with a) phytochemicals in 5 v/v% DMSO aqueous solution or b) NCs. This figure was illustrated using a 3-color limited mixing setting (blue: 0%, white: 100%, and red: 200%). Data points were averaged viability (n = 3) determined using alamarBlue assay. Black bullets indicated $MBEC_{90}$ if applicable.

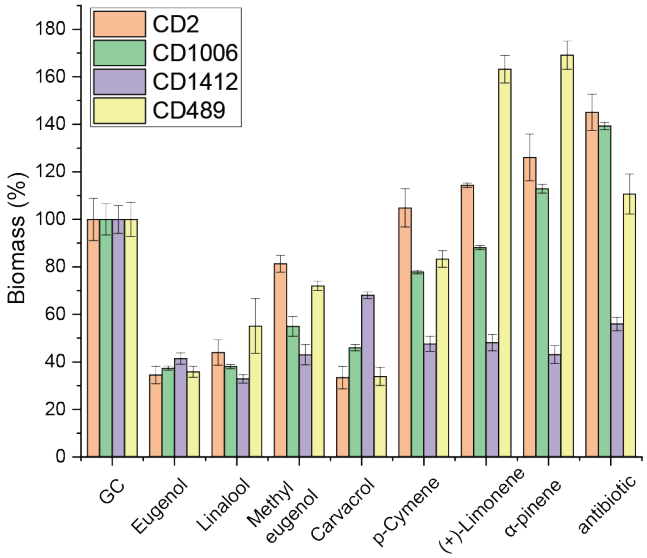

Figure 3. 3. Biomass of *E. coli* (CD2), *P. aeruginosa* (CD1006), *E. cloacae* complex (CD1412), and methicillin-resistant *S. aureus* (MRSA, CD489) biofilms after a 3 h treatment with NCs. The concentrations were either the corresponding $MBEC_{90}$ of the NCs (if applicable) or 48 v/v%. Furthermore, biofilms were treated with antibiotics as controls. Specifically, Gram-negative bacterial biofilms were treated with 10 × MIC of colistin while Gram-positive biofilms were treated with 10 × MIC of vancomycin. Data were presented as mean ± standard deviation and represented three independent experiments.

We also prepared phytochemical solutions in 5 v/v% DMSO solutions to compare antibiofilm efficacy of bulk oils with the NCs. As shown in Figure 3. 2, these oils demonstrated weak to moderate antimicrobial activity even at high concentrations. The results indicated that NC delivery also improved phytochemical antimicrobial activity for recalcitrant biofilms. Notably, this delivery strategy is potentially useful in targeting *E. cloacae* complex populations in multi-species biofilm as *P. aeruginosa and E. coli* biofilms were less susceptible to NCs loaded with high log P phytochemicals.[34]

3.2.4 Antimicrobial Activity of Nanocomposites against Gram-positive Planktonic Bacteria and Their Biofilms

Besides *P. aeruginosa, Staphylococcus aureus* is also one of the most common bacteria isolated from chronic wounds.[35-37] Therefore, we also evaluated the growth inhibition ability of NCs to planktonic clinical isolated methicillin-resistant *S. aureus* (CD489, MRSA). As before, MICs of NCs were lower than free phytochemicals (Table 3. 3). In addition, we found that more hydrophobic oils were less effective against CD489 even delivered using PONI-GMT.

Table 3. 3. MICs (v/v%) against CD489. Bacteria were treated with phytochemical dissolved in 5 v/v% DMSO aqueous solution or NCs. Vancomycin was used as control. MIC experiments were performed using 15:85 TSB/M9 medium.

Treatment	**Phytochemical**	**Nanocomposites**
	CD489 (*S. aureus*, MRSA)	
Eugenol	16	4
Linalool	>32	16
Methyl eugenol	16	8
Carvacrol	32	4
p-cymene	>32	>32
(+)-limonene	>32	>32
α-pinene	>32	32
Vancomycin	0.5 mg/L	--

Subsequently, we selected eugenol, linalool, methyl eugenol, and carvacrol NCs, which showed the highest antimicrobial activity, to test against *S. aureus* biofilms. As shown in Figure 3. 4, after a three-hour treatment, eugenol, linalool, and carvacrol NCs eliminated 90% of bacteria at 9.27, 37.9 and 3.55 v/v%, respectively. However, CD489 biofilm was not susceptible to methyl eugenol NCs. We also performed a CV staining assay against CD489. These NCs demonstrated biofilm-dispersal ability while vancomycin promoted building biomass of the biofilm (Figure 3. 3). These experiments demonstrated that eugenol, linalool, and carvacrol NCs have broad-spectrum biofilm combating ability.

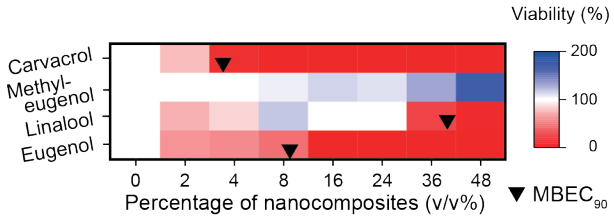

Figure 3. 4. Viabilities of CD489 biofilms after a three-hour treatment with NCs. This figure was illustrated using a 3-color limited mixing setting (blue: 0%, white: 100%, and red: 200%). Data points were averaged viability (n = 3) determined using alamarBlue assay. Black bullets indicated $MBEC_{90}$ if applicable.

3.2.5 Cytotoxicity of NCs to 3T3 Fibroblast Cells

Next, we evaluated the cytotoxicity of NCs towards fibroblast cells[38] for assessing the potential utility of NCs for cutaneous wound biofilms. In this study, 3T3 fibroblast cell monolayers were treated with NCs for 3 hours. Subsequently, cell viability was determined using Pierce LDH cytotoxicity assay. As shown in Figure 3. 5, higher log P phytochemicals such as carvacrol, limonene, *p*-cymene, and *α*-pinene were more cytotoxic to 3T3 fibroblast cells. Cell viabilities were less than 50% at 8-16 v/v% after the treatment. In contrast, methyl eugenol and linalool were less cytotoxic, as their

concentrations to inhibit 50% fibroblast cell proliferations (GI_{50}) were not detected in this study and 27.14 v/v%, respectively.

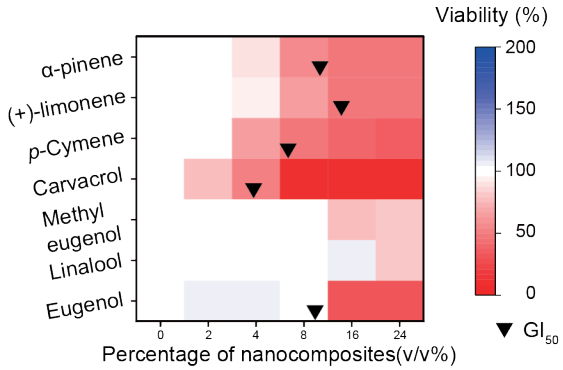

Figure 3. 5. Viabilities of 3T3 fibroblast cells after a three-hour treatment with NCs. This figure was illustrated using a 3-color limited mixing setting (blue: 0%, white: 100%, and red: 200%). Data points were averaged viability (n =3) determined using LDH assay. Black bullets indicated GI_{50} if applicable.

While eugenol had the lowest log P phytochemical in this study, it demonstrated strong cytotoxicity at higher concentrations (> 8 v/v%). This cytotoxicity was possibly due to the phenolic hydroxyl group in its structure.[39] Other proposed mechanisms such as inhibition of Na^+-K^+-ATPase and mitochondrial damage were also reported.[40-42] Similarly, the presence of phenolic hydroxyl group in carvacrol could contribute to its cytotoxicity. The combination of this functional group and carvacrol's higher log P could lead to the highest cytotoxicity toward 3T3 fibroblast cells among the phytochemicals in this study. Consequently, using lower log P phytochemicals without a phenolic hydroxyl group potentially eliminated safety concerns of this therapeutic method.

3.3 Conclusion

In summary, we evaluated the antimicrobial activities and cytotoxicity of phytochemicals delivered using a cross-linked polymeric scaffold. In general, this

delivery strategy dramatically improves their antimicrobial efficacy against both planktonic bacteria and biofilms. Specifically, phytochemicals with lower log P value are promising candidates for this delivery system. Moreover, encapsulating phytochemicals with lower log P and no phenolic hydroxyl groups provides particularly low cytotoxicity nanocomposites. Taken together, loading phytochemicals with the above-mentioned properties, such as linalool and methyl eugenol, into nanocomposites offers a promising direction to address wound biofilm infections.

3.4 Experimental Section

3.4.1 Materials and Reagents

All reagents/materials were purchased from Fisher Scientific as well as Sigma-Aldrich and used as received. Clinical isolated bacterial strains were obtained from the Cooley Dickson Hospital Microbiology Laboratory (Northampton, MA). NIH-3T3 cells (ATCC CRL-1658) were purchased from American Type Culture Collection (ATCC). Dulbecco's Modified Eagle's Medium (DMEM, ATCC 30-2002) and fetal bovine serum (Fisher Scientific, SH3007103) were used in cell culture.

3.4.2 Preparation of NCs

Stock nanocomposite solutions were prepared in 600 μL Eppendorf tubes. To prepare the NCs emulsions, 3 μL of the selected phytochemical (containing 3 wt% DTDS) was added to 497 μL of Milli-Q H_2O containing 6.04 μM of PONI-GMT and emulsified using an amalgamator for 50 s. The emulsions were allowed to rest overnight prior to use.

3.4.3 Determination of Minimum Inhibitory Concentration

Bacteria were cultured in Lysogeny broth at 37°C and 275 rpm until stationary phase. The cultures were then collected by centrifugation (7000 rpm, 5 min) and washed with 0.85% sodium chloride solution for three times. The bacteria culture was then resuspended in phosphate-buffered saline (PBS) to determine its OD_{600}. OD_{600} of the solution was then diluted to 0.001 using M9 minimal media, giving a final bacterial concentration of 1 x 10^6 CFU/mL. Afterwards, 50 µL of these solutions was added into a 96-well plate and mixed with 50 µL of NCs solutions. NCs solutions were serially diluted to give a concentration range of 0 – 32 v/v%. A growth control group was prepared containing only M9 and the bacterial solution. In addition, a sterile control group with only the growth medium was carried out at the same time. Cultures were performed in triplicates, and at least two independent experiments were repeated on different days. The MIC is defined as the lowest concentration of NCs that inhibits visible growth as observed with the unaided eye.

3.4.4 Biofilm Formation

Bacteria culture was prepared using the method described above. To prepare biofilm seeding solutions, bacteria except *S. aureus* were resuspended in M9 medium to reach OD_{600} of 0.1. *S. aureus* were resuspended in M9 medium containing 15 v/v% TSB to reach OD_{600} of 0.1. 100 µL of the seeding solution was added to each well of the 96-well plate. The plate was covered and incubated under static conditions at room temperature overnight.

NCs solutions were prepared with various concentrations ranging from 0 to 48 v/v%. 100 µL of these solutions was added into a 96-well plate. Subsequently, the plate

was incubated at 37°C under static condition. After 3 hours, the biofilms were washed with PBS three times, then 10 v/v% of alamarBlue cell viability reagent was added to each well, then incubated for 1 hour. Biofilm viability was determined by measuring fluorescence intensity (excitation: 560 nm; emission: 590 nm). Readings from the wells containing 10 v/v% of alamarBlue cell viability reagent only were considered as the blank (I_{blank}), and readings from wells having untreated biofilms were used as growth control (I_{control}). Biofilm viability was calculated using the equation below:

$$\text{Biofilm viability (\%)} = 100\% \times \frac{I_{\text{sample}} - I_{\text{blank}}}{I_{\text{control}} - I_{\text{blank}}}$$

3.4.5 Crystal Violet Assay for Biofilm Quantification

We followed the crystal violet staining protocol with some modifications.[43] Briefly, biofilms were prepared using the method described above. NCs solutions were prepared at calculated $MBEC_{90}$ or 48 v/v%. 10 × MIC of antibiotic solutions were also prepared as controls. 100 µL of these solutions was added into a 96-well plate. Subsequently, the plate was incubated at 37°C under static conditions. After 3 hours, the biofilms were washed with PBS three times, then 150 µL of a 0.1% crystal violet aqueous solution was added to each well. Then, the plate was incubated at room temperature for 15 minutes. Afterwards, the biofilms were wash with PBS four times to remove excess crystal violet. The 96-well plate was then allowed to air dry.

To quantifying the biofilms, 150 µL of 20:80 acetone/ethanol solution was added to each well. The 96-well plate was incubated at room temperature for 20 minutes. Subsequently, 125 µL of the solubilized CV solutions in each well were transferred to a new flat bottom 96-well plate. OD_{590} of the solutions were then measured using a plate reader.

3.4.6 3T3 Fibroblast Cell Viability Assay

A total of 20000 NIH 3T3 (ATCC CRL-1658) cells were cultured in Dulbecco's modified Eagle medium (DMEM; ATCC 30-2002) with 10% bovine calf serum and 1% Penicillin-Streptomycin at 37°C in a humidified atmosphere of 5% CO_2 for 48 h. Then, DMEM media was removed and cells were washed once with PBS before addition of NCs prepared using pre-warmed media containing 10% bovine calf serum. Cells were incubated for 3 h at 37ºC under a humidified atmosphere of 5% CO_2. Cell viability was determined using Pierce LDH cytotoxicity assay according to the manufacturer's protocol.

3.5 References

1. Potera, C. Forging a Link Between Biofilms and Disease. *Science* **1999**, *283*, 1837 LP-1839.

2. Hall-stoodley, L.; Stoodley, P. Evolving Concepts in Biofilm Infections. *Cell Microbiol* **2009**, *11*, 1034–1043.

3. Wolcott, R. D.; Rhoads, D. D.; Dowd, S. E. Biofilms and Chronic Wound Inflammation. *J. Wound Care* **2008**, *17*, 333–341.

4 Moreau-Marquis, S.; Stanton, B. A.; O'Toole, G. A. Pseudomonas Aeruginosa Biofilm Formation in the Cystic Fibrosis Airway. *Pulm. Pharmacol. Ther.* **2008**, *21*, 595–599.

5. Flemming, H.; Wingender, J. The Biofilm Matrix. *Nat. Rev. Microbiol.* **2010**, *8*, 623–633.

6. Mah, T. C.; Toole, G. A. O. Mechanisms of Biofilm Resistance to Antimicrobial Agents. *Trends Microbiol* **2001**, *9*, 34–39.

7. del Pozo, J. L.; Patel, R. The Challenge of Treating Biofilm-Associated Bacterial Infections. *Clin. Pharmacol. Ther.* **2007**, *82*, 204–209.

8. Olsen, I. Biofilm-Specific Antibiotic Tolerance and Resistance. *Eur. J. Clin. Microbiol. Infect. Dis*. **2015**, *34*, 877–886.

9. Stewart, P. S.; William Costerton, J. Antibiotic Resistance of Bacteria in Biofilms. *Lancet* **2001**, *358*, 135–138.

10. Wu, H.; Moser, C.; Wang, H.-Z.; Hoiby, N.; Song, Z.-J. Strategies for Combating Bacterial Biofilm Infections. *J. Oral. Sci.* **2015**, *7*, 1–7.

11. Wolcott, R. D.; Rhoads, D. D.; Bennett, M. E.; Wolcott, B. M.; Gogokhia, L.; Costerton, J. W.; Dowd, S. E. Chronic Wounds and the Medical Biofilm Paradigm. *J. Wound Care* **2010**, *19*, 45–53.

12. Hammer, K. A.; Carson, C. F.; Riley, T. V. Antimicrobial Activity of Essential Oils and Other Plant Extracts. *J. Appl. Microbiol.* **1999**, *86*, 985–990.

13. Dorman, H. J. D.; Deans, S. G. Antimicrobial Agents from Plants: Antibacterial Activity of Plant Volatile Oils. *J. Appl. Microbiol.* **2000**, *88*, 308–316.

14. Das, K.; Tiwari, R. K. S.; Shrivastava, D. K. Techniques for Evaluation of Medicinal Plant Products as Antimicrobial Agent : Current Methods and Future Trends. *J. Med. Plants Res.* **2010**, *4*, 104–111.

15. Monte, J.; Abreu, C. A.; Borges, A.; Simões, C. L.; Simões, M. Antimicrobial Activity of Selected Phytochemicals against Escherichia Coli and Staphylococcus Aureus and Their Biofilms. *Pathogens* **2014**, *3*, 473–498.

16. Simões, M.; Bennett, R. N.; Rosa, E. A. S. Understanding Antimicrobial Activities of Phytochemicals against Multidrug Resistant Bacteria and Biofilms. *Nat. Prod. Rep.* **2009**, *26*, 746–757.

17. Chang, Y.; McLandsborough, L.; McClements, D. J. Physicochemical Properties and Antimicrobial Efficacy of Carvacrol Nanoemulsions Formed by Spontaneous Emulsification. *J. Agric. Food Chem.* **2013**, *61*, 8906–8913.

18. Gomes, C.; Moreira, R. G.; Castell-Perez, E. Poly (DL-Lactide-Co-Glycolide) (PLGA) Nanoparticles with Entrapped Trans-Cinnamaldehyde and Eugenol for Antimicrobial Delivery Applications. *J. Food Sci.* **2011**, *76*, 16–24.

19. Lin, L.; Cui, H.; Zhou, H.; Zhang, X.; Bortolini, C. Nanoliposomes Containing Eucalyptus Citriodora as Antibiotic with Specific Antimicrobial Activity. *Chem. Commun.* **2015**, *51*, 2653–2655.

20. Landis, R. F.; Li, C. H.; Gupta, A.; Lee, Y. W.; Yazdani, M.; Ngernyuang, N.; Altinbasak, I.; Mansoor, S.; Khichi, M. A. S.; Sanyal, A.; et al. Biodegradable Nanocomposite Antimicrobials for the Eradication of Multidrug-Resistant Bacterial Biofilms without Accumulated Resistance. *J. Am. Chem. Soc.* **2018**, *140*, 6176–6182.

21. Reichling, J.; Suschke, U. Essential Oils of Aromatic Plants with Antibacterial , Antifungal , Antiviral , and Cytotoxic Properties – an Overview. *Complement. Med. Res.* **2009**, 79–90.

22. Zhou, Z.; Zheng, A.; Zhong, J. Interactions of Biocidal Guanidine Hydrochloride Polymer Analogs with Model Membranes: A Comparative Biophysical Study. *Acta Biochim. Biophys. Sin. (Shanghai)*. **2011**, *43*, 729–737.

23. Pounder, R. J.; Stanford, M. J.; Brooks, P.; Richards, S. P.; Dove, A. P. Metal Free Thiol-Maleimide “Click” Reaction as a Mild Functionalisation Strategy for Degradable Polymers. *Chem. Commun.* **2008**, 5158–5160.

24. Ali, S. M.; Khan, A. A.; Ahmed, I.; Musaddiq, M.; Ahmed, K. S.; Polasa, H.; Rao, L. V.; Habibullah, C. M.; Sechi, L. A.; Ahmed, N. Antimicrobial Activities of Eugenol and Cinnamaldehyde against the Human Gastric Pathogen Helicobacter Pylori. *Ann. Clin. Microbiol. Antimicrob.* **2005**, *4*, 20–26.

25. Sybiya Vasantha Packiavathy, I. A.; Agilandeswari, P.; Musthafa, K. S.; Karutha Pandian, S.; Veera Ravi, A. Antibiofilm and Quorum Sensing Inhibitory Potential of Cuminum Cyminum and Its Secondary Metabolite Methyl Eugenol against Gram Negative Bacterial Pathogens. *Food Res. Int.* **2012**, *45*, 85–92.

26. Lambert, R. J. W.; Skandamis, P. N.; Coote, P. J.; Nychas, G.-J. E. E. A Study of the Minimum Inhibitory Concentration and Mode of Action of Oregano Essential Oil, Thymol and Carvacrol. *J. Appl. Microbiol.* **2001**, *91*, 453–462

27. Park, S.; Kyong, Y.; Oliveira, M.; Cho, E.; Jin, D.; Kook, J. Anaerobe Antimicrobial Effect of Linalool and a -Terpineol against Periodontopathic and Cariogenic Bacteria. *Anaerobe* **2012**, *18*, 369–372.

28. Aggarwal, K. K.; Khanuja, S. P. S.; Ahmad, A.; Santha Kumar, T. R.; Gupta, V. K.; Kumar, S.; Khanuja, Ł. S. P. S.; Ahmad, A.; Kumar, T. R. S.; Gupta, V. K. Antimicrobial Activity Profiles of the Two Enantiomers of Limonene and Carvone Isolated from the Oils of Mentha Spicata and Anethum Sowa. *Flavour Fragr. J.* **2002**, *17*, 59–63.

29. Castilho, P. C.; Savluchinske-Feio, S.; Weinhold, T. S.; Gouveia, S. C. Evaluation of the Antimicrobial and Antioxidant Activities of Essential Oils, Extracts and Their Main Components from Oregano from Madeira Island, Portugal. *Food Control* **2012**, *23*, 552–558.

30. Leite, A. M.; Lima, E. D. O.; Souza, E. L. De; De, M. Inhibitory Effect of β -Pinene , α -Pinene and Eugenol on the Growth of Potential Infectious Endocarditis Causing Gram-Positive Bacteria. *Rev. Bras. Cienc. Farm.* **2007**, *43*, 121–126.

31 Ultee, A.; Bennik, M. H. J.; Moezelaar, R. The Phenolic Hydroxyl Group of Carvacrol Is Essential for Action against the Food-Borne Pathogen Bacillus Cereus. *Appl. Environ. Microbiol.* **2002**, *68*, 1561–1568.

32 Liu, L.; Xu, K.; Wang, H.; Jeremy Tan, P. K.; Fan, W.; Venkatraman, S. S.; Li, L.; Yang, Y.-Y. Self-Assembled Cationic Peptide Nanoparticles as an Efficient Antimicrobial Agent. *Nat. Nanotechnol.* **2009**, *4*, 457–463.

33 Ramalingam, K.; Amaechi, B. T.; Ralph, R. H.; Lee, V. A. Antimicrobial Activity of Nanoemulsion on Cariogenic Planktonic and Biofilm Organisms. *Arch. Oral Biol*. **2012**, *57*, 15–22.

34. Eckert, R.; He, J.; Yarbrough, D. K.; Qi, F.; Anderson, M. H.; Shi, W. Targeted Killing of Streptococcus Mutans by a Pheromone-Guided “Smart” Antimicrobial Peptide. *Antimicrob. Agents Chemother.* **2006**, *50*, 3651–3657.

35. Giacometti, A.; Cirioni, O.; Schimizzi, A. M.; Del Prete, M. S.; Barchiesi, F.; D’Errico, M. M.; Petrelli, E.; Scalise, G. Epidemiology and Microbiology of Surgical Wound Infections. *J. Clin. Microbiol.* **2000**, *38*, 918–922.

36. Miller, L. S.; Cho, J. S. Immunity against Staphylococcus Aureus Cutaneous Infections. *Nat. Rev. Immunol.* **2011**, *11*, 505–518.

37. Serra, R.; Grande, R.; Butrico, L.; Rossi, A.; Settimio, U. F.; Caroleo, B.; Amato, B.; Gallelli, L.; de Franciscis, S. Chronic Wound Infections: The Role of Pseudomonas Aeruginosa and Staphylococcus Aureus. *Expert Rev. Anti. Infect. Ther.* **2015**, *13*, 605–613.

38. Singer, A. J.; Clark, R. A. F. Cutaneous Wound Healing. *N. Engl. J. Med.* **1999**, *341*, 738–746.

39. Borges, A.; Serra, S.; Abreu, A. C.; Saavedra, M. J.; Simões, M.; Borges, A.; Serra, S.; Abreu, A. C.; Saavedra, M. J. Evaluation of the Effects of Selected Phytochemicals on Quorum Sensing Inhibition and in Vitro Cytotoxicity. *Biofouling* **2014**, *30*, 183–195.

40. Kreydiyyeh, S. I.; Usta, J.; Copti, R. Effect of Cinnamon, Clove and Some of Their Constituents on the Na+-K+-ATPase Activity and Alanine Absorption in the Rat Jejunum. *Food Chem. Toxicol.* **2000**, *38*, 755–762.

41. Yoo, C.-B.; Han, K.-T.; Cho, K.-S.; Ha, J.; Park, H.-J.; Nam, J.-H.; Kil, U.-H.; Lee, K.-T. Eugenol Isolated from the Essential Oil of Eugenia Caryophyllata Induces a Reactive Oxygen Species-Mediated Apoptosis in HL-60 Human Promyelocytic Leukemia Cells. *Cancer Lett*. **2005**, *225*, 41–52.

42. Prashar, A.; Locke, I. C.; Evans, C. S. Cytotoxicity of Clove (Syzygium Aromaticum) Oil and Its Major Components to Human Skin Cells. *Cell Prolif.* **2006**, 39, 241–248.

43. O'Toole, G. A. Microtiter Dish Biofilm Formation Assay. *J. Vis. Exp.* **2011**, 2437-2438.

CHAPTER 4

4. NANOTHERAPEUTICS USING ALL-NATURAL MATERIALS. EFFECTIVE TREATMENT OF WOUND BIOFILM INFECTIONS USING CROSSLINKED NANOEMULSIONS

Material from: Li, C.-H.*; Landis, R.*; Makabenta, J. M.*; Nabawy, A.; Tronchet, T.; Archambault, D.; Liu, Y.; Huang, R.; Golan, M.; Cui, W.; *et al.* Nanotherapeutics Using All-Natural Materials. Effective Treatment of Wound Biofilm Infections Using Crosslinked Nanoemulsions. *Mater. Horiz.*, 2021, Advance Article , **DOI:** 10.1039/D0MH01826K with permission from the Royal Society of Chemistry

* indicates equal contribution

4.1 Introduction

Antibiotics are the current treatment of choice for bacterial infections.[1] Unfortunately, bacteria are rapidly acquiring resistance against these agents through different mechanisms they have developed over billions of years to remove and/or deactivate toxins or evade their activities.[2-4] The ability of pathogenic bacteria, including *Pseudomonas aeruginosa* and *Staphylococcus aureus*, to form biofilms results in particularly problematic infections in wounds and on implanted devices.[5,6] The extracellular polymeric substance (EPS) matrix of biofilms has evolved as a barrier to some antibiotics and host immune responses. The slow growth and presence of persister cells in biofilms further foster resistance against traditional antibiotics.[7] Biofilms also impede the wound healing process, resulting in chronic wounds associated with increased morbidity, mortality, and decreased quality of life.[8,9] The lack of effective antibiofilm agents has led to an annual multibillion-dollar (US) burden to healthcare systems worldwide.[10]

Plant-derived essential oils provide a potential resource to combat bacterial biofilm-associated infections.[11] Essential oils are produced by plants as protection against infections by bacteria.[12] These oils have been extensively used in traditional medicine as antioxidant, anti-inflammatory, and antibacterial agents, and their efficacy has been scientifically validated.[13,14] The additional benefits of using essential oils, including aroma,[15] safety,[16] and sustainability, have contributed to their increasing use in therapeutics. The low aqueous solubility of essential oils, however, limits their use in combating planktonic bacterial infections.[17] Moreover, these hydrophobic oils are not able to efficiently penetrate into the highly charged EPS of biofilms,[18] making them of limited use against biofilm-associated infections.

Synthetic nanoparticles and polymers provide a strategy for enhancing the activity of essential oil-based antimicrobials.[19,20] We set out to generate an all-natural platform that delivers active antimicrobials derived from essential oils for treatment of wound biofilms, with the potential for increased safety and community acceptance. In this platform, riboflavin (vitamin B_2) is used to cross-link[21, 22] gelatin that stabilizes nanodroplets of carvacrol, a key antimicrobial component of oregano oil. Our approach combines nature-derived ingredients to generate well-defined nanostructured-materials with size and stability required for potent antimicrobial and antibiofilm applications.[23,24] These nanoemulsions eradicated both Gram-positive and -negative bacterial biofilms *in vitro*. Significantly, the nanoemulsion system was highly active *in vivo*, reducing bacterial loads in the wound site and enhancing the rate of wound healing in a murine wound biofilm model. Taken together, the described nanoemulsions use only bio-derived

GRAS (generally regarded as safe) components to provide a safe, sustainable and effective treatment for wound biofilms.

4.2 Results and Discussion

The choice of oil for fabricating the nanoemulsions plays a critical role in therapeutic effects.[25] Oregano oil is among the most potent antimicrobial essential oils.[19,26] Carvacrol is the primary active component of oregano oil,[19] and was chosen to provide the GRAS benefits of oregano oil without the batch-to-batch variability observed with unpurified oils. Moreover, commercial gelatin was chosen as the scaffold for the oil-in-water nanoemulsion engineered to overcome the poor water solubility of carvacrol. Gelatin is naturally-derived, inherently biocompatible, biodegradable, non-cytotoxic, and has low antigenicity.[27] Structurally, gelatin is hydrophilic with hydrophobic domains, allowing it to encapsulate and stabilize hydrophobic oils, such as carvacrol, in aqueous conditions.[28] The gelatin matrix was stabilized through a cross-linking technique used for therapeutic corneal collagen cross-linking.[21] This strategy employs riboflavin (vitamin B_2) as a photo-initiator for cross-linking gelatin fibers. Nanoemulsions were fabricated by emulsifying a suspension of riboflavin in carvacrol into an aqueous suspension of gelatin (Figure 4. 1a), generating a transiently stable emulsion. This emulsion was then irradiated (365 nm) to activate the cross-linking process, resulting in stable nanoemulsions.

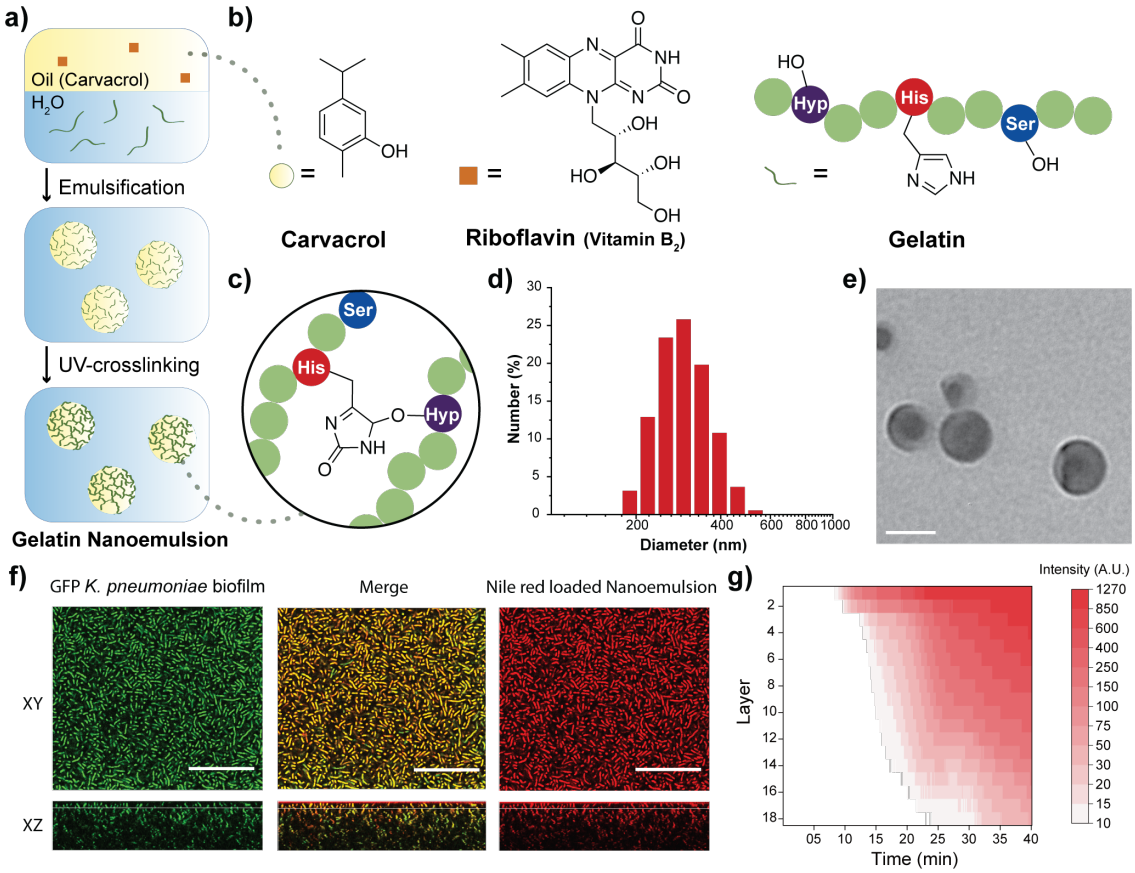

Figure 4. 1. Fabrication and characterization of gelatin nanoemulsions. a) Riboflavin (UV-cross-linking initiator) was dissolved in carvacrol. The oil mixture was then emulsified in an aqueous gelatin solution and cross-linked using long wavelength UV-A light (365 nm) to fabricate gelatin nanoemulsions. b) Chemical structures of carvacrol, riboflavin, and the functional groups of gelatin participating in the cross-linking reaction. c) Proposed cross-linked structure of gelatin nanoemulsions. d) Dynamic light scattering histogram of nanoemulsions in phosphate buffered saline (150 mM). e) Transmission electron microscopy images of nanoemulsions. Scale bar is 100 nm. f) Confocal laser scanning microscopy images of green fluorescent protein-expressing *Klebsiella pneumoniae* (IDRL-11999) biofilm after 40 minutes of treatment with Nile red-loaded nanoemulsions (XY top view, XZ side view). Scale bars are 50 µm and the thickness of this biofilm is ~37 µm. g) Spatial and time distribution of red fluorescence within the biofilm after the addition of Nile red-loaded nanoemulsions, indicating complete penetration after 35 min.

Dynamic light scattering (DLS), transmission electron microscopy (TEM) and attenuated total reflectance-Fourier transform infrared spectroscopy (ATR-FTIR) were used to characterize the nanoemulsions. DLS analysis showed that the hydrodynamic

diameter of nanoemulsions is ~310 nm with a narrow size distribution (polydispersity index = 0.017) (Figure 4. 1d). These nanoemulsions are stable at room temperature for at least 30 days and are degraded in the presence of collagenase (Figure 4. 2). TEM photographs revealed a spherical morphology of the nanoemulsions (Figure 4. 1e and Figure 4. 3). The size observed in TEM (~100 nm) is smaller than observed by DLS, presumably due to partial collapse upon removal of carvacrol under vacuum during TEM. Finally, the chemical nature of the cross-linking was demonstrated by the emergence of a band at 1033 cm^{-1} arising from aliphatic-aromatic ether formation, an additional aromatic ether signature at 1242 cm^{-1}, and appearance of sp^3 C-H stretches at 2957 cm^{-1} (Figure 4. 1c and Figure 4. 4).

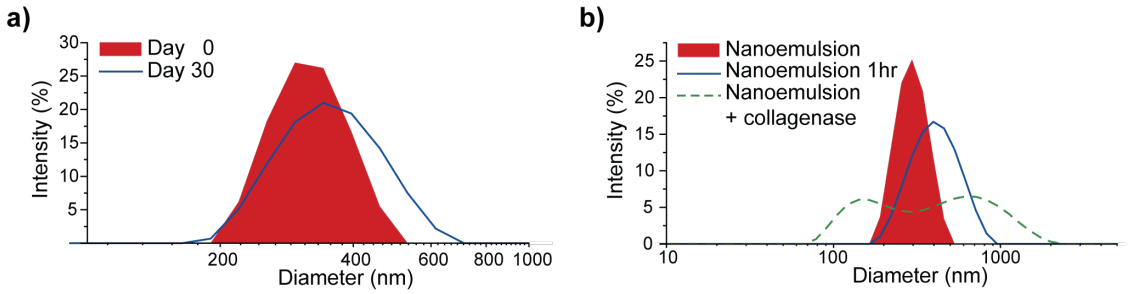

Figure 4. 2. Stability and biodegradation of gelatin nanoemulsion. a) Gelatin nanoemulsion demonstrates ≥ 30 days stability at room temperature. Cross-linked nanoemulsions were stable in storage, with only a modest change in DLS. b) Collagenase type I degrades the gelatin nanoemulsion at 37°C. The broadened DLS profile indicates the degradation of nanoemulsion.

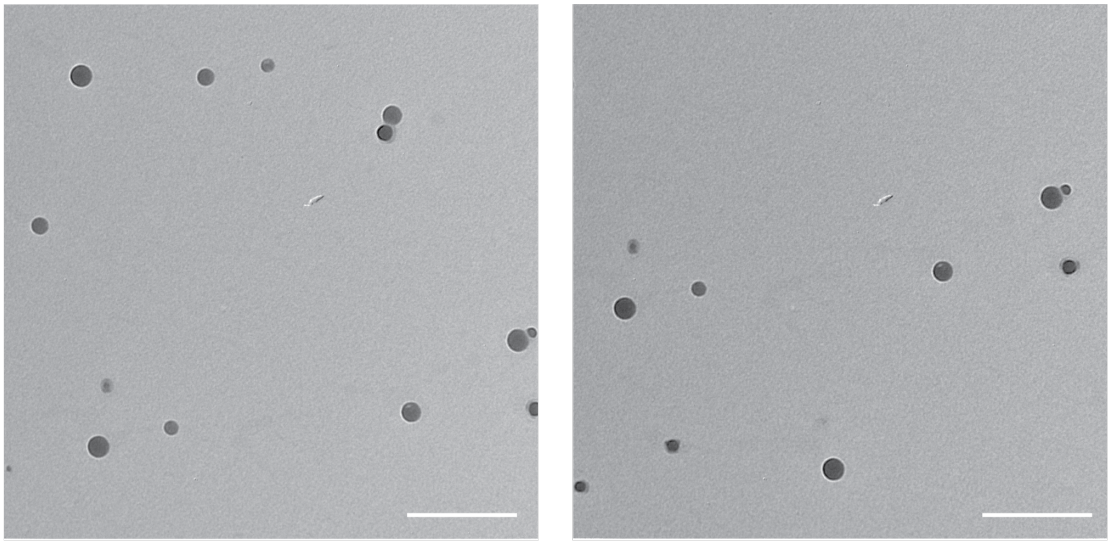

Figure 4. 3. Additional transmission electron microscopy images of the gelatin nanoemulsions. Scale bar is 500 nm.

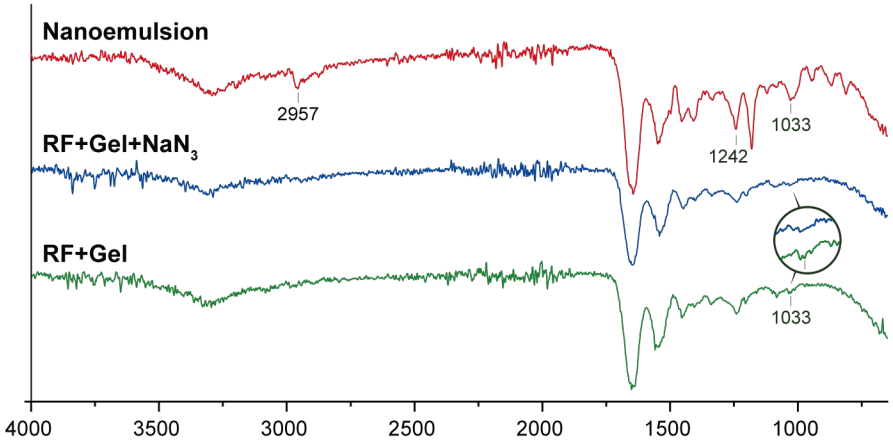

Figure 4. 4. IR spectra of nanoemulsion cross-linking and control experiments. As reported previously,[29, 30] irradiation of riboflavin with UV-A light generates singlet oxygen, oxidizing the imidazole moiety of the histidines of collagen to electrophilic imidazolones. These imidazolones then react with hydroxyl moieties of hydroxyproline, serine, or tyrosine, resulting in cross-linking. Cross-linking after irradiation was demonstrated by the emergence of a band at 1033 cm^{-1} arising from aliphatic-aromatic ether formation, similar to that obtained from riboflavin and gelatin without carvacrol. Compared with irradiation of gelatin and riboflavin alone, carvacrol nanoemulsions featured broadening at 1033 cm^{-1}, an additional aromatic ether signature at 1242 cm^{-1}, and appearance of sp^3 C-H stretches at 2957 cm^{-1}, consistent with an imidazolone reaction with the hydroxyl groups of carvacrol, imparting further hydrophobic domains and additionally stabilizing the oil domains. Irradiation in the presence of the singlet oxygen inhibitor sodium azide resulted in no new bands, consistent with the proposed cross-linking mechanism. All three reactions underwent dialysis and were lyophilized to remove by-product noise (riboflavin, residual carvacrol oil, sodium azide, and water) prior to the IR measurement.

Carvacrol and other hydrophobic materials fail to penetrate biofilms.[18] We hypothesized that the cationic charge of gelatin at the low pH[31] found in biofilms[32] would facilitate transport of nanoemulsions into biofilms. Confocal laser scanning microscopy (CLSM) was used to demonstrate effective and complete penetration of gelatin nanoemulsions into biofilms. Transport was tracked by loading the vehicle with the hydrophobic dye Nile red. Nanoemulsions were incubated with 4-day old biofilms of green fluorescent protein (GFP)-expressing *K. pneumoniae* IDRL-11999. As shown in

Figure 4. 1f, gelatin nanoemulsions penetrated the biofilm matrix completely, as indicated by visualization of Nile red throughout the thickness of the biofilm, with colocalization of red and green signals. Time-dependent z-stack scanning demonstrated that complete penetration of nanoemulsions occurred within 40 minutes (Figure 4. 1g).

We next probed the mechanism of action of gelatin nanoemulsions. We hypothesized that gelatin nanoemulsions kill bacteria in the same manner as carvacrol, namely through disrupting the cell membrane. We used propidium iodide (PI) staining to monitor the membrane permeability of bacteria.[33] Planktonic bacteria (*P. aeruginosa,* ATCC-27853) were treated with gelatin nanoemulsions or the antibiotic Ceftazidime (from 0.125X to 4X of their respective minimum inhibitory concentrations (MICs)) in the presence of PI. Gelatin nanoemulsion treatment immediately generated fluorescence inside bacteria, indicating that PI penetrated through the compromised cell membrane and bound to DNA (Figure 4. 5). In contrast, bacteria treated with Ceftazidime did not generate fluorescence, as Ceftazidime does not directly act on the membrane. Studies have shown that therapeutics causing membrane disruption are unlikely to trigger development of resistance.[19]

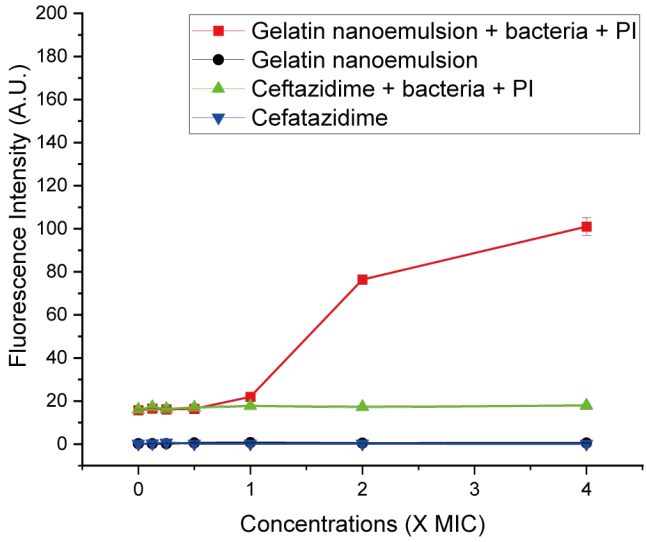

Figure 4. 5. Killing mechanism of gelatin nanoemulsions. *P. aeruginosa* (ATCC-27853) was treated with gelatin nanoemulsions and Ceftazidime in concentrations ranging from 0.125 to 4X of MIC. Upon addition, gelatin nanoemulsions quickly disrupted bacterial cell membranes, therefore allowing propidium iodide to bind to nucleic acids and generate fluorescence. However, no fluorescence was observed with Ceftazidime, as its mechanism of action is through inhibition of enzymes for cell-wall synthesis rather than membrane disruption.

After validating the biofilm penetration profile and the mechanism of action, we used Alamar blue assay to assess antimicrobial activity of nanoemulsions against biofilms of four clinical bacterial isolates (*P. aeruginosa* CD-1006, methicillin-resistant *S. aureus* [MRSA] CD-489, *Escherichia coli* CD-2, and *Enterobacter cloacae* complex CD-1412). Treatment of these biofilms with nanoemulsions for 3 hours eliminated bacteria within the biofilms at 5% v/v (1.95 mM of carvacrol) (Figure 4. 6), with individual components of the nanoemulsions having minimal effect. Notably, treatment of bacteria with only gelatin (nutrient[34]) or riboflavin (nutrient/potential quorum sensing signal[35]) can enhance biofilm viability. We further quantified the minimum biofilm inhibitory concentrations (MBICs) and minimum biofilm eradication concentrations (MBECs) towards several clinical isolates (Table 4. 1), including *P. aeruginosa* (CD-

1006, IDRL-11442, ATCC 27583) and MRSA (IDRL-6169) to represent bacterial species that are common constituents of wound biofilm infections.[36] All biofilms were suppressed or eradicated by nanoemulsions at concentrations ranging from 4% v/v (1.56 mM) to 8% v/v (3.12 mM). This activity was mirrored in more challenging dual-species biofilm models (MRSA/*P. aeruginosa* and MRSA/*E. coli*) (Table 4. 2).[37]

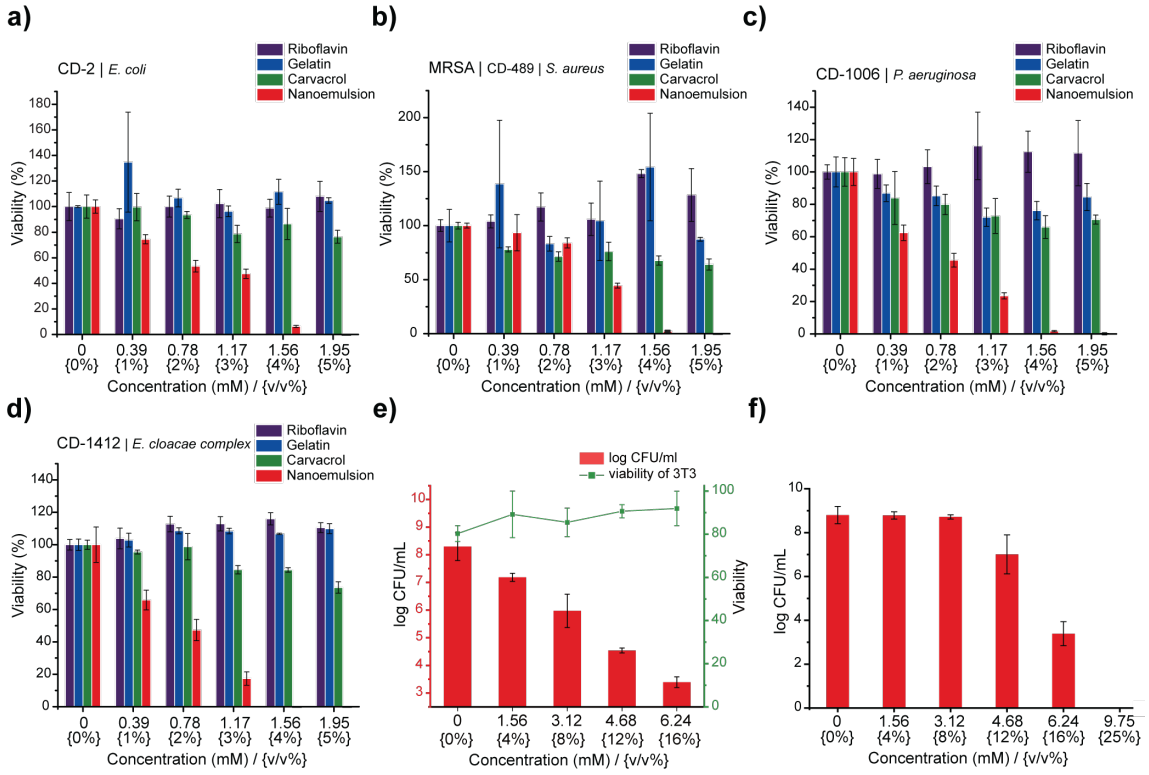

Figure 4. 6. Gelatin nanoemulsions kill the bacteria within biofilms. Viability of a) *Escherichia coli* CD-2, b) methicillin-resistant *Staphylococcus aureus* CD-489, c) *Pseudomonas aeruginosa* CD-1006, and d) *Enterobacter cloacae* complex CD-1412 biofilms after 3 hours of treatment with riboflavin, gelatin, carvacrol, or nanoemulsions. e) Viability of 3T3 fibroblast cells and *P. aeruginosa* biofilms in the co-culture model after 3 h treatment with nanoemulsions. The line represents 3T3 fibroblast cell viability. Bars represent $\log_{10}$ of colony forming units of bacteria in biofilms. f) Gelatin nanoemulsions kill the biofilm bacteria in simulated wound conditions. Log colony forming units (CFU) of methicillin-resistant *S. aureus* IDRL-6169 biofilms after 3 hours of treatment with gelatin nanoemulsions in simulated wound fluid. Data are presented as mean ± standard deviation and represent three independent experiments.

Table 4. 1. MBICs and MBECs of gelatin nanoemulsions against single-species bacterial biofilms

	Single-species biofilms				
Species	*P. aeruginosa*			*E. coli*	*S. aureus*
Strain	CD-1006	IDRL-11442[2]	ATCC 27583	IDRL-10366[2]	IDRL-6169[1]
MBIC	4%	4%	8%	4%	4%
MBEC	4%	4%	8%	4%	4%

[1]Methicillin-resistant
[2]Multidrug-resistant

Table 4. 2 MBICs and MBECs of gelatin nanoemulsions against dual-species bacterial biofilms

	Dual-species biofilms	
Species	*S. aureus* + *P. aeruginosa*	*S. aureus* + *E. coli*
Strain	IDRL-6169[1] + IDRL-11442[2]	IDRL-6169[1] + IDRL-10366[2]
MBIC	4%	4%
MBEC	4%	4%

We next used an *in vitro* bacterial biofilm-mammalian cell coculture model to evaluate antimicrobial activity and biocompatibility of gelatin nanoemulsions. *P. aeruginosa* (ATCC-27853) was seeded on a monolayer of NIH 3T3-fibroblast cells for 6 hours to mimic biofilm infections on mammalian cells. Subsequently, the cocultures were treated with gelatin nanoemulsion for three hours. The viabilities of mammalian cells and bacteria were determined using LDH assay and colony counting, respectively. As shown in Figure 4. 6e, gelatin nanoemulsions effectively reduce bacterial colonies up to 5 $\log_{10}$ colony forming units (CFUs), while the toxicity toward 3T3 fibroblast cells remained negligible. Moreover, the activity of the nanoemulsions was determined using a simulated wound fluid (SWF) model, mimicking the interference/deactivation of antimicrobial activity by wound fluids.[38] In this experiment, 4-day old MRSA (IDRL-6169) biofilms were grown using tryptic soy broth (TSB)/SWF (1:1) solution. Gelatin nanoemulsions were serially diluted with SWF solution and added to the biofilms; three hours after, antimicrobial efficacy was determined using quantitative colony counting.

Nanoemulsions were active against the biofilms in SWF, with 12% v/v (4.68 mM) and 16% v/v (6.24 mM) of nanoemulsions resulting in ~2 and ~5 $\log_{10}$ CFU reduction, respectively (Figure 4. 6f).

Encouraged by the *in vitro* efficacy of the nanoemulsions, their *in vivo* activity was evaluated using a murine wound biofilm model (Figure 4. 7a). In this model, MRSA IDRL-6169 biofilms were established in a wound created using a 5-mm skin puncture, and allowed to mature for 4 days. Mice were then separated into three groups: 100% v/v nanoemulsions (39 mM carvacrol), vancomycin (110 mg/kg), and saline solution only. Treatments were administered every other day (topical application of nanoemulsions and PBS, and intraperitoneal injection of vancomycin) until the day of sacrifice. Photographs were taken daily, and wound sizes and weights of the mice were monitored every day. The degree of purulence was also evaluated daily using a purulence reaction scoring system described in Figure 4. 8.

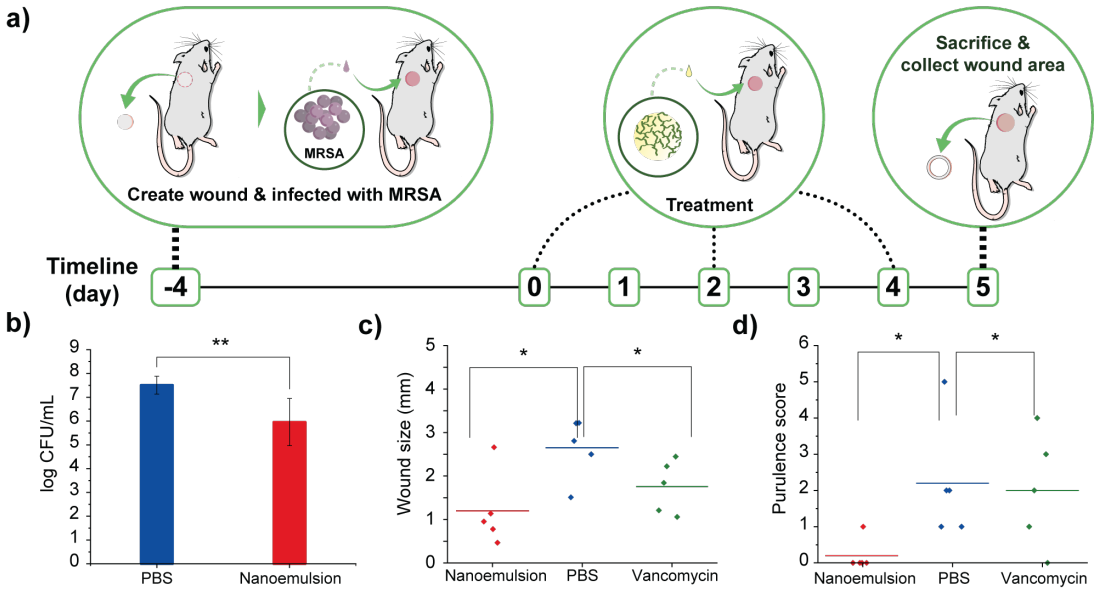

Figure 4. 7. Gelatin nanoemulsions reduce bacterial load and expedite wound healing in a murine model *in vivo*. a) Schematic overview of the murine biofilm-associated wound infection model. b) Colony counts from the infected wounds treated with PBS and nanoemulsions. c) Wound size on the day of sacrifice. d) Purulence score on the day of sacrifice (*, ** = P values < 0.05 or 0.01, respectively

Purulence score	0	1	2	3	4	5
Photo						
Description	normal wound bed	slight turbid exudate	mild whitish exudate	whitish exudate	yellowish exudate	gross pus

Figure 4. 8. Purulence scoring system. We used a 6-point system, from 0 to 5, to evaluate the degree of pus formation in wound beds. Scores of 5 indicate that the wound is heavily infected, with pus extending beyond the wound edge. Scores of 4 indicate that the infected wound has significant pus formation but is limited to the wound bed. Scores of 3 are given to wounds completely covered with whitish exudate. Scores of 2 are assigned to wounds with a whitish exudate, and a visible wound bed. Scores of 1 are assigned to wounds with a slightly turbid exudate, while scores of 0 indicate a normal appearing wound without any sign of exudate.

Treatment with nanoemulsions significantly reduced bacterial load in the wound as compared with PBS controls, with ~1.5 $\log_{10}$ unit reduction after administration of two treatments (Figure 4. 7b), while vancomycin only had ~0.5 $\log_{10}$ bacterial reduction (Figure 4. 9). This antimicrobial effect was mirrored by enhanced wound healing with the

nanoemulsions. The group treated with nanoemulsions showed a greater reduction in wound size after treatment as compared to those treated with vancomycin or PBS (Figure 4. 7c), with the two control group wound beds still containing pus (Figure 4. 10-11). The wounds were likewise better healed: mice in the nanoemulsion group had a purulence score of 0, with normal-appearing healed wound beds. In contrast, vancomycin and PBS groups had purulence scores ~2, indicating the presence of pus (Figure 4. 7d and Figure 4. 13).

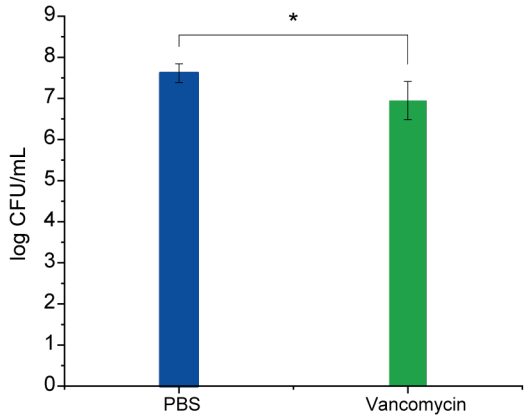

Figure 4. 9. Colony counts from the infected wounds treated with PBS and vancomycin. Treatment with vancomycin slightly reduced wound bacterial loads as compared with PBS controls (~ 0.5 $\log_{10}$ unit reduction) after administration of two treatments (* = P values < 0.05).

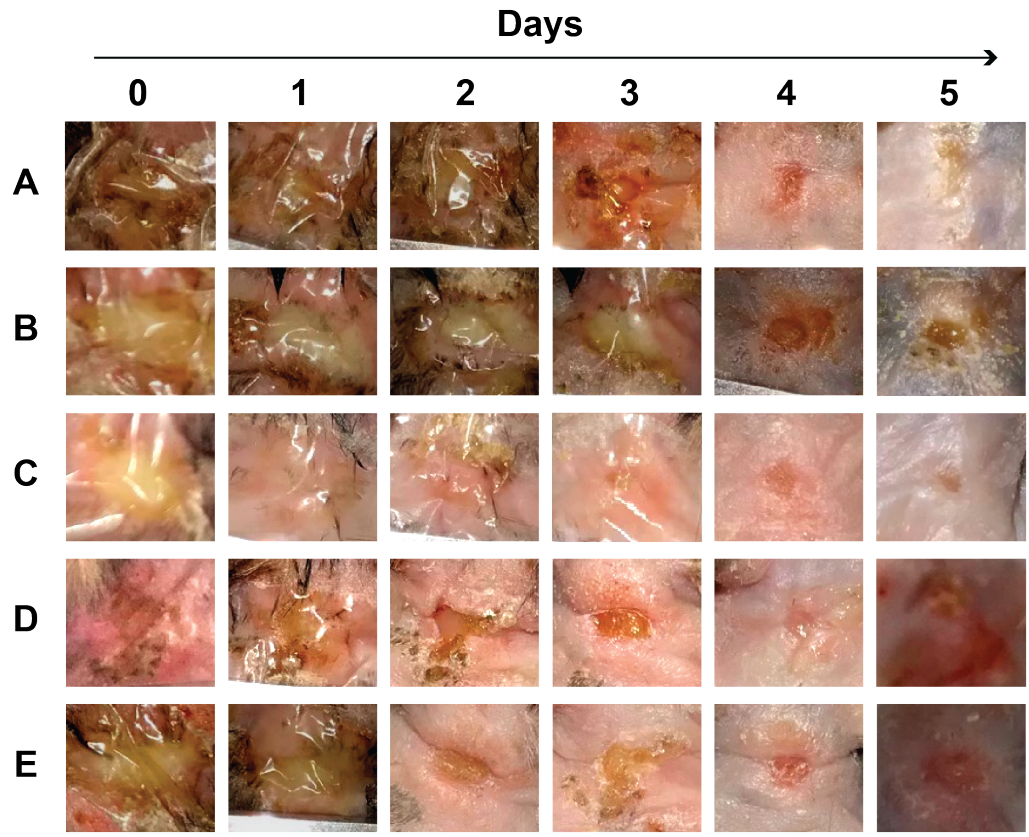

Figure 4. 10. Photographs of infected wounds treated with gelatin nanoemulsions. Photographs were taken daily over the duration of the experiment. Images were used for the blinded evaluation of degrees of purulence.

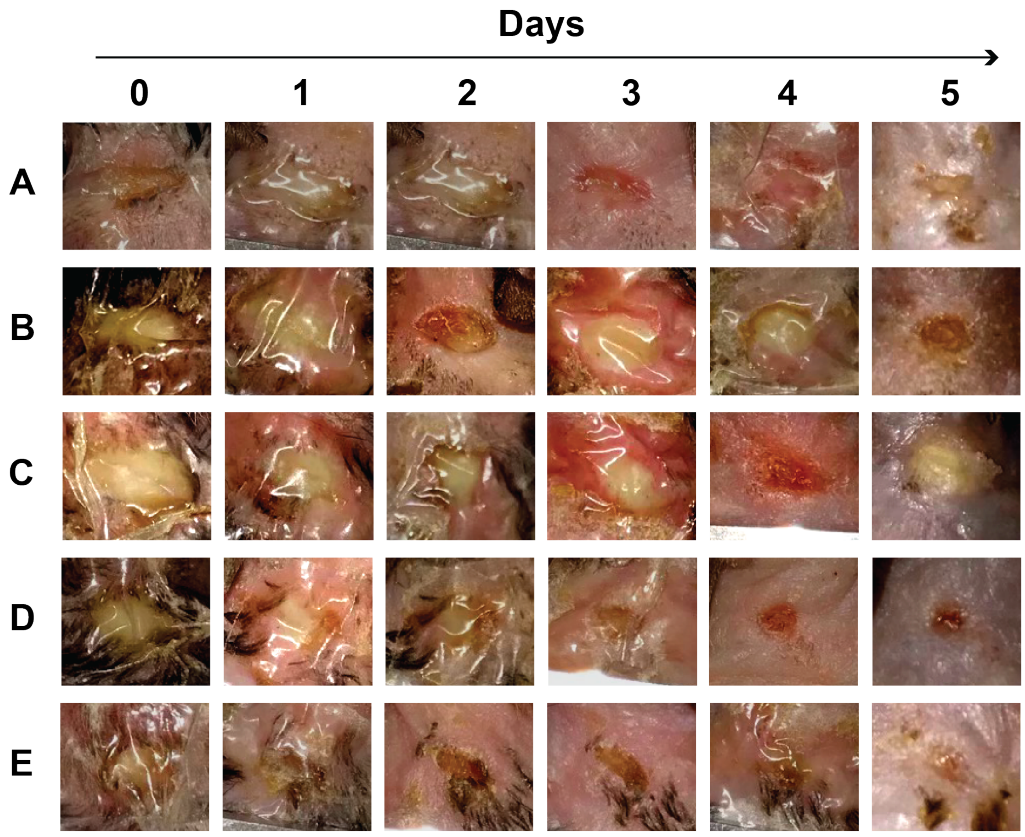

Figure 4. 11. Photographs of infected wounds treated with PBS. Photographs were taken daily over the duration of the experiment. Images were used for the blinded evaluation of degrees of purulence.

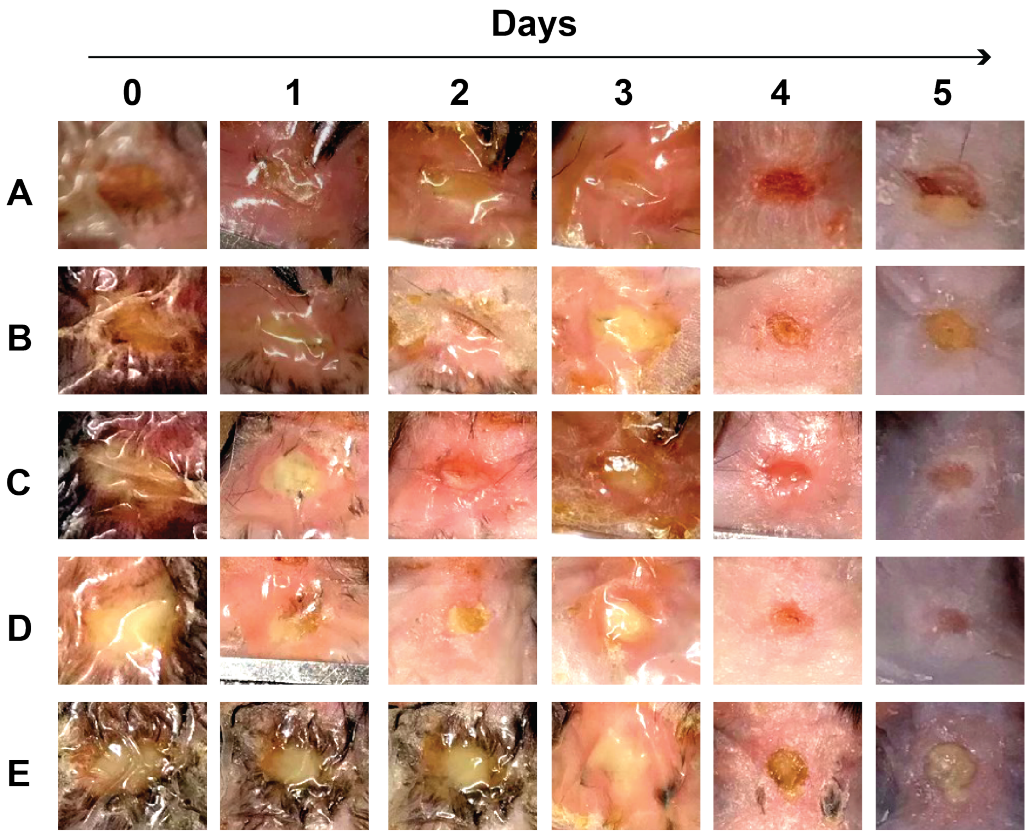

Figure 4. 12. Photographs of infected wounds treated with vancomycin. Photographs were taken daily over the duration of the experiment. Images were used for blinded evaluation of degrees of purulence.

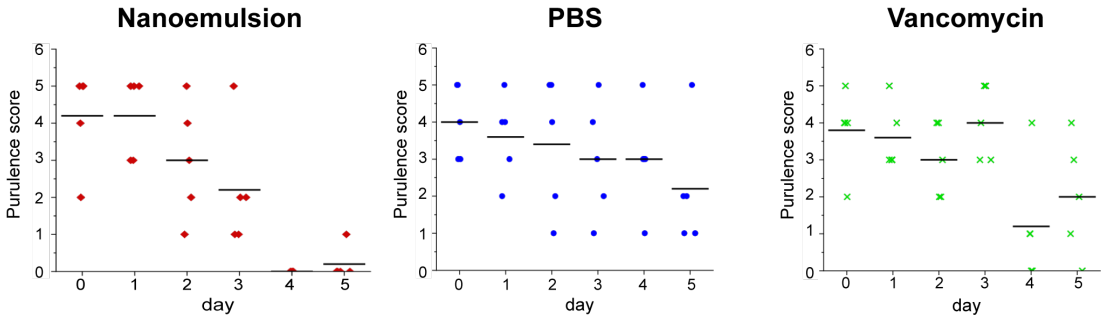

Figure 4. 13. Purulence scores of wounds treated with nanoemulsions, PBS, and vancomycin. Photos of infected wounds were taken daily and were used to rate the extent of pus in a blinded fashion. The results showed that treatment with gelatin nanoemulsions resulted in better wound healing than treatment with vancomycin or PBS.

Histological analysis of the wound beds similarly indicated enhanced healing with the nanoemulsions. Hematoxylin and eosin staining (H&E staining) revealed regeneration

of keratin and epithelial layers, and collagen matrix for the nanoemulsion group. In contrast, for the vancomycin and PBS groups, inflammatory cells were still abundantly found in the area, indicating that the wounds were in the early stages of the wound healing cascade (Figure 4. 14 and Figure 4. 15). Notably, the healed skin had a normal appearing epidermis and dermis, suggesting that nanoemulsions do not alter morphology of the skin undergoing repair. The relative lack of inflammatory cells could also suggest an anti-inflammatory role for the nanoemulsions in wound healing.

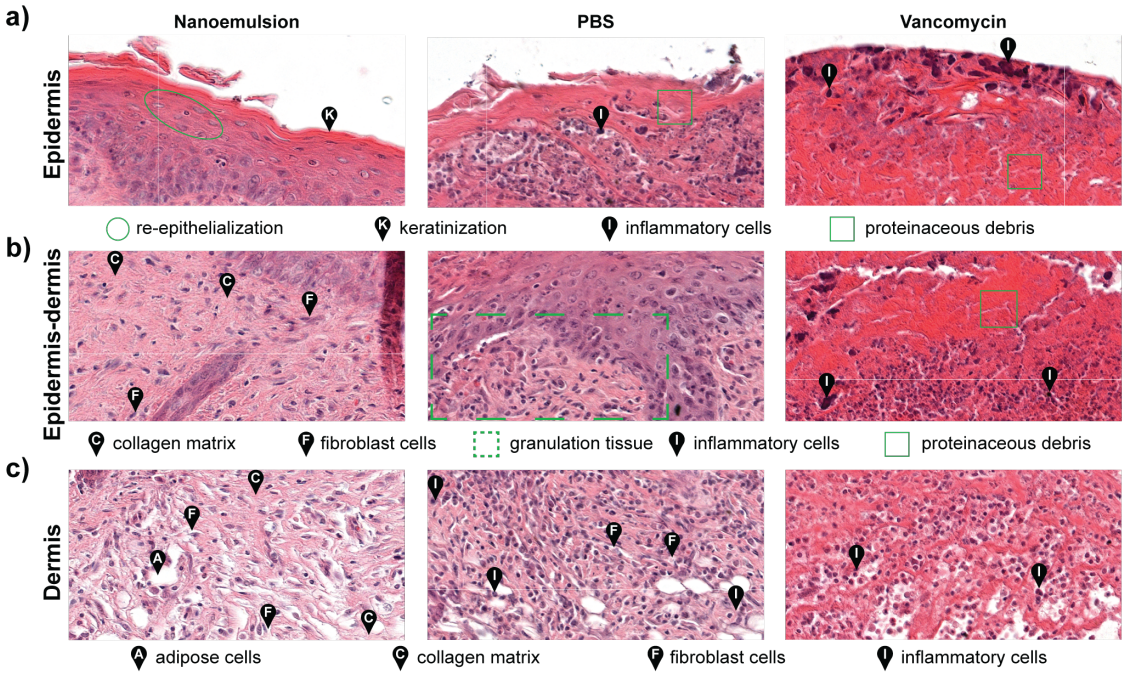

Figure 4. 14. Histological analysis of the tissues surrounding infected wounds show enhanced healing with nanoemulsions. a) Epidermis samples showed regeneration of keratin and the epithelial layer with nanoemulsion treatment. In contrast, inflammatory cells and proteinaceous debris were observed with PBS and vancomycin treatments. b) Substantial formation of collagen matrix at the epidermis-dermis junction was observed after nanoemulsion treatment, whereas immature epidermis and granulation were observed with PBS. Necrosis and cell debris were also detected in the vancomycin-treated sample. c) The dermis was restored with nanoemulsion treatment, while inflammatory cells were still present in the PBS and vancomycin controls.

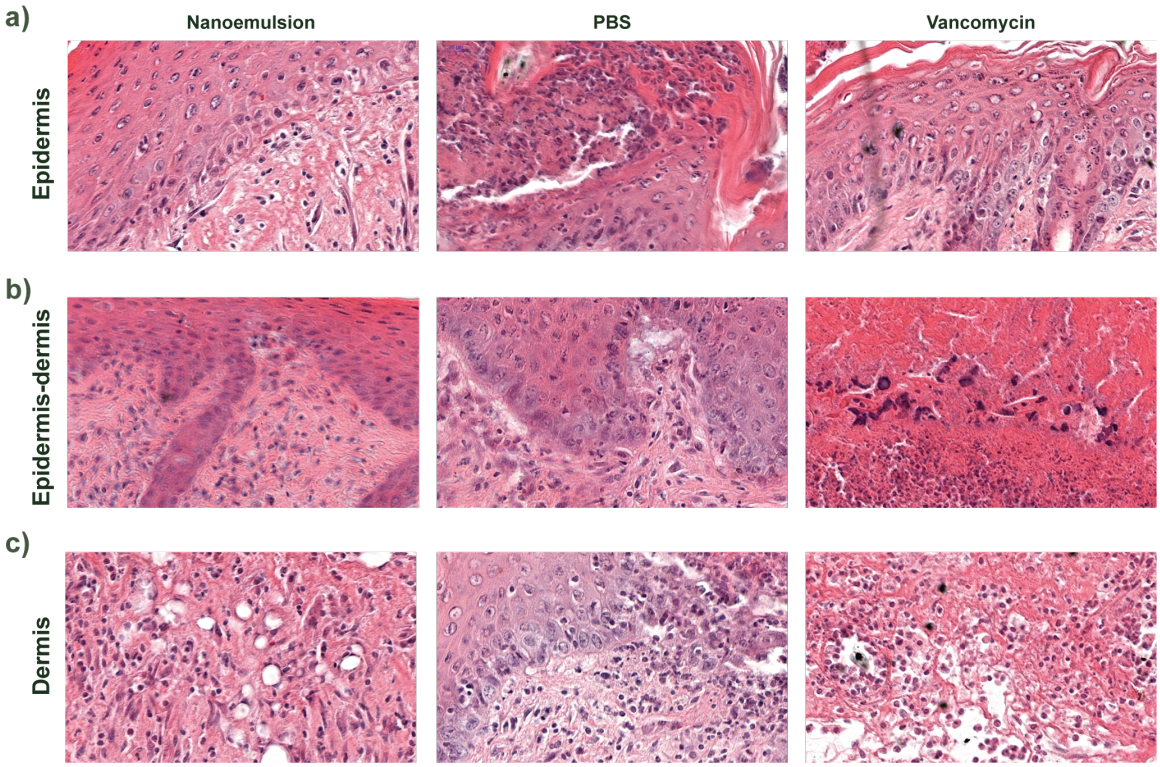

Figure 4. 15. Additional histological samples of skin surrounding infected wounds. a) Epidermis samples showing regeneration of keratin and epithelial layer with nanoemulsion treatment. Inflammatory cells and proteinaceous debris were observed with PBS and vancomycin treatments. b) Formation of collagen matrix in epidermis-dermis junction after nanoemulsion treatment. Immature epidermis and granulation were observed with PBS. Necrosis and cell debris were detected in the vancomycin-treated sample. c) The dermis was restored with nanoemulsion treatment, while inflammatory cells were still present in other controls.

4.3 Conclusion

In summary, integration of nanostructured biomaterials with essential oil payloads provides effective treatment of challenging wound biofilms. Emulsification of oregano oil and gelatin followed by vitamin B_2 cross-linking provided stable nanoemulsions comprised solely of naturally-occurring components. These described nanoemulsions effectively penetrate into biofilms, and kill embedded Gram-positive and -negative bacteria effectively *in vitro*. This antibacterial effect is observed in an *in vivo* murine model, and translates into enhancement in wound healing both in terms of wound size

and degree of purulence. Crucially, this platform is highly modular, providing a general platform for the delivery of a wide variety of oils and other payloads. Overall, integration of the inherent bactericidal activity of essential oils with materials properties provided by biomaterials presents a new path of treatment for wound biofilms, with potential for treating other life-threatening bacterial infections.

4.4 Experimental Sections

4.4.1 Materials

Riboflavin, carvacrol, and Nile red were purchased from Acros. Gelatin (Type B, 100 Bloom) and Luria-Burtani (LB) liquid medium were purchased from Fisher Chemical. Phosphate-buffered saline was purchased from HyClone. Sodium chloride and Pepton were purchased from Fisher BioReagents. M9 minimum medium was purchased from Teknova. Tryptic soy broth (TSB) was purchase from Becton Dickinson. AlamarBlue™ cell viability reagent was purchased from Invitrogen. Fetal bovine serum (FBS) was purchased from Gibco. Pegged lids were purchased from Nunc. Paraformaldehyde (PFA) was purchased from Sigma-Aldrich.

4.4.2 Preparation of gelatin nanoemulsions

Nanoemulsions were prepared through emulsification of a suspension of riboflavin in carvacrol into an aqueous gelatin solution, followed by irradiation with 365 nm UV-light. Briefly, suspension of riboflavin in carvacrol (3 μL, 0.1 wt%) was added to the gelatin aqueous solution (497 μL, 0.24 mg/ml). This solution was then emulsified for 50 seconds using an amalgamator. The emulsion was then exposed to UV lamp for 20

minutes. The concentration of this nanosemulsion stock solution was defined as 100 v/v% (39 mM of carvacrol)

4.4.3 Characterization

The hydrodynamic diameter of nanoemulsions was measured in triplicate using DLS (Malvern Zetasizer). TEM samples were prepared on 300 square mesh nickel grids with Formvar film (Electron Microscopy Sciences). IR was performed on a Bruker Alpha FTIR spectrophotometer fitted with a platinum ATR QuickSnap sampling module.

4.4.4 Biofilm penetration study

Red fluorescent nanoemulsions were prepared as above, using a solution of Nile red in carvacrol (1 mg/ 1000 μL). GFP-expressing *K. pneumoniae* biofilms were prepared using the preparation method described below for mono-species biofilms. These biofilms were then treated with prepared red fluorescent nanoemulsions (5 v/v%) for 1 hour at room temperature. A Nikon A1 spectral detector confocal with FLIM module was used to monitor penetration profile of the nanoemulsions. A penetration profile study was performed using Nikon A1 resonant scanning confocal with TIRF module. The images were processed using NIS-Elements.

4.4.5 Evaluation of antimicrobial activity *in vitro*

Frozen (-80°C) cultures of all bacteria strains used: a.) Clinical isolates *E. coli* (CD-2), MDR *E. coli* (IDRL-10366), *P. aeruginosa* (CD-1006), MDR *P. aeruginosa* (IDRL-11442), *E. cloacae* complex (CD-1412), MRSA (CD-489), MRSA (IDRL-6169); b.) GFP-expressing *K. pneumoniae* (IDRL-11999); and c.) reference strain *P. aeruginosa*

(ATCC 27583) were grown aerobically using Luria-Burtani agar. Overnight cultures of bacteria were prepared by transferring isolated colony from the agar plate to culture tubes with sterile LB broth. Bacterial cultures were then incubated overnight at 37°C with agitation (275 rpm), until the stationary phase was reached. Bacteria were then collected by centrifugation (7000 rpm, 5 min) and washed thrice with sodium chloride (0.85%). Subsequently, the culture was resuspended in PBS (1 mL) to determine its OD_{600} (SpectraMax M2, Molecular Devices). All clinical isolates with code CD were obtained from Cooley Dickinson Hospital, while those denoted by IDRL were from the Infectious Diseases Research Laboratory at the Mayo Clinic.

For mono-species biofilms, bacteria (except *S. aureus*) were prepared by dilution with M9 medium to 0.1 OD_{600} for biofilm formation. For *S. aureus* biofilms, cultures were prepared in M9/TSB (85:15) to the same concentration. Subsequently, the seeding solutions (100 μL) were added to each well of a 96-well clear flat-bottomed plate. The plate was covered and incubated under static conditions at room temperature overnight. The seeding solutions were removed, and biofilms were washed thrice with PBS. Gelatin nanoemulsion solutions ranging from 0 to 48 v/v% were then administered (100 μL) to the biofilms. The plates were incubated statically at 37°C. After 3 h, the biofilms were washed thrice with PBS; then alamarBlue cell viability reagent[39] (10 v/v%) was added to each well, and incubated for 1 h. Biofilm viability was determined by measuring fluorescence intensity (excitation: 560 nm; emission: 590 nm). Readings from the wells containing alamarBlue cell viability reagent (10 v/v%) alone were considered as the blank (I_{blank}), and readings from wells with untreated biofilms were used as growth controls ($I_{control}$). Biofilm viability was calculated using the equation below:

$$Biofilm\ viability\ (\%) = 100\% \times \frac{I_{sample} - I_{blank}}{I_{control} - I_{blank}}$$

Biofilm-3T3 fibroblast cell coculture model was performed using the previously reported protocol.[40] Briefly, NIH 3T3 (ATCC CRL-1658) cells (20k/well) were cultured in a 96 well plate overnight to form a monolayer. Afterward, the mammalian cells were washed and 100 μL of bacterial seeding solutions (108 CFU/mL) were added. The cocultures were then stored at 37°C for six hours without shaking. Gelatin nanoemulsions and other control solutions were diluted in DMEM media prior to use to obtain the desired testing concentrations. The cocultures were washed again and the freshly prepared testing solutions were then added. After 3 h incubation at 37°C, the cocultures were then analyzed using LDH cytotoxicity assay. To determine the bacteria viability in biofilms, the testing solutions were removed and cocultures were washed with PBS. Fresh PBS was then added, and the plate was sealed and sonicated for 20 min to disperse biofilms. The solutions containing dispersed bacteria were quantitatively determined using the colony counting forming unit method.

For the SWF experiment, we followed an established SWF protocol.[41] Briefly, bacterial cultures were prepared using the method described above. Biofilm seeding solutions were prepared in SWF/TSB (1:1) solutions. SWF was comprised of fetal bovine serum (50%) and sodium chloride (50%) in Pepton water (0.1%). This seeding solution (100 μL) was added to each well of the 96-well plate. The plate was covered and incubated under static conditions at ~23°C for 4 days. The activity of gelatin nanoemulsions towards this model was determined using quantitative colony counting.

MBIC and MBBC assays[42] of single- and dual-species biofilms were carried out using a Calgary biofilm device.[43] For the single-species biofilms, bacteria were grown in

TSB (2.5 mL) at 275 rpm and 37°C until the concentration reached 0.5 McFarland standard. These solutions (150 μL) were then transferred to each well of a 96-well plate. The plate was covered with a pegged lid and incubated for 6 h at 50 rpm and 37°C. The pegged lid was then removed, rinsed with PBS for 30 seconds, and then transferred to a plate with antimicrobial agents (200 μL) in each well. MBIC values were determined after the plate was incubated 24 h at 37°C statically. Subsequently, the same pegged lid was rinsed with PBS for 30 seconds again, and transferred to a plate with broth (200 μL) in each well. MBBC values were determined after the plates were statically incubated for another 24 hours at 37°C. For dual-species biofilms, the same procedure was followed except that 75 μL of each of the component bacterial species were added into the 96-well microplate then mixed.

4.4.6 Study of killing mechanism of gelatin nanoemulsions

Bacteria solution (OD_{600} = 0.5) containing propidium iodide (PI) (10 μL/ 1000 μL) was prepared for the killing mechanism study. The bacteria solutions (50 μL) were added to each well of a black 96-well flat-bottomed plate. Fluorescence intensities were measured immediately after adding 50 μL of PBS containing 0.125 to 4X MIC of gelatin nanoemulsions or Ceftazidime (Excitation/Emission: 535 nm/617 nm).

4.4.7 Ethics statement

C57BL/6 mice were supplied by Jackson Laboratory. Mice were housed in sterile cages with a 12 hours light/12 hours dark cycle. They were allowed to acclimatize for at least a week before any of the procedures were carried out. All animal experiments were performed in accordance with the authorized protocol (IACUC Protocol ID 2018-0011)

and the policies issued by Institutional Animal Care and Use Committee at University of Massachusetts Amherst.

4.4.8 *In vivo* wound biofilm murine model

The biofilm model was generated using C57BL/6 mice that were anesthetized and the skin on their dorsum shaved and disinfected using a sterile alcohol pad.[44] Afterwards, a sterile 5-mm circular full thickness skin wound was punched using a skin puncture biopsy tool. Using a micropipette, 10^7 colony forming units (CFU) of a clinical isolate of MRSA (IDRL-6169) in saline (10 μL) was inoculated onto the wound bed. Semi-occlusive transparent Tegaderm® was placed over the wound using Mastisol® as an adhesive to prevent secondary bacterial contamination. Biofilm was then allowed to form for four days. The mice were then separated into three groups of five: one group treated with nanoemulsions (100% v/v; 39 mM), a second with vancomycin (110 mg/kg) that served as the positive control and a third with vehicle control (saline solution only). Test agents (100 μL) were administered every other day until the day of sacrifice (day 5); nanoemulsions and saline were administered topically, while vancomycin was injected intraperitoneally. Photographs were taken daily, and purulence scores, wound sizes and weights of the mice were monitored every day. On the day of the sacrifice, the mice were euthanized via CO_2 asphyxiation. Then, 10-mm circular full thickness skin covering the infection area was collected using a skin biopsy punch for histological analysis.

4.4.9 *In vivo* wound closure measurement and purulence score grading

All photographs were taken from a standard height at the same time over the entire treatment period. Three blinded observers determined the sizes of the wounds

using the taken images with ImageJ software and graded the degree of pus formation using a standard purulence scoring system. At the same time, a blinded observer present through the duration of the study measured wound size using a digital caliper (Neiko tools) and rated the degree of purulence of the mice.

4.4.10 Preparation of skin samples for histological analysis

The skin tissue was fixed in paraformaldehyde (4%) in 4°C overnight and transferred into PBS. After 24 hours, the tissue was dehydrated in a series of ethanol washes and stored at 4°C. The tissue samples were cut, dividing the wound in half. Subsequently, the tissues were cleared in xylene for 1 hour, with a xylene change after 30 minutes. After 1 hour, xylene was removed and replaced with paraffin wax, followed by fresh wax changes every 30 minutes. Half tissue sections were aligned in the wax and sectioned at 7 μm.

4.4.11 Hematoxylin and eosin (H&E) staining

The sectioned tissues were deparaffinized and rehydrated for subsequent procedures. Slides were then stained with hematoxylin for 45 seconds, placed under gently running tap water for 1 minute, submerged in Scott's Tap Water Substitute (20 g $MgSO_4$ and 3.5 g $NaHCO_2$ in 1 L of Milli-Q® H_2O) for 1 minute, and then washed in still tap water for another minute. Slides were quickly dipped into ethanol (95%), stained with eosin for 15 seconds, and then again washed in ethanol (95%) with two 2-minute washes in ethanol (100%). Lastly, slides were washed with xylene three times for 1 minute each, and then sealed with Cytoseal™ 60. H&E stained sections were imaged with a Panoramic MIDI II slide scanner (3DHISTECH).

4.4.12 *In vivo* antimicrobial activity

Separate experiments were done to assess bacterial reduction midway through the wound healing process. After formation of 4-day old MRSA biofilms on wounds as above, mice were separated into groups of five for each treatment group: nanoemulsions (100% v/v; 39 mM), saline solution only, and vancomycin (110 mg/kg). Treatments were administered every other day until the day of sacrifice (day 2). At day 2, mice were sacrificed 3 h after test materials were administered. The mice were euthanized via CO_2 asphyxiation. Then, 3-mm circular full thickness skin in the inner portion of the infection area was collected using a skin biopsy punch for quantitative colony counting. Skin samples were homogenized in PBS, diluted, and plated into mannitol salt agar to quantitatively determine remaining bacteria counts.

4.5 References

1 Col, N. F.; O'Connor, R. W. Estimating Worldwide Current Antibiotic Usage: Report of Task Force 1. *Rev. Infect. Dis.* **1987**, *9*, S232–S243.

2 Blair, J. M. A.; Webber, M. A.; Baylay, A. J.; Ogbolu, D. O.; Piddock, L. J. V. Molecular Mechanisms of Antibiotic Resistance. *Nat. Rev. Microbiol.* **2015**, *13*, 42–51.

3 Aminov, R. A Brief History of the Antibiotic Era: Lessons Learned and Challenges for the Future. *Front. Microbiol.* **2010**, *1*, 134.

4 Liu, X.; Wang, Z.; Feng, X.; Bai, E.; Xiong, Y.; Zhu, X.; Shen, B.; Duan, Y.; Huang, Y. Platensimycin-Encapsulated Poly(Lactic-Co-Glycolic Acid) and Poly(Amidoamine) Dendrimers Nanoparticles with Enhanced Anti-Staphylococcal Activity in Vivo. *Bioconjug. Chem.* **2020**, *31*, 1425–1437.

5 James, G. A.; Swogger, E.; Wolcott, R.; Pulcini, E. deLancey; Secor, P.; Sestrich, J.; Costerton, J. W.; Stewart, P. S. Biofilms in Chronic Wounds. *Wound Repair Regen.* **2008**, *16*, 37–44.

6 Arciola, C. R.; Campoccia, D.; Speziale, P.; Montanaro, L.; Costerton, J. W. Biofilm Formation in Staphylococcus Implant Infections. A Review of Molecular Mechanisms and Implications for Biofilm-Resistant Materials. *Biomaterials* **2012**, *33*, 5967–5982.

7 Lewis, K. Multidrug Tolerance of Biofilms and Persister Cells. *Curr. Top. Microbiol. Immunol.* **2008**, *322*, 107-131.

8 Percival, S. L.; McCarty, S. M.; Lipsky, B. Biofilms and Wounds: An Overview of the Evidence. *Adv. Wound Care* **2014**, *4*, 373–381.

9 Xu, C.; Akakuru, O. U.; Ma, X.; Zheng, J.; Zheng, J.; Wu, A. Nanoparticle-Based Wound Dressing: Recent Progress in the Detection and Therapy of Bacterial Infections. *Bioconjug. Chem.* **2020**, *31*, 1708–1723.

10 Järbrink, K.; Ni, G.; Sönnergren, H.; Schmidtchen, A.; Pang, C.; Bajpai, R.; Car, J. The Humanistic and Economic Burden of Chronic Wounds: A Protocol for a Systematic Review. *Syst. Rev.* **2017**, *6*, 1–7.

11 Simões, M.; Bennett, R. N.; Rosa, E. A. S. Understanding Antimicrobial Activities of Phytochemicals against Multidrug Resistant Bacteria and Biofilms. *Nat. Prod. Rep.* **2009**, *26*, 746–757.

12 Tiwari, B. K.; Valdramidis, V. P.; O' Donnell, C. P.; Muthukumarappan, K.; Bourke, P.; Cullen, P. J. Application of Natural Antimicrobials for Food Preservation. *J. Agric. Food Chem.* **2009**, *57*, 5987–6000.

13 Baratta, M. T.; Dorman, H. J. D.; Deans, S. G.; Biondi, D. M.; Ruberto, G. Chemical Composition, Antimicrobial and Antioxidative Activity of Laurel, Sage, Rosemary, Oregano and Coriander Essential Oils. *J. Essent. Oil Res.* **1998**, *10*, 618–627.

14 Farzaei, M. H.; Bahramsoltani, R.; Abbasabadi, Z.; Rahimi, R. A Comprehensive Review on Phytochemical and Pharmacological Aspects of Elaeagnus Angustifolia L. *J. Pharm. Pharmacol.* **2015**, *67*, 1467–1480.

15 Etman, M.; Amin, M.; Nada, A. H.; Shams-Eldin, M.; Salama, O. Emulsions and Rectal Formulations Containing Myrrh Essential Oil for Better Patient Compliance. *Drug Discov. Ther.* **2011**, *5*, 150–156.

16 Freire Rocha Caldas, G.; Araújo, A. V.; Albuquerque, G. S.; Silva-Neto, J. D. C.; Costa-Silva, J. H.; De Menezes, I. R. A.; Leite, A. C. L.; Da Costa, J. G. M.; Wanderley, A. G.; Caldas, G. F. R.; *et al.* Repeated-Doses Toxicity Study of the Essential Oil of Hyptis Martiusii Benth. (Lamiaceae) in Swiss Mice. *Evidence-Based Complement. Altern. Med.* **2013**, *2013*, No. 856168.

17 Samperio, C.; Boyer, R.; Eigel, W. N.; Holland, K. W.; McKinney, J. S.; O'Keefe, S. F.; Smith, R.; Marcy, J. E. Enhancement of Plant Essential Oils' Aqueous Solubility and Stability Using Alpha and Beta Cyclodextrin. *J. Agric. Food Chem.* **2010**, *58*, 12950–12956.

18 Iannitelli, A.; Grande, R.; Di Stefano, A.; Di Giulio, M.; Sozio, P.; Bessa, L. J.; Laserra, S.; Paolini, C.; Protasi, F.; Cellini, L. Potential Antibacterial Activity of Carvacrol-Loaded Poly(DL-Lactide-Co-Glycolide) (PLGA) Nanoparticles against Microbial Biofilm. *Int. J. Mol. Sci.* **2011**, *12*, 5039–5051.

19 Landis, R. F.; Li, C. H.; Gupta, A.; Lee, Y. W.; Yazdani, M.; Ngernyuang, N.; Altinbasak, I.; Mansoor, S.; Khichi, M. A. S.; Sanyal, A.; Rotello, V. M. Biodegradable Nanocomposite Antimicrobials for the Eradication of Multidrug-Resistant Bacterial Biofilms without Accumulated Resistance. *J. Am. Chem. Soc.* **2018**, *140*, 6176–6182.

20 Guarda, A.; Rubilar, J. F.; Miltz, J.; Galotto, M. J. The Antimicrobial Activity of Microencapsulated Thymol and Carvacrol. *Int. J. Food Microbiol.* **2011**, *146*, 144–150.

21 Wollensak, G.; Spoerl, E.; Seiler, T. Riboflavin/Ultraviolet-a–Induced Collagen Crosslinking for the Treatment of Keratoconus. *Am. J. Ophthalmol.* **2003**, *135*, 620–627.

22 Ribes, J.; Beztsinna, N.; Bailly, R.; Castano, S.; Rascol, E.; Taib-Maamar, N.; Badarau, E.; Bestel, I. Flavin-Conjugated Nanobombs: Key Structural Requirements Governing Their Self-Assemblies' Morphologies. *Bioconjug. Chem.* **2021**, *32*, 553–562.

23 Makabenta, J. M. V.; Nabawy, A.; Li, C.-H.; Schmidt-Malan, S.; Patel, R.; Rotello, V. M. Nanomaterial-Based Therapeutics for Antibiotic-Resistant Bacterial Infections. *Nat. Rev. Microbiol.* **2021**, *19*, 23–36.

24 Liu, Y.; Shi, L.; Su, L.; Van der Mei, H. C.; Jutte, P. C.; Ren, Y.; Busscher, H. J. Nanotechnology-Based Antimicrobials and Delivery Systems for Biofilm-Infection Control. *Chem. Soc. Rev.* **2019**, *48*, 428–446.

25 Terjung, N.; Löffler, M.; Gibis, M.; Hinrichs, J.; Weiss, J. Influence of Droplet Size on the Efficacy of Oil-in-Water Emulsions Loaded with Phenolic Antimicrobials. *Food Funct.* **2012**, *3*, 290–301.

26 Nostro, A.; Blanco, A. R.; Cannatelli, M. A.; Enea, V.; Flamini, G.; Morelli, I.; Roccaro, A. S.; Alonzo, V. Susceptibility of Methicillin-Resistant Staphylococci to Oregano Essential Oil, Carvacrol and Thymol. *FEMS Microbiol. Lett.* **2004**, *230*, 191–195.

27 Elzoghby, A. O. Gelatin-Based Nanoparticles as Drug and Gene Delivery Systems: Reviewing Three Decades of Research. *J. Control. Release* **2013**, *172*, 1075–1091.

28 Dickinson, E. Hydrocolloids as Emulsifiers and Emulsion Stabilizers. *Food Hydrocoll.* **2009**, *23*, 1473–1482.

29 Au, V.; Madison, S. A. Effects of Singlet Oxygen on the Extracellular Matrix Protein Collagen: Oxidation of the Collagen Crosslink Histidinohydroxylysinonorleucine and Histidine. *Arch. Biochem. Biophys.* **2000**, *384*, 133–142.

30 McCall, A. S.; Kraft, S.; Edelhauser, H. F.; Kidder, G. W.; Lundquist, R. R.; Bradshaw, H. E.; Dedeic, Z.; Dionne, M. J. C.; Clement, E. M.; Conrad, G. W. Mechanisms of Corneal Tissue Cross-Linking in Response to Treatment with Topical Riboflavin and Long-Wavelength Ultraviolet Radiation (UVA). *Invest. Ophthalmol. Vis. Sci.* **2010**, *51*, 129–138.

31 Gaihre, B.; Khil, M. S.; Lee, D. R.; Kim, H. Y. Gelatin-Coated Magnetic Iron Oxide Nanoparticles as Carrier System: Drug Loading and in Vitro Drug Release Study. *Int. J. Pharm.* **2009**, *365*, 180–189.

32 Vroom, J. M.; De Grauw, K. J.; Gerritsen, H. C.; Bradshaw, D. J.; Marsh, P. D.; Watson, G. K.; Birmingham, J. J.; Allison, C. Depth Penetration and Detection of PH Gradients in Biofilms by Two-Photon Excitation Microscopy. *Appl. Environ. Microbiol.* **1999**, *65*, 3502–3511.

33 Arndt-Jovin, D. J.; Jovin, T. M. Chapter 16 Fluorescence Labeling and Microscopy of DNA. In *Fluorescence Microscopy of Living Cells in Culture Part B. Quantitative Fluorescence Microscopy—Imaging and Spectroscopy*; Taylor, D. L.; Wang, Y.-L. B. T.-M. in C. B., Eds.; Academic Press, 1989; Vol. 30, pp. 417–448.

34 Koser, S. A.; Chinn, B. D.; Saunders, F. Gelatin as a Source of Growth-Promoting Substances for Bacteria. *J. Bacteriol.* **1938**, *36*, 57–65.

35 Rajamani, S.; Bauer, W. D.; Robinson, J. B.; Farrow, J. M.; Pesci, E. C.; Teplitski, M.; Gao, M.; Sayre, R. T.; Phillips, D. A. The Vitamin Riboflavin and Its Derivative Lumichrome Activate the LasR Bacterial Quorum-Sensing Receptor. Mol. *Plant-Microbe Interact.* **2008**, *21*, 1184–1192.

36 Serra, R.; Grande, R.; Butrico, L.; Rossi, A.; Settimio, U. F.; Caroleo, B.; Amato, B.; Gallelli, L.; de Franciscis, S. Chronic Wound Infections: The Role of Pseudomonas Aeruginosa and Staphylococcus Aureus. *Expert Rev. Anti. Infect. Ther.* **2015**, *13*, 605–613.

37 DeLeon, S.; Clinton, A.; Fowler, H.; Everett, J.; Horswill, A. R.; Rumbaugh, K. P. Synergistic Interactions of Pseudomonas Aeruginosa and Staphylococcus Aureus in an In Vitro Wound Model. *Infect. Immun.* **2014**, *82*, 4718–4728.

38 Craig, W. A.; Welling, P. G. Protein Binding of Antimicrobials: Clinical Pharmacokinetic and Therapeutic Implications. *Clin. Pharmacokinet.* **1977**, *2*, 252–268.

39 Pettit, R. K.; Weber, C. A.; Pettit, G. R. Application of a High Throughput Alamar Blue Biofilm Susceptibility Assay to Staphylococcus Aureus Biofilms. *Ann. Clin. Microbiol. Antimicrob.* **2009**, *8*, 28.

40 Duncan, B.; Li, X.; Landis, R. F.; Kim, S. T.; Gupta, A.; Wang, L. S.; Ramanathan, R.; Tang, R.; Boerth, J. A.; Rotello, V. M. Nanoparticle-Stabilized Capsules for the Treatment of Bacterial Biofilms. *ACS Nano* **2015**, *9*, 7775–7782.

41 Werthén, M.; LINA, H.; Jensen, P. Ø.; Sternberg, C.; M. Givskov, M.; Bjarnsholt, T. An in Vitro Model of Bacterial Infections in Wounds and Other Soft Tissues. *APMIS* **2010**, *118*, 156–164.

42 Ceri, H.; Olson, M. E.; Stremick, C.; Read, R. R.; Morck, D.; Buret, A. The Calgary Biofilm Device: New Technology for Rapid Determination of Antibiotic Susceptibilities of Bacterial Biofilms. *J. Clin. Microbiol.* **1999**, *37*, 1771–1776.

43 Harrison, J. J.; Stremick, C. A.; Turner, R. J.; Allan, N. D.; Olson, M. E.; Ceri, H. Microtiter Susceptibility Testing of Microbes Growing on Peg Lids: A Miniaturized Biofilm Model for High-Throughput Screening. *Nat. Protoc.* **2010**, *5*, 1236–1254.

44 Kim, C. K.; Karau, M. J.; Greenwood-Quaintance, K. E.; Tilahun, A. Y.; Krogman, A.; David, C. S.; Pritt, B. S.; Patel, R.; Rajagopalan, G. Superantigen-Producing Staphylococcus Aureus Elicits Systemic Immune Activation in a Murine Wound Colonization Model. *Toxins (Basel).* **2015**, *7*, 5308–5319.

CHAPTER 5

5. PENETRATION PROFILES OF NANOEMULSIONS IN KLEBSIELLA PNEUMONIAE BIOFILM

5.1 Introduction

Bacterial biofilm has been recognized as a key factor in chronic infections.[1,2] The formation of biofilm including bacterial aggregation and biosynthesis of extracellular polymeric substances (EPS) provides a unique biofilm structure and microenvironment for survival.[3] Specifically, the EPS restricts or even inhibits penetration of antimicrobials, resulting in a dramatic increase of antimicrobial tolerance.[4,5] Moreover, the EPS also regulates nutrients and water dynamics, leading to a diverse habitat including the formation of antimicrobial tolerant persister cells.[6] Therefore, understanding the interactions between EPS, embedded bacteria, and antimicrobials is essential for the management of biofilm infections.[7]

Nanomaterials are promising tools for probing dynamics between external molecules and biofilms.[8] The interactions of nanomaterials with cells and biofilms correlate with the nanomaterials' surface functionality.[9,10] Coupled with fluorescent-labeling techniques and confocal laser scanning microscopy (CLSM), nanomaterials reveal factors including charge and hydrophobicity/hydrophilicity that determine the nanomaterial-biofilm interactions.[11,12] However, relevant studies often only provide end-point observations, revealing no spatiotemporal-detailed dynamics of the nanomaterial within the bacterial biofilm settings.

Herein, I generated penetration profiles of nanoemulsions into bacterial biofilms. The interaction between the nanoemulsions and the bacteria within the biofilm was

probed using Nile red-loaded emulsions derived from our established platform,[13] minimizing the organic synthetic workload and changes of surface properties of the resulted nanoemulsions. The spatial and temporal dynamics of the nanoemulsions in the biofilm setting were monitored using 4D (xyzt) confocal imaging. Coupled with the quantitative technique, these readily prepared nanoemulsions provide penetration profiles for designing potential synthetic polymers for antimicrobial nanoemulsions and identifying bacterial strains of the biofilm.

5.2 Results and Discussion

5.2.1 Fabrication and characterization of dye-loaded nanoemulsions

Fluorescent labeling of the nanoemulsions was implemented by loading Nile red into carvacrol, minimizing changes to the surface properties of the resulting nanoemulsions. Additionally, Nile red probes only the interaction of the bacteria and the nanoemulsions, as Nile red is only fluorescent in lipid-rich environments.[14] Nanoemulsions with opposite charges were fabricated to explore the relationship between surface charge and penetration behavior.[9] The nanoemulsions with positive surface charges and negative surface charges were generated using a cationic polymer (PONI-GMT)[13] and an anionic polymer (PONI-AMT), respectively (Figure 5. 1). Specifically, nanoemulsions were fabricated by emulsifying a Nile red-loaded carvacrol into the aqueous polymer solution.

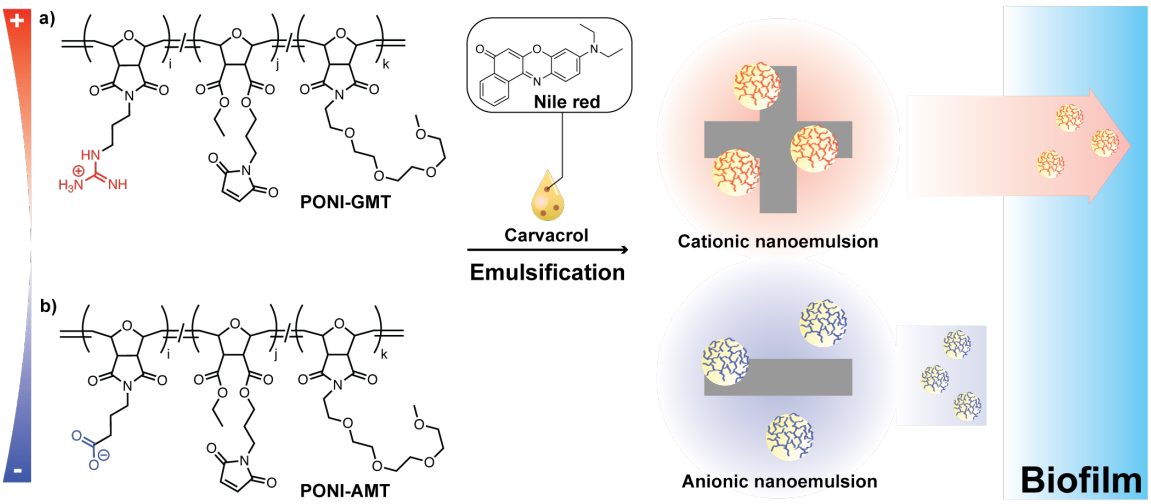

Figure 5. 1. Schematic depiction of the preparation of the nanoemulsions and the chemical structures of a) PONI-GMT and b) PONI-AMT

Dynamic light scattering (DLS) and zeta potential were used to characterize the nanoemulsions. DLS analysis demonstrated that the hydrodynamic diameter of the cationic and anionic nanoemulsion were ~ 220 and ~ 250 nm, respectively. Additionally, both nanoemulsions showed a narrow size distribution (polydispersity index < 0.26) (Figure 5. 2) These nanoemulsions are stable at room temperature for at least 1 day. The colloidal stability of these nanoemulsions is sufficient for determining their penetration profiles to biofilms. Zeta potentials revealed that the surface charge of the cationic nanoemulsion is ~ 23 mV and its anionic counterpart is ~ - 33 mV (Figure 5. 3)

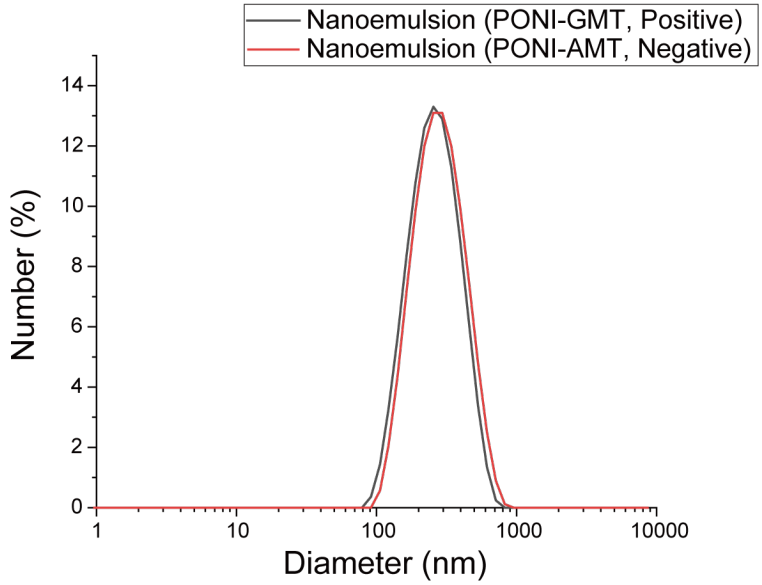

Figure 5. 2. Dynamic light scattering analysis of the nanoemulsions in phosphate buffered saline (150 mM).

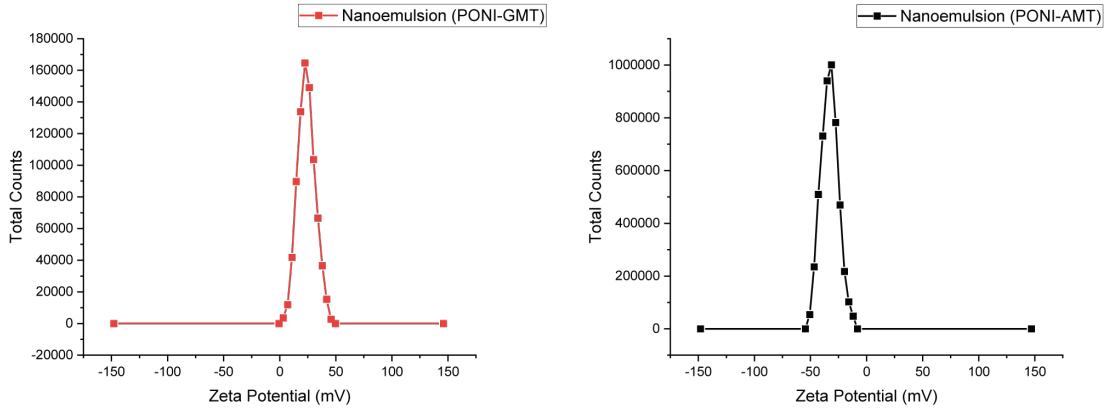

Figure 5. 3. Zeta potentials of the nanoemulsions in 0.1x phosphate buffered saline.

5.2.2 Penetration profiles of nanoemulsions to biofilms

After the basic characterization of the nanoemulsions, we used confocal laser scanning microscopy (CLSM) to monitor the interactions of the nanoemulsions and the biofilm. We used 4-day old biofilms of green fluorescent protein (GFP)-expressing *K. pneumoniae* (IDRL-11999), as the thicker EPS may amplify the difference in the diffusive penetration behavior. The biofilms were first scanned along z-axis using the

green channel with the same interval (0.5 µm). As shown in Figure 5. 4, the two biofilms had different thickness. Figure 5. 4a had 52 layers and Figure 5. 4b had 60 layers, even though the biofilms were grown in the same conditions. Additionally, the distribution of the bacteria within the biofilm were also different. Figure 5. 4b showed more bacteria distributed in the bottom of the biofilm (z = 30 - 50) than Figure 5. 4a. Therefore, the distribution along z-axis was converted to the percentage of bacteria within biofilm along z-axis for comparisons (Figure 5. 5). Figure 5. 5 demonstrated that 80% of the bacteria were distributed in 0 – 20 layers of the left biofilm, while the right biofilm had 80% of the bacteria in 0 – 30 layers.

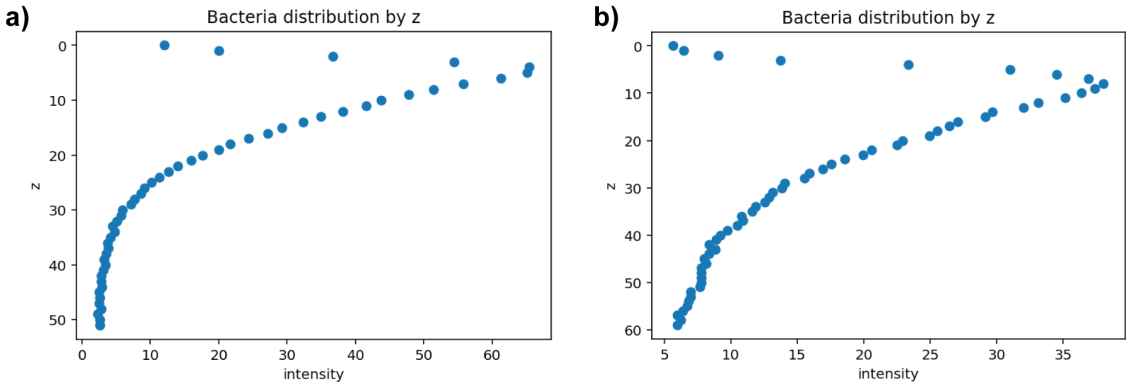

Figure 5. 4. Fluorescent intensity of the bacteria within the biofilm along z-axis. a) and b) were grown in the same condition but showing different thickness (z_a = 52, z_b = 60) and bacterial distributions with respect to z-axis.

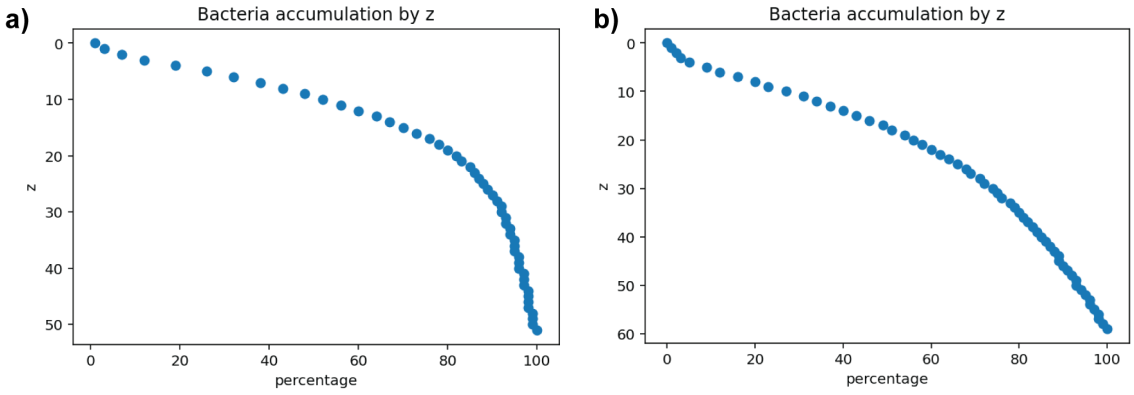

Figure 5. 5. Percentage of the bacteria within the biofilm along z-axis. a) indicated that 80% of the bacteria distributed in the upper biofilm. b) showed a relative uniform distribution of the bacteria within the biofilm.

The nanoemulsions were added to the biofilm and allowed to diffuse freely. As shown in Figure 5. 6a, the cationic nanoemulsion contacted the biofilm after ~ 10 min of the addition. The cationic nanoemulsion then penetrated the biofilm and stained ~ 90% of the bacteria within 35 min. The anionic nanoemulsion contacted the biofilm at about the same time, indicating the diffusion rates of the cationic and anionic nanoemulsions are similar in the M9 medium. However, the anionic nanoemulsion was unable to penetrate the biofilm (Figure 5. 6b). These preliminary results were consistent with the previous literature.[9,15]

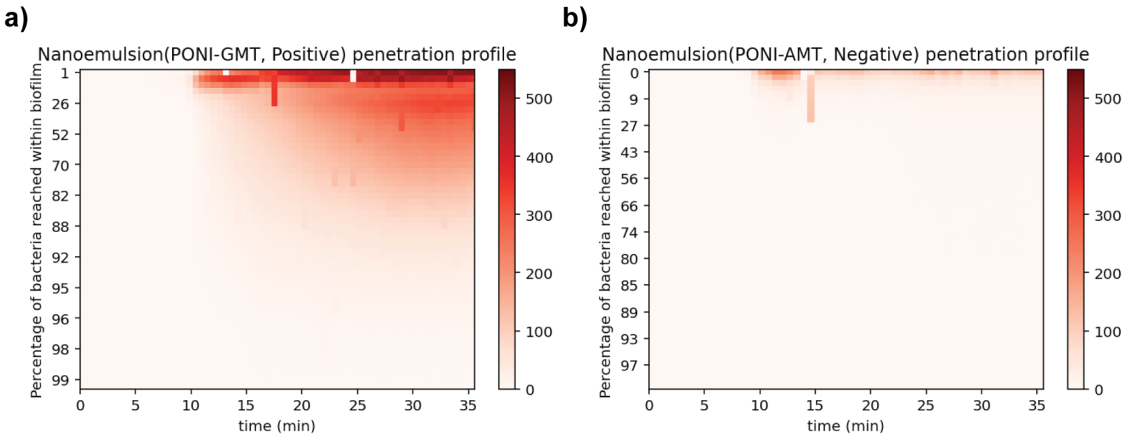

Figure 5. 6. Spatial and time distribution of red fluorescence within the biofilm after the addition of Nile red-loaded a) PONI-GMT, Positive and b) PONI-AMT, Negative nanoemulsions.

Additionally, the experiment monitored the diffusive penetration profile of the nanoemulsions by collecting fluorescent intensities of the bacteria stained with the nanoemulsions and the nanoemulsions themselves (Figure 5. 7a). To better quantify the delivery of the nanoemulsions to the bacteria within the matrix, I isolated the signals from the bacteria (Figure 5. 7b) and calculated penetration without the nanoemulsions' signals (Figure 5. 8b) as the delivery profile. The difference between the penetration profile and the delivery profile was attributed to the fluorescence signals from the

nanoemulsions. The much stronger signals from the top right corner of the penetration profile indicated that the EPS impedes the entry of the nanoemulsions (Figure 5. 8).

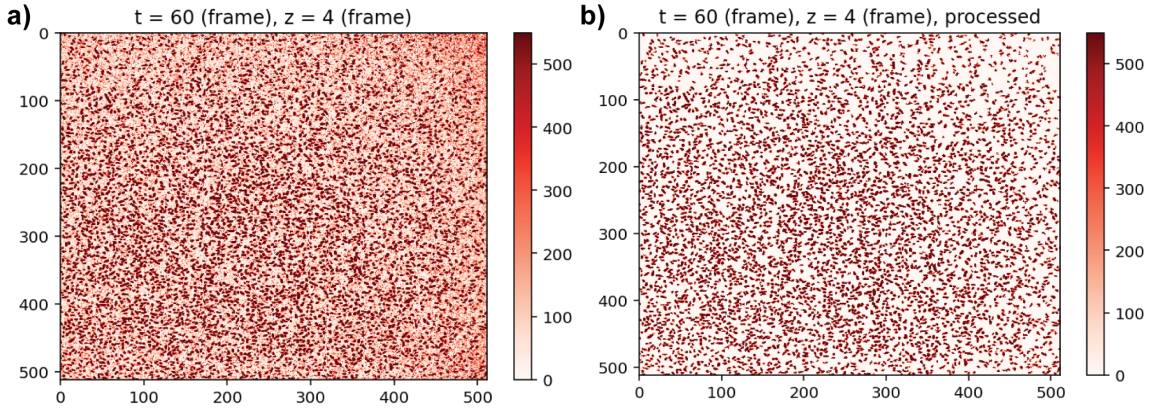

Figure 5. 7. Example of the confocal images of the biofilm a) before and b) after removing signals from the nanoemulsions.

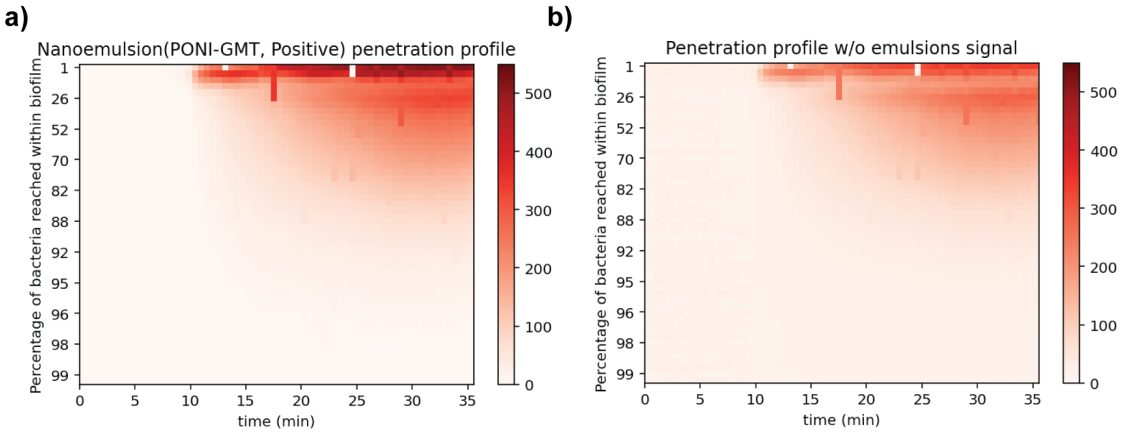

Figure 5. 8. Penetration profiles a) with the signals from the nanoemulsions and b) without the signals from the nanoemulsions.

5.3 Conclusion

Loading Nile red into oil-in-water nanoemulions provides a fluorescent probe for visualizing the interaction between the nanoemulsion and the bacteria within the biofilm in real-time. This fluorescent labeling strategy minimizes physical and chemical changes of the nanomaterials, eliminating behavioral differences between dye-labeled materials

and the original materials. Additionally, these nanoemulsions only label lipids, as Nile red is only fluorescent in lipid-rich environments, minimizing the signal interference from other hydrophilic components within the biofilms. Finally, through image processing and quantification, the Nile red-loaded nanoemulsions reveal the penetration profiles to bacterial biofilms. In this preliminary study, we have used this technique to demonstrate that surface charges play a critical role in the interaction of the nanoemulsions and bacteria within biofilms. The resulting penetration profiles have potential for use in rapid identification of bacterial species of the biofilm infection.

5.4 Experimental Section

5.4.1 Synthesis of PONI-GMT

PONI-GMT and its monomer were synthesized according to the procedures reported in literature.[13]

5.4.2 Synthesis of ONI-C3-carboxylic acid-Boc (3)

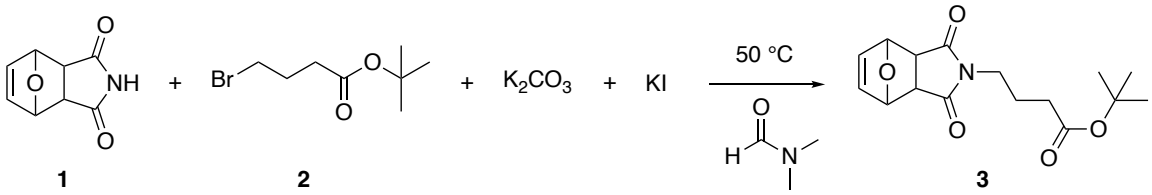

1 **2** **3**

A stirred solution of **1** (3.53 g, 21.34 mmol) and K_2CO_3 (8 g, 64 mmol) in dimethylformamide (DMF, 30 mL) was heated to 50°C. This solution was further stirred for 5 min. Subsequently, a solution of **2** (5 g, 22.41 mmol) and KI (0.7 g, 4.27 mmol) in DMF (10 mL) was added to the stirred solution. The combined reaction was stirred at 50°C overnight and monitored with thin-layer chromatography (ethyl acetate:hexane = 1:1). The solvent was then removed under reduced pressure. The crude product was

dissolved in ethyl acetate then washed with brine three times. The crude product was purified by flash chromatography on silica gel (ethyl acetate:hexane = 1:1) to give a white solid (**3**, 3.08 g, 46.88%). (^{1}H NMR, $CDCl_3$, 400 MHz) 6.5 (s, 2H), 5.26 (s, 2H), 3.52 (t, 2H), 2.83 (s, 2H), 2.2 (t, 2H), 1.84 (quin, 2H), 1.43 (s, 9H).

5.4.3 Synthesis of PONI-AMT

5.4.3.1 Synthesis of PONI-AMT-Boc (6)

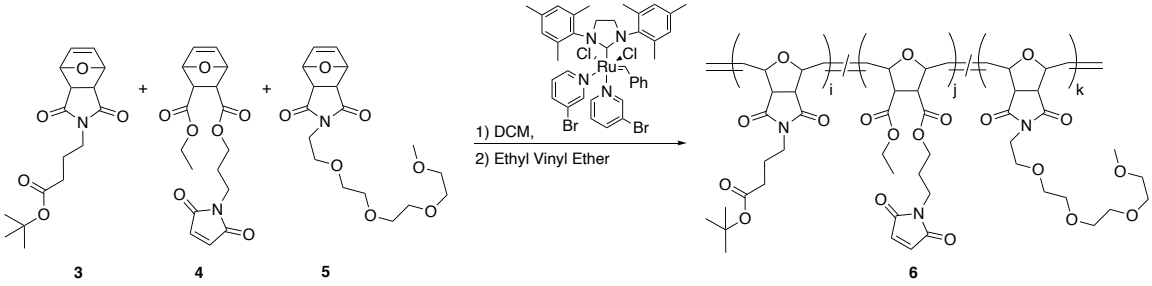

To a 10 mL pear-shaped air-free flask equipped with a stir-bar was added **3** (196 mg, 0.57 mmol, 4 eq), **4**[13] (50 mg, 0.14 mmol, 1 eq), **5**[13] (254 mg, 0.72 mmol, 5 eq), and 1 mL of dichloromethane (DCM). In a separate 10 mL pear-shaped air-free flask was added Grubbs 3rd generation catalyst (9.45 mg, 0.011 mmol) and 1mL of DCM. Both flasks were sealed with septa and attached to a Schlenk nitrogen/vacuum line, and then both flasks were freeze-pump-thawed three times. After thawing, the catalyst solution was transferred to the flask containing the monomers and allowed to react for 20 min. Ethyl vinyl ether (300 μL) was added and allowed to stir for 15 min. The reaction mixture was then diluted to two times the volume and precipitated into a heavily stirred solution of hexane (500 mL) to yield Polymer **6**. MW = 34000, PDI = 1.86, as determined by THF GPC using a polystyrene calibration curve). ^{1}H NMR (400MHz, $CDCl_3$) 6.5 (br s, 2H, C*H*=C*H* of **4**), 6.07 and 5.77 (br s, 2H, =C*H*-CH-O of **3** or **5** backbone), 6.0 and 5.69 (br s, 2H, =C*H*-CH-O of **4** backbone), 5 and 4.46 (br m, 2H,

=CH-C*H*-O of **3** or **5** backbone), 4.75 (br s, 2H, =CH-C*H*-O of **4** backbone), 4.13 (br m, 4H, O-CH_2-CH_3 and O-CH_2-CH_2 of **4**), 3.75-3.25 (br m, 25H, overlapping of O-CH_2-CH_2-O (**5**), C(O)-N-CH_2- (**3**), and CH-C*H*-C(O) of **3** or **5** backbone) 3.12 (br, 2H, CH-C*H*-C(O) of **4** backbone), 2.2 (br, t, 2H, CH_2-CH_2-C(O) of **3**), 1.98 (br, 2H, CH_2-CH_2-CH_2 of **4**), 1.83 (br, 2H, CH_2-CH_2-CH_2 of **3**), 1.44 (br s, 9H, C-$(CH_3)_3$ of **3**), 1.23 (br m, 3H, O-CH_2-CH_3 of **4**).

5.4.3.2 Synthesis of PONI-AMT

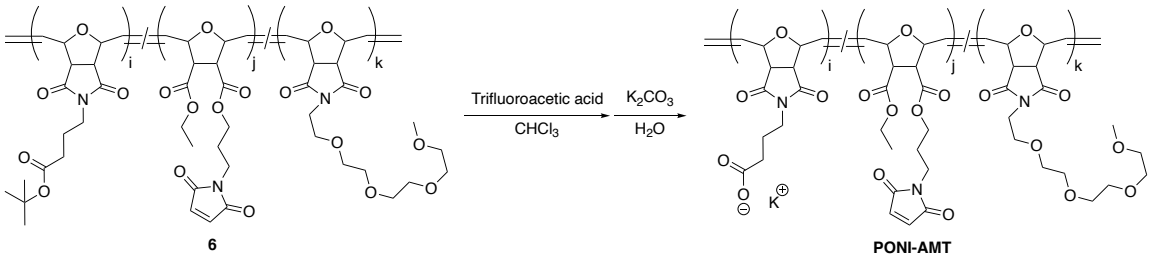

To a 50 mL round bottom flask equipped with a stir-bar was added Polymer **6** (340 mg). Chloroform was purged with nitrogen for 5 min and 12 mL was added to the flask, sealed with a septum and purged with nitrogen for 5 min. The main nitrogen line was left in the septum and the nitrogen pressure was reduced to a steady stream. 1 mL of trifluoroacetic acid (TFA, excess) was added and the reaction was stirred for 4 h. Afterwards, the excess TFA was removed. The reaction residue was dissolved in a minimal amount of K_2CO_3 (aq.), filtered through a polyethersulfone (PES) syringe filter and lyophilized to yield polymer **PONI-AMT** as a white solid which readily dissolves in water. MW ~ 32200, as calculated from the GPC result of **6**. ^{1}H NMR (400MHz, D_2O) 6.2-5.7 (br s, 2H, =C*H*-CH-O of **3** , **4** or **5** backbone), 5.1 and 4.64 (br m, 2H, =CH-C*H*-O of **3** or **5** backbone), 4.16 (br m, 4H, O-CH_2-CH_3 and O-CH_2-CH_2 of **4**), 3.8-3.25 (br m, 25H, overlapping of O-CH_2-CH_2-O (**5**), C(O)-N-CH_2- (**3**), and CH-C*H*-C(O) of **3** or **5**

backbone), 3.12 (br, 2H, CH-C*H*-C(O) of **4** backbone), 2.19 (br, t, 2H, CH_2-CH_2-C(O) of **3**), 1.92 (br, 2H, CH_2-CH_2-CH_2 of **4**), 1.82 (br, 2H, CH_2-CH_2-CH_2 of **3**), 1.25 (br m, 3H, O-CH_2-CH_3 of **4**).

5.4.4 Preparation of the nanoemulsions

Nanoemulsions were prepared through emulsification of a suspension of Nile red in carvacrol into an aqueous polymer solution. To prepare the cationic nanoemulsion, suspension of Nile red in carvacrol (3 μL carvacrol, 1 mg Nile red/1000 μL nanoemulsion) was added to the PONI-GMT aqueous solution (497 μL, 6.04 μM) then emulsified for 50 seconds using an amalgamator. The anionic nanoemulsions were prepared in a similar way but using PONI-AMT aqueous solution (497 μL, 0.8 μg/ μL). The concentration of these nanosemulsion stock solution were defined as 100 v/v% (39 mM of carvacrol).

5.4.5 Characterization of the nanoemulsions

5.4.5.1 Dynamic light scattering

The hydrodynamic diameter of nanoemulsions was measured in triplicate using DLS (Malvern Zetasizer). Sample was prepared by adding 100 μL of the nanoemulsion to 900 μL of PBS.

5.4.5.2 Zeta potentials

The zeta potential of nanoemulsions was measured in triplicate using DLS (Malvern Zetasizer). Sample was prepared by adding 100 μL of the nanoemulsion to 900 μL of 0.1x PBS.

5.4.6 Biofilm formation

GFP-expressing *K. pneumoniae* (IDRL-11999) was grown in Tryptic Soy Broth (TSB) medium with agitation (275 rpm) at 37°C overnight until stationary phase was reached. Bacteria were then collected by centrifugation (7000 rpm, 5 min) and washed 3 times with sterilized sodium chloride (0.85%). Subsequently, the culture was resuspended in PBS (1 mL) to determine its OD_{600} (SpectraMax M2, Molecular Devices). 2 mL of 0.1 OD_{600} of the bacterial solution prepared in TSB containing 1 mM Isopropyl ß-D-1-thiogalactopyranoside (IPTG) was prepared and added to a confocal dish. This culture was then incubated under static conditions at room temperature for 4 days and the medium was changed every 2 days.

5.4.7 Biofilm penetration study

The medium in the GFP-expressing *K. pneumoniae* biofilm was first removed. The biofilm was then washed with PBS 3 times to remove planktonic bacteria. 1 mL of PBS was added to the biofilm to maintain the hydration of the biofilm. Subsequently, the red fluorescent nanoemulsions (20 µL, 100 v/v%) was added to the biofilm and allowed to freely diffuse at room temperature. A Nikon A1 spectral detector confocal with FLIM module was used to monitor penetration profile of the nanoemulsions. Real-time penetration profile study was performed using Nikon A1 resonant scanning confocal with TIRF module.

5.4.8 Confocal images analysis

Penetration profiles were generated using Python with nd2reader, matplotlib, and numpy. The code is available at https://github.com/chl1221/process_time_dependent_z_stacking

5.5 References

1 Wu, Y.-K.; Cheng, N.-C.; Cheng, C.-M. Biofilms in Chronic Wounds: Pathogenesis and Diagnosis. *Trends Biotechnol.* **2019**, *37*, 505–517.

2 Cooper, R. A.; Bjarnsholt, T.; Alhede, M. Biofilms in Wounds: A Review of Present Knowledge. *J. Wound Care* **2014**, *23*, 570–582.

3 Karygianni, L.; Ren, Z.; Koo, H.; Thurnheer, T. Biofilm Matrixome: Extracellular Components in Structured Microbial Communities. *Trends Microbiol.* **2020**, *28*, 668–681.

4 Tseng, B. S.; Zhang, W.; Harrison, J. J.; Quach, T. P.; Song, J. L.; Penterman, J.; Singh, P. K.; Chopp, D. L.; Packman, A. I.; Parsek, M. R. The Extracellular Matrix Protects Pseudomonas Aeruginosa Biofilms by Limiting the Penetration of Tobramycin. *Environ. Microbiol.* **2013**, *15*, 2865–2878.

5 Singh, R.; Ray, P.; Das, A.; Sharma, M. Penetration of Antibiotics through Staphylococcus Aureus and Staphylococcus Epidermidis Biofilms. *J. Antimicrob. Chemother.* **2010**, *65*, 1955–1958.

6 Flemming, H.-C.; Wingender, J.; Szewzyk, U.; Steinberg, P.; Rice, S. A.; Kjelleberg, S. Biofilms: An Emergent Form of Bacterial Life. *Nat. Rev. Microbiol.* **2016**, *14*, 563–575.

7 Fulaz, S.; Vitale, S.; Quinn, L.; Casey, E. Nanoparticle–Biofilm Interactions: The Role of the EPS Matrix. *Trends Microbiol.* **2019**, *27*, 915–926.

8 Ikuma, K.; Decho, A. W.; Lau, B. L. T. When Nanoparticles Meet Biofilms - Interactions Guiding the Environmental Fate and Accumulation of Nanoparticles. *Front. Microbiol.* **2015**, *6*, 1–6.

9 Li, X.; Yeh, Y. C.; Giri, K.; Mout, R.; Landis, R. F.; Prakash, Y. S.; Rotello, V. M. Control of Nanoparticle Penetration into Biofilms through Surface Design. *Chem. Commun.* **2015**, *51*, 282–285.

10 Mitzel, M. R.; Sand, S.; Whalen, J. K.; Tufenkji, N. Hydrophobicity of Biofilm Coatings Influences the Transport Dynamics of Polystyrene Nanoparticles in Biofilm-Coated Sand. *Water Res.* **2016**, *92*, 113–120.

11 Daddi Oubekka, S.; Briandet, R.; Fontaine-Aupart, M.-P.; Steenkeste, K. Correlative Time-Resolved Fluorescence Microscopy To Assess Antibiotic Diffusion-Reaction in Biofilms. *Antimicrob. Agents Chemother.* **2012**, *56*, 3349–3358.

12 Peulen, T.; Wilkinson, K. J. Diffusion of Nanoparticles in a Biofilm. *Environ. Sci. Technol.* **2011**, *45*, 3367–3373.

13 Landis, R. F.; Li, C.-H.; Gupta, A.; Lee, Y.-W. W.; Yazdani, M.; Rotello, V. M.; Ngernyuang, N.; Altinbasak, I.; Mansoor, S.; Khichi, M. A. S. S.; *et al.* Biodegradable Nanocomposite Antimicrobials for the Eradication of Multidrug-Resistant Bacterial Biofilms without Accumulated Resistance. *J. Am. Chem. Soc.* **2018**, *140*, 6176–6182.

14 Diaz, G.; Melis, M.; Batetta, B.; Angius, F.; Falchi, A. M. Hydrophobic Characterization of Intracellular Lipids in Situ by Nile Red Red/Yellow Emission Ratio. *Micron* **2008**, *39*, 819–824.

15 Harper, R. A.; Carpenter, G. H.; Proctor, G. B.; Harvey, R. D.; Gambogi, R. J.; Geonnotti, A. R.; Hider, R.; Jones, S. A. Diminishing Biofilm Resistance to Antimicrobial Nanomaterials through Electrolyte Screening of Electrostatic Interactions. *Colloids Surfaces B Biointerfaces* **2019**, *173*, 392–399.

CHAPTER 6

6. POLYMER-BACTERIOPHAGE NANOASSEMBLY AS TREATMENT FOR BACTERIAL BIOFILMS

6.1 Introduction

Antibiotics are the frontline treatment for bacterial infections[1]. These small molecule-based systems have been used by microbes for over a billion years to kill competing organisms. During this time, bacteria have developed defenses against these agents that remove or deactivate antibiotics.[2,3,4] Bacteria carry the genetic information required to activate these defense mechanisms, allowing rapid acquisition of resistance.[5] Moreover, the ability of pathogenic bacteria, including *Pseudomonas aeruginosa* and *Staphylococcus aureus* to form biofilms creates particular challenges to treat infections in wounds and on implanted devices.[6,7,8,9] Extracellular polymeric substances (EPS) found in biofilms have evolved to become potent barriers to both antibiotics and host immune responses. Additionally, the slow growth and presence of persister cells in these infections further foster the development of antibiotic resistance.[10,11,12] Recent studies have shown that biofilms impede the wound healing process, resulting in chronic wounds with increased morbidity, mortality, and decreased quality of life.[13,14] The lack of effective antibiofilm agents has led to a multibillion US dollar burden to healthcare systems worldwide annually.[15,16]

Bacteriophage therapy has recently been considered as an alternative strategy to combat bacterial infections.[17,18] Bacteriophages are bacteria-specific viruses, and their specificity can be at the strain level.[19] They lyse the pathogens at the site of infection,

while they are inherently non-toxic to mammalian cells, and are thereby generally considered to be safe.[20] Bacteriophage therapy is particularly promising for biofilm-related infections, as high bacterial density of biofilms facilitates the replication of bacteriophage. Moreover, bacteriophages can also infect persister cells and lyse them after those cells become metabolically active again.[21] However, the EPS slows or inhibits the penetration of bacteriophages, dramatically reducing antimicrobial efficacy of the bacteriophage therapy against biofilm infections.[22,23]

Surface properties of nanomaterials play a critical role in determing the penetration profiles of bacterial biofilms.[24] I hypothesized that the negative surface charge of bacteriophages slows or inhibits their penetration into biofilms. Herein, we developed a polymer-bacteriophage nanoassembly with improved antimicrobial activity against *S. aureus* bacterial biofilms. We demonstrated that encapsulation of bacteriophages using functionalized cationic polymers retains infectivity of the bacteriophage toward planktonic bacteria. Moreover, these polymer-bacteriophage nanoassemblies showed improved antimicrobial and antibiofilm activity within the biofilm matrix. These promising preliminary results validate delivery of bacteriophage using polymers and provide a gateway to improve bacteriophage therapy.

6.2 Results and Discussion

6.2.1 Preparation and characterization of polymer-bacteriophage nanoassembly

We chose *Staphylococcus aureus* subsp. *aureus* bacteriophage (ATCC 23360-B1) for encapsulation as it targets *Staphylococcus aureus*, a common pathogen isolated from infected wounds.[25] Additionally, ATCC 23360-B1 has a relative broad host range,

allowing it to affect more *Staphylococcus aureus* strains. Moreover, a guanidinium-functionalized poly(oxanorbornene)imide polymer (PONI-C3-Guan, MW: 68000, PDI: 1.01) was chosen to encapsulate the bacteriophage, as it is cationic, non-toxic to mammalian cells, and has been demonstrated to encapsulate biomolecules.[26] The polymer-bacteriophage nanoassemblies were prepared by mixing the bacteriophage solution and the polymer solutions in ratios ranging from 68 ng: 9 x10^6 PFU to 680 ng: 9 x10^6 PFU for 60 min at ambient temperature (Figure 6. 1)

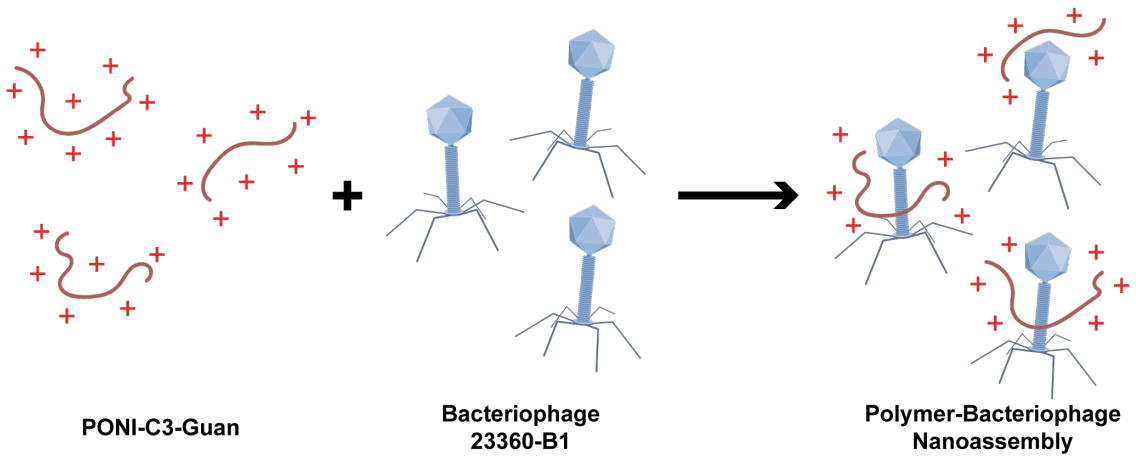

Figure 6. 1. Schematic depiction of the generation of the Polymer-Bacteriophage Nanoassembly.

The particle size of the bacteriophage (23360-B1), polymer (PONI-C3-Guan), and polymer-bacteriophage nanoassemblies were first characterized using dynamic light scattering (DLS). As shown in Figure 6. 2, the particle size of 23360-B1 is ~180 nm, matching the size of most *S. aureus* bacteriophages measured using transmission electronic microscopy (TEM) reported in the literature.[27,28] Moreover, the PONI-C3-Guan forms ~ 90 nm particles in aqueous solution. Finally, the mixtures of the polymer and the bacteriophage prepared with ratios ranging from 136 ng: 9 x 10^6 PFU to 340 ng: 9 x 10^6 PFU form nanoassemblies and their particle sizes are all ~ 250 nm. The increased sizes suggests that the bacteriophages were successfully encapsulated by the polymer.

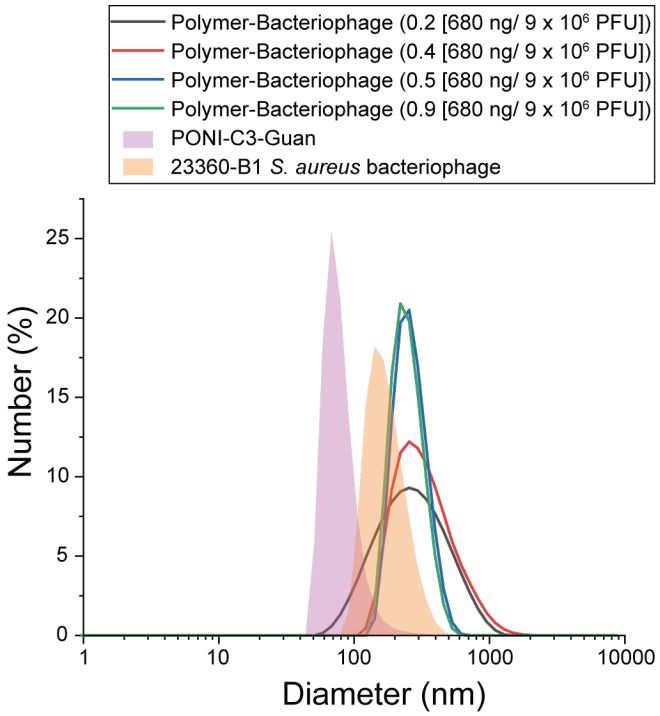

Figure 6. 2. Dynamic light scattering analysis of PONI-C3-Guan, bacteriophage (23360-B1) and the polymer-bacteriophage nanoassembly prepared with varied ratios of polymer to bacteriophage in Milli-Q water.

Additionally, the zeta potentials of the assemblies were monitored to validate the formation of the nanoassemblies. As show in Figure 6. 3, the surface charge of 23360-B1 is ~ -13 mV. The zeta potential demonstrated a concentration dependent shift towards positive surface charge with the addition of PONI-C3-Guan, presumably due to adsorption of the cationic polymer onto the anionic surface of the bacteriophage.[29] The zeta potential of the bacteriophage shifted to positive and finally became > 10 mV after the addition of 408 ng of PONI-C3-Guan to 9 x 10^6 PFU of 23360-B1. Current preliminary data suggest the formation of the polymer-bacteriophage nanoassembly. Further characterization including electrophoresis and transmission electronic microscopy (TEM) may be required to prove the formation of the nanoassemblies.

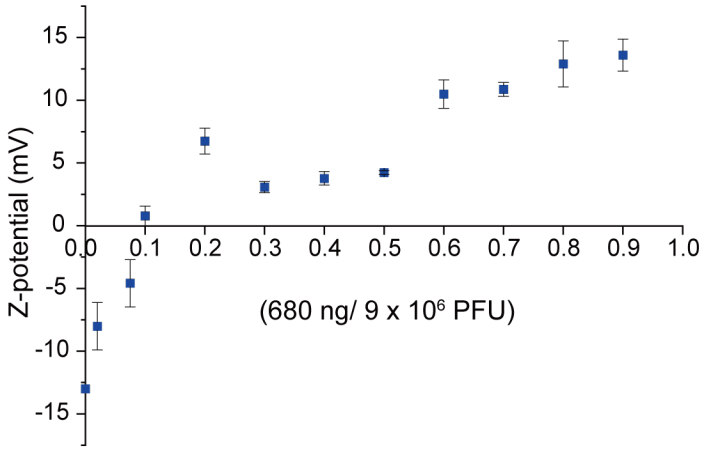

Figure 6. 3. Zeta potentials of the mixtures with various ratios of the bacteriophage and PONI-C3-Guan

6.2.2 Antimicrobial activity of polymer-bacteriophage nanoassembly against planktonic bacteria

We next examined the infectivity of the polymer-bacteriophage nanoassembly as surface modification of biomolecules often deactivates the biomolecules.[30] The infectivity of the polymer-bacteriophage nanoassembly was determined using a double agar overlay plaque assay.[31] The polymer-bacteriophage nanoassembly was first prepared by mixing 340 to 680 ng of PONI-C3-Guan to 9 x 10^6 PFU of 23360-B1, as these ratios lead to the formation of nanoassemblies with positive surface charges. Subsequently, these nanoassemblies were further serially diluted to up to 1: 10^6 and mixed with their bacteria host (*S. aureus*, ATCC-23360). As shown in Table 6. 1, the polymer-bacteriophage nanoassemblies formed similar number of plaques compared to the positive control, suggesting that they retained infectivity. However, we observed that the nanoassembly formulated with a higher polymer ratio showed reduced infectivity, presumably due to “over-encapsulation”. Additionally, PONI-C3-Gaun demonstrated no

antimicrobial activity toward *S. aureus* (Table 6. 2), further validating the retained infectivity of the nanoassemblies.

Table 6. 1. Photographs of the double agar overlay assay results of the polymer-bacteriophage nanoassemblies and the positive control (bacteriophage only)

	n*	0.9 n	0.8 n	0.5 n	Phage only
1: 10 (polymer 10^{-2} µM)	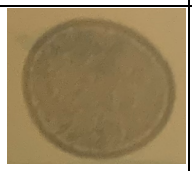	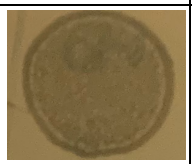	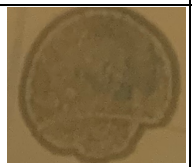	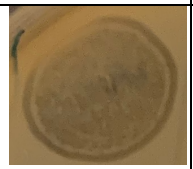	
1: 10^2 (polymer 10^{-3} µM)	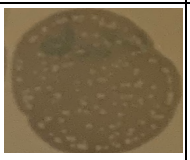	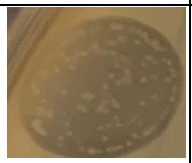	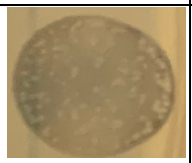	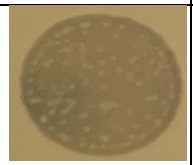	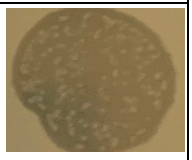
1: 10^3 (polymer 10^{-4} µM)	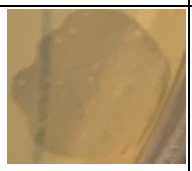	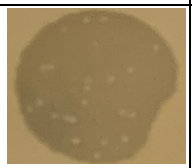	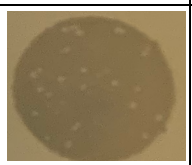	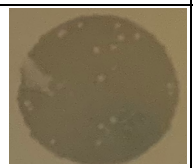	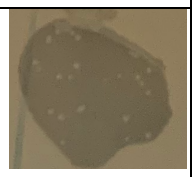
1: 10^4 (polymer 10^{-5} µM)	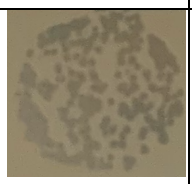	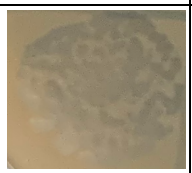	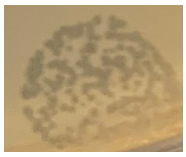	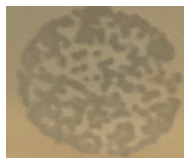	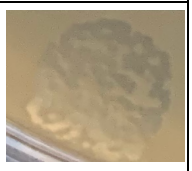
1: 10^5 (polymer 10^{-6} µM)	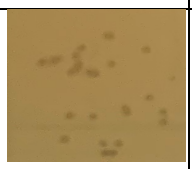	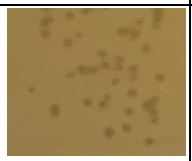	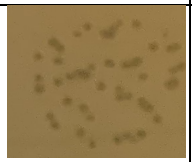	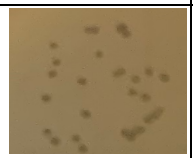	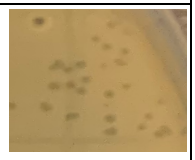
1: 10^6 (polymer 10^{-7} µM)	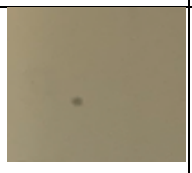	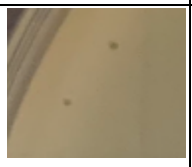	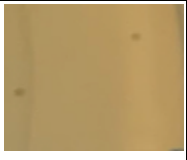		

n*: polymer/ bacteriophage = 680 ng/ 9 x 10^6 PFU

Table 6. 2. Photographs of the double agar overlay assay results of tPONI-C3-Guan and the negative control (PBS)

0 μM	0.05 μM	0.1 μM	0.25 μM	0.5 μM	1 μM
				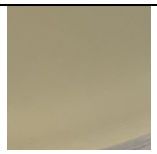	

6.2.3 Antimicrobial activity of polymer-bacteriophage nanoassembly against bacterial biofilms

After validating the infectivity of polymer-bacteriophage nanoassemblies, we used an alamarBlue[32] assay to assess antimicrobial activity of the nanoassemblies against *S. aureus* biofilms (ATCC-23360). The 2-day biofilms were treated with phosphate-buffered saline (PBS), the bacteriophage, the polymer-bacteriophage nanoassemblies, and PONI-C3-Guan for 12 hr, respectively. Phage treatments including the phage and the polymer-bacteriophage nanoassemblies were prepared using two concentrations (10^8 PFU/mL and 10^7 PFU/mL) with respect to the concentration of bacteriophage to explore multiplicity of infection (MOI) effect. As shown in Figure 6. 4, 23360-B1 shows negligible antimicrobial activity against its host, while nanoassemblies demonstrated noticeable antimicrobial activity and reduced viability of the bacteria up to 60%. This enhanced antimicrobial activity is presumably due to the overall positive surface charge of the nanoassemblies, which enables bacteriophage to further penetrate biofilms in a protected manner by an assembly formation with positively charged polymers. Their increased mobility within the biofilm matrix also improves antimicrobial activity. Moreover, nanoassembly treatments of lower MOI (10^7 PFU/mL) demonstrated better antimicrobial activity overall. In higher MOI condition (10^8 PFU/mL), we noticed that

bacteria had a higher viability after the treatment of nanoassemblies with a higher polymer to bacteriophage ratio. This could be due to their lower infectivity. The polymeric encapsulation inhibits the binding between of the phage and the receptor on the bacterial cell surface, as discussed in the previous section. Moreover, this phenomenon could result from the different mobility of the bacteriophage within biofilms and the coexistence pattern of bacteria and bacteriophage. Specifically, we have discussed that different ratios of PONI-C3-Guan and 23360-B1 form the nanoassemblies with varied surface charges (Figure 6. 3). The surface charge might be a critical factor for the mobility of bacteriophages within biofilm[24] and determines the time point of the beginning of the coexistence.[33] Additionally, the populations of the bacteria and bacteriophage in this system may exist in an oscillation pattern as a predator-prey cycle,[22] in which the viability is time-dependent rather than concentration-dependent. In other words, we might observe a reversed result at another time point, and a similar result after a full cycle period of the oscillation.

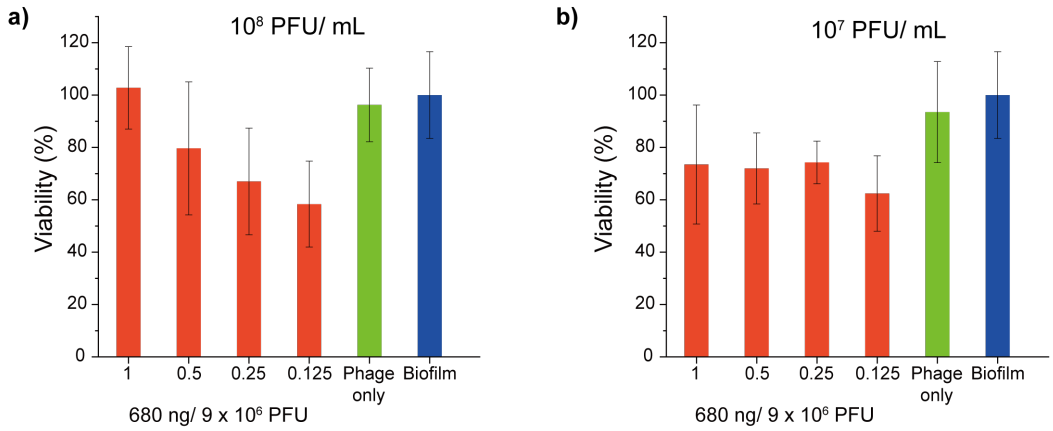

Figure 6. 4. Viabilities of the *S. aureus* within the biofilms after the treatment of 23360-B1 and the nanoassemblies prepared with varied ratio of PONI-C3-Guan and 23360-B1. The bacteriophage concentration in each treatment is a) 10^8 PFU/mL and b) 10^7 PFU/mL

Additionally, we used the safranin staining method[34] to quantify the biomass after the treatments. We noticed that the phage treatment increased the biomass in the system (Figure 6. 5). This could be due to the low adsorption of the bacteriophages onto their hosts, as the alamarBlue results indicate no reduced bacterial metabolism. On the other hand, the trapped phages in the EPS could also contribute to the biomass. Overall, all the phage treatments showed a low biomass removal. 23360-B1 may lack EPS-degrading enzymes to disperse bacterial biofilms.[35]

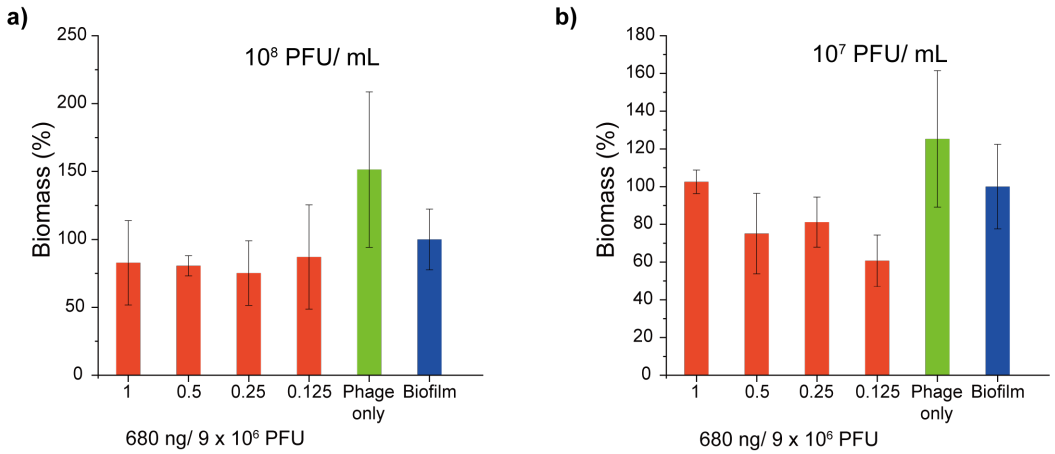

Figure 6. 5. Biomass of the *S. aureus* biofilms after the treatment of 23360-B1 and the nanoassemblies prepared with varied ratios of PONI-C3-Guan and 23360-B1. The bacteriophage concentration in each treatment is a) 10^8 PFU/mL and b) 10^7 PFU/mL

Finally, we demonstrated that the PONI-C3-Guan has negligible antimicrobial activity towards *S. aureus* ATCC-23360 biofilms (Figure 6. 6). In fact, PONI-C3-Guan slightly promoted the growth of the biofilms.

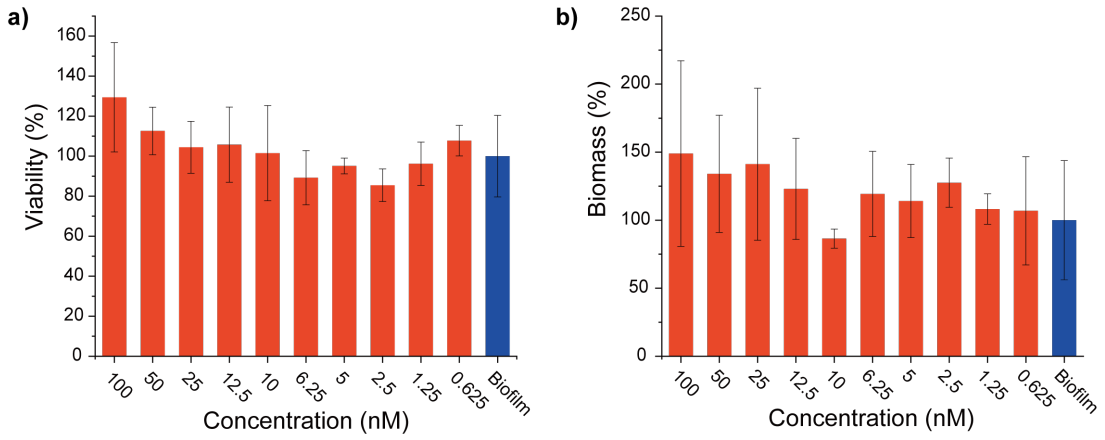

Figure 6. 6. a) Viability of bacteria within the *S. aureus* biofilms and b) biomass of the *S. aureus* biofilms after PONI-C3-Guan treatment.

6.3 Conclusion

In summary, I reported the preparation and preliminary characterization of the polymer-bacteriophage nanoassembly. This strategy retains the bacteriophage's infectivity towards its planktonic host. Additionally, these polymer-bacteriophage nanoassemblies demonstrated improved antimicrobial activity within the biofilm matrix. More importantly, this polymer-based delivery strategy is highly modular. Theoretically, PONI-C3-Guan can encapsulate bacteriophages with similar particle size and surface charge, improving antimicrobial activity of a wide range of bacteriophages against bacterial biofilms. Furthermore, bacteriophages can be encapsulated using other functional polymers to customize other properties such as improved shelf life and increased blood circulation time. Overall, this preliminary study provides evidence that polymer-bacteriophage nanoassemblies have the potential to improve phage therapy for the treatment for bacteria-related infections.

6.4 Experimental Section

6.4.1 Materials

All reagents and materials were purchased from Fisher Scientific or Sigma-Aldrich and used as received unless otherwise specified. Phosphate-buffered saline was purchased from HyClone. M9 minimum medium was purchased from Teknova. Tryptic soy broth (TSB) was purchased from Becton Dickinson. AlamarBlue cell viability reagent was purchased from Invitrogen. *S. aureus* (23360) and the bacteriophage (23360-B1) were kindly provided by Dr. Robin Patel at Mayo clinic.

6.4.2 Synthesis of PONI-C3-Guan

PONI-C3-guan and its monomer were synthesized according to the procedures reported in the literature.[26]

6.4.3 Preparation of polymer-bacteriophage nanoassembly

10 μL of PONI-C3-guan aqueous solution (1 μM to 0.1 μM) and 90 μL of 23360-B1 (10^8 PFU/ml) were added to a 7 mL vial with a stir bar. The mixture was then gently stirred for 60 min at ambient temperature. These solutions were directly used for characterization and antimicrobial use without further purification.

6.4.4 Characterization of polymer-bacteriophage nanoassembly

6.4.4.1 DLS

The hydrodynamic diameter of PONI-C3-Guan, the bacteriophage and the polymer-bacteriophage nanoassemblies were measured in triplicate using DLS (Malvern

Zetasizer). The solution was prepared by adding 20 μL of the polymer-bacteriophage solution to 980 μL of Milli-Q water.

6.4.4.2 Zeta potential

The zeta potentials of the bacteriophage and the polymer-bacteriophage nanoassemblies were measured in triplicate using a Malvern Zetasizer. The solution was prepared by adding 100 μL of the sample solution to 900 μM of 0.1x PBS.

6.4.5 Preparation of underlay and overlay agar

30 g TSB and 15 g bacteriological agar were added to 1000 mL Milli-Q water. This solution was then autoclaved and cooled to no less than 55°C. Subsequently, 18 mL of the cooled underlay agar solution was transferred to 100 mm petri dishes. The underlay agar plates were ready for use once the agar medium solidified.

The overlay agar was prepared by autoclaving a 500 mL Milli-Q water containing 15 g TSB and 2.75 g bacteriological agar. The solution was then cooled down to no less than 55°C and 5 mL of filtered 1 M $MgSO_4$ solution was added to the cooled solution. 3-4 mL of this solution was transferred to a sterilized culture tube.

6.4.6 Biofilm eradication

S. aureus (23360) was incubated overnight at 37°C with agitation (275 rpm) until the stationary phase was reached. The bacterial solution was then collected by centrifugation (3500 rpm, 5 min) and washed 3 times with sodium chloride (0.85%). The collected culture was diluted to 0.1 OD_{600} using TSB. Subsequently, the seeding solutions (100 μL) were added to each well of a 96-well clear flat-bottomed plate and incubated

under static conditions at room temperature. After 2 days, the seeding solutions were removed, and the biofilms were gently washed with PBS 3 times to remove planktonic bacteria. The biofilm in each well was then treated with 100 µL of 10^8 PFU/mL of the bacteriophage (23360-B1) for 12 h. The antimicrobial activity was evaluated using alamarBlue[32] and safranin[34] described below.

6.4.6.1 AlamarBlue assay

After the treatment, the biofilms were washed 3 times with PBS and 120 µL of alamarBlue cell viability reagent (10 v/v%, PBS solution) was added to each well and incubated for 1 h. Biofilm viability was determined by measuring fluorescence intensity (excitation: 560 nm; emission: 590 nm). Readings from the wells containing alamarBlue cell viability reagent (10 v/v%) alone were considered as the blank (I_{blank}), and readings from wells with untreated biofilms were used as growth controls ($I_{control}$). Biofilm viability was calculated using the equation below:

$$Biofilm\ viability\ (\%) = 100\% \times \frac{I_{sample} - I_{blank}}{I_{control} - I_{blank}}$$

6.4.6.2 Safranin

The safranin stock solution was prepared by dissolving 2.5 g safranin in 100 mL 95% ethanol. 10 mL of this stock solution was further diluted with DI water to 100 mL as a safranin working solution. 100 µL of the working solution was added to the biofilm in each well. After 10 min, all the biofilms were washed with DI water to remove non-bound safranin and allowed to dry for another 30 min. 100 mL of 33% glacial acetic acid aqueous solution was then added to the biofilm for releasing the safranin. Optical density at 530 nm was measured to determine the biomass.

6.5 References

1 Col, N. F.; O'Connor, R. W. Estimating Worldwide Current Antibiotic Usage: Report of Task Force 1. *Rev. Infect. Dis.* **1987**, *9*, S232–S243.

2 Blair, J. M. A.; Webber, M. A.; Baylay, A. J.; Ogbolu, D. O.; Piddock, L. J. V. Molecular Mechanisms of Antibiotic Resistance. *Nat. Rev. Microbiol.* **2015**, *13*, 42–51.

3 Aminov, R. A Brief History of the Antibiotic Era: Lessons Learned and Challenges for the Future. *Front. Microbiol.* **2010**, *1*, 134.

4 Levy, S. B. Active Efflux, a Common Mechanism for Biocide and Antibiotic Resistance. *J. Appl. Microbiol.* **2002**, *92*, 65S-71S.

5 Courvalin, P. Transfer of Antibiotic Resistance Genes between Gram-Positive and Gram-Negative Bacteria. *Antimicrob. Agents Chemother.* **1994**, *38*, 1447–1451.

6 James, G. A.; Swogger, E.; Wolcott, R.; Pulcini, E. deLancey; Secor, P.; Sestrich, J.; Costerton, J. W.; Stewart, P. S. Biofilms in Chronic Wounds. *Wound Repair Regen.* **2008**, *16*, 37–44.

7 Arciola, C. R.; Campoccia, D.; Speziale, P.; Montanaro, L.; Costerton, J. W. Biofilm Formation in Staphylococcus Implant Infections. A Review of Molecular Mechanisms and Implications for Biofilm-Resistant Materials. *Biomaterials* **2012**, *33*, 5967–5982.

8 Costerton, J. W.; Montanaro, L.; Arciola, C. R. Biofilm in Implant Infections: Its Production and Regulation. *Int. J. Artif. Organs* **2005**, *28*, 1062–1068.

9 Donlan, R. Biofilms and Device-Associated Infections. *Emerg. Infect. Dis.* **2001**, *7*, 277–281.

10 Lewis, K. Multidrug Tolerance of Biofilms and Persister Cells BT - Bacterial Biofilms. In; Romeo, T., Ed.; Springer Berlin Heidelberg: Berlin, Heidelberg, 2008; pp. 107–131.

11 Roberts, M. E.; Stewart, P. S. Modelling Protection from Antimicrobial Agents in Biofilms through the Formation of Persister Cells. *Microbiology* **2005**, *151*, 75–80.

12 Stewart, P. S.; William Costerton, J. Antibiotic Resistance of Bacteria in Biofilms. *Lancet* **2001**, *358*, 135–138.

13 Percival, S. L.; McCarty, S. M.; Lipsky, B. Biofilms and Wounds: An Overview of the Evidence. *Adv. Wound Care* **2014**, *4*, 373–381.

14 Franks, P. J.; Moffatt, C. J. Quality of Life Issues in Chronic Wound Management. *Br. J. Community Nurs.* **1999**, *4*, 283–289.

15 Sen, C. K.; Gordillo, G. M.; Roy, S.; Kirsner, R.; Lambert, L.; Hunt, T. K.; Gottrup, F.; Gurtner, G. C.; Longaker, M. T. Human Skin Wounds: A Major and Snowballing Threat to Public Health and the Economy. *Wound Repair Regen.* **2009**, *17*, 763–771.

16 Järbrink, K.; Ni, G.; Sönnergren, H.; Schmidtchen, A.; Pang, C.; Bajpai, R.; Car, J. The Humanistic and Economic Burden of Chronic Wounds: A Protocol for a Systematic Review. *Syst. Rev.* **2017**, *6*, 1–7.

17 Lu, T. K.; Koeris, M. S. The Next Generation of Bacteriophage Therapy. *Curr. Opin. Microbiol.* **2011**, *14*, 524–531.

18 Golkar, Z.; Bagasra, O.; Pace, D. G. Bacteriophage Therapy: A Potential Solution for the Antibiotic Resistance Crisis. *J. Infect. Dev. Ctries.* **2014**, *8*, 129–136.

19 Denou, E.; Bruttin, A.; Barretto, C.; Ngom-Bru, C.; Brüssow, H.; Zuber, S. T4 Phages against Escherichia Coli Diarrhea: Potential and Problems. *Virology* **2009**, *388*, 21–30.

20 Borysowski, J.; Górski, A. Is Phage Therapy Acceptable in the Immunocompromised Host? *Int. J. Infect. Dis.* **2008**, *12*, 466–471.

21 Harper, D. R.; Parracho, H. M. R. T.; Walker, J.; Sharp, R.; Hughes, G.; Werthén, M.; Lehman, S.; Morales, S. Bacteriophages and Biofilms. *Antibiotics*, **2014**, *3*, 270–284.

22 Simmons, M.; Drescher, K.; Nadell, C. D.; Bucci, V. Phage Mobility Is a Core Determinant of Phage-Bacteria Coexistence in Biofilms. *ISME J.* **2018**, *12*, 531–543.

23 Parasion, S.; Kwiatek, M.; Gryko, R.; Mizak, L.; Malm, A. Bacteriophages as an Alternative Strategy for Fighting Biofilm Development. *Polish J. Microbiol.* **2014**, *63*, 137–145.

24 Li, X.; Yeh, Y. C.; Giri, K.; Mout, R.; Landis, R. F.; Prakash, Y. S.; Rotello, V. M. Control of Nanoparticle Penetration into Biofilms through Surface Design. *Chem. Commun.* **2015**, *51*, 282–285.

25 Pastar, I.; Nusbaum, A. G.; Gil, J.; Patel, S. B.; Chen, J.; Valdes, J.; Stojadinovic, O.; Plano, L. R.; Tomic-Canic, M.; Davis, S. C. Interactions of Methicillin Resistant Staphylococcus Aureus USA300 and Pseudomonas Aeruginosa in Polymicrobial Wound Infection. *PLoS One* **2013**, *8*, 1–11.

26 Lee, Y.-W.; Luther, D. C.; Goswami, R.; Jeon, T.; Clark, V.; Elia, J.; Gopalakrishnan, S.; Rotello, V. M. Direct Cytosolic Delivery of Proteins through Coengineering of Proteins and Polymeric Delivery Vehicles. *J. Am. Chem. Soc.* **2020**, *142*, 4349–4355.

27 Xia, G.; Wolz, C. Phages of Staphylococcus Aureus and Their Impact on Host Evolution. *Infect. Genet. Evol.* **2014**, *21*, 593–601.

28 Chang, Y.; Shin, H.; Lee, J.-H.; Park, C. J.; Paik, S.-Y.; Ryu, S. Isolation and Genome Characterization of the Virulent Staphylococcus Aureus Bacteriophage SA97. *Viruses* **2015**, *7*, 5225–5242.

29 Yata, T.; Lee, K.-Y.; Dharakul, T.; Songsivilai, S.; Bismarck, A.; Mintz, P. J.; Hajitou, A. Hybrid Nanomaterial Complexes for Advanced Phage-Guided Gene Delivery. *Mol. Ther. Nucleic Acids* **2014**, *3*, e185–e185.

30 Kim, K.-P.; Cha, J.-D.; Jang, E.-H.; Klumpp, J.; Hagens, S.; Hardt, W.-D.; Lee, K.-Y.; Loessner, M. J. PEGylation of Bacteriophages Increases Blood Circulation Time and Reduces T-Helper Type 1 Immune Response. *Microb. Biotechnol.* **2008**, *1*, 247–257.

31 Kropinski, A. M.; Mazzocco, A.; Waddell, T. E.; Lingohr, E.; Johnson, R. P. Enumeration of Bacteriophages by Double Agar Overlay Plaque Assay BT - Bacteriophages: Methods and Protocols, Volume 1: Isolation, Characterization, and Interactions. In; Clokie, M. R. J.; Kropinski, A. M., Eds.; Humana Press: Totowa, NJ, 2009; pp. 69–76.

32 Pettit, R. K.; Weber, C. A.; Pettit, G. R. Application of a High Throughput Alamar Blue Biofilm Susceptibility Assay to Staphylococcus Aureus Biofilms. *Ann. Clin. Microbiol. Antimicrob.* **2009**, *8*, 28.

33 Tait, K.; Skillman, L. C.; Sutherland, I. W. The Efficacy of Bacteriophage as a Method of Biofilm Eradication. *Biofouling* **2002**, *18*, 305–311.

34 Ommen, P.; Zobek, N.; Meyer, R. L. Quantification of Biofilm Biomass by Staining: Non-Toxic Safranin Can Replace the Popular Crystal Violet. *J. Microbiol. Methods* **2017**, *141*, 87–89.

35 Lu, T. K.; Collins, J. J. Dispersing Biofilms with Engineered Enzymatic Bacteriophage. *Proc. Natl. Acad. Sci.* **2007**, *104*, 11197–11202.

CHAPTER 7

7. CONCLUSION AND OUTLOOK

Integration of polymers with therapeutic payloads provides effective treatment of recalcitrant bacterial biofilms. In this dissertation, I have demonstrated that engineered polymers (PONI-GMT) stabilize a library of antimicrobial phytochemicals in relevant biomedical conditions. Their antimicrobial activities are enhanced through this delivery strategy, owing to the careful design of the polymer. Additionally, this polymer-based nanoemulsion platform is promising for monitoring dynamics of the nanomaterial in bacterial biofilms. I have demonstrated a preliminary correlation of polymer structure and penetration profile using engineered polymers (PONI-GMT and PONI-AMT) coupled with confocal microscopy imaging and quantitative analysis. In related work, natural polymers are particularly promising materials for delivery of therapeutics, as they are intrinsically biocompatible and biodegradable. I have demonstrated that gelatin-based nanoemulsions effectively reduce bacterial burden and promote wound healing *in vivo*. Finally, I utilized another related engineered polymer (PONI-C3-Guan) to develop a polymer-bacteriophage nanoassembly. The polymeric encapsulation alters the surface charge of the raw bacteriophage and thus improves its antimicrobial activity against the corresponding biofilm. Overall, polymer-based delivery strategies present promising approaches to develop treatments for bacterial biofilm infections.

Although I have presented evidence showing that polymers aid in combating bacterial infections, all the reported nanomaterials still need further engineering prior to their use in clinical trials. To this end, a fundamental study about the interactions of the nanoemulsion and biofilm is necessary. I have developed a platform for probing the

nanoemulsions' dynamics within the biofilm in Chapter 5. A follow-up study using this platform in other strains of bacterial biofilms could contribute to the future design of the nanoemulsion. Additionally, biosafety of these nanomaterials is still a matter of concern, even though I have implemented a delivery strategy using only GRAS materials. Bacteriophages in Chapter 6 especially need attention as they are reported to trigger immune responses. This issue might be resolved by integrating ethylene glycol or zwitterionic structures into the polymer. Future work in pursuit of further understanding of the system as well as alternative antimicrobial strategies demonstrated in this dissertation should address these concerns.

BIBLIOGRAPHY

Aggarwal, K. K.; Khanuja, S. P. S.; Ahmad, A.; Santha Kumar, T. R.; Gupta, V. K.; Kumar, S.; Khanuja, Ł. S. P. S.; Ahmad, A.; Kumar, T. R. S.; Gupta, V. K.; *et al.* Antimicrobial Activity Profiles of the Two Enantiomers of Limonene and Carvone Isolated from the Oils of Mentha Spicata and Anethum Sowa. *Flavour Fragr. J.* **2002**, *17*, 59–63.

Ahmad, I.; Beg, A. Z. Antimicrobial and Phytochemical Studies on 45 Indian Medicinal Plants against Multi-Drug Resistant Human Pathogens. *J. Ethnopharmacol.* **2001**, *74*, 113–123.

Ali, S. M.; Khan, A. A.; Ahmed, I.; Musaddiq, M.; Ahmed, K. S.; Polasa, H.; Rao, L. V.; Habibullah, C. M.; Sechi, L. A.; Ahmed, N. Antimicrobial Activities of Eugenol and Cinnamaldehyde against the Human Gastric Pathogen Helicobacter Pylori. *Ann. Clin. Microbiol. Antimicrob.* **2005**, *4*, 20–26.

Aminov, R. A Brief History of the Antibiotic Era: Lessons Learned and Challenges for the Future. *Front. Microbiol.* **2010**, *1*, 134.

Anderl, J. N.; Franklin, M. J.; Stewart, P. S. Role of Antibiotic Penetration Limitation in Klebsiella Pneumoniae Biofilm Resistance to Ampicillin and Ciprofloxacin. *Antimicrob. Agents Chemother.* **2000**, *44*, 1818–1824.

Anwer, M. K.; Jamil, S.; Ibnouf, E. O.; Shakeel, F. Enhanced Antibacterial Effects of Clove Essential Oil by Nanoemulsion. *J. Oleo Sci.* **2014**, *63*, 347–354.

Arciola, C. R.; Campoccia, D.; Montanaro, L. Implant Infections: Adhesion, Biofilm Formation and Immune Evasion. *Nat. Rev. Microbiol.* **2018**, *16*, 397–409.

Arndt-Jovin, D. J.; Jovin, T. M. Chapter 16 Fluorescence Labeling and Microscopy of DNA. In *Fluorescence Microscopy of Living Cells in Culture Part B. Quantitative Fluorescence Microscopy—Imaging and Spectroscopy*; Taylor, D. L.; Wang, Y.-L. B. T.-M. in C. B., Eds.; Academic Press, 1989; Vol. 30, pp. 417–448.

Au, V.; Madison, S. A. Effects of Singlet Oxygen on the Extracellular Matrix Protein Collagen: Oxidation of the Collagen Crosslink Histidinohydroxylysinonorleucine and Histidine. *Arch. Biochem. Biophys.* **2000**, *384*, 133–142.

Baratta, M. T.; Dorman, H. J. D.; Deans, S. G.; Biondi, D. M.; Ruberto, G. Chemical Composition, Antimicrobial and Antioxidative Activity of Laurel, Sage, Rosemary, Oregano and Coriander Essential Oils. *J. Essent. Oil Res.* **1998**, *10*, 618–627.

Beyth, N.; Houri-Haddad, Y.; Domb, A.; Khan, W.; Hazan, R. Alternative Antimicrobial Approach: Nano-Antimicrobial Materials. *Evidence-Based Complement. Altern. Med.* **2015**, *2015*, 1–16.

Bjarnsholt, T. The Role of Bacterial Biofilms in Chronic Infections. *APMIS* **2013**, *121*, 1–58.

Blair, J. M. A.; Webber, M. A.; Baylay, A. J.; Ogbolu, D. O.; Piddock, L. J. V. Molecular Mechanisms of Antibiotic Resistance. *Nat. Rev. Microbiol.* **2015**, *13*, 42–51.

Borges, A.; Serra, S.; Abreu, A. C.; Saavedra, M. J.; Simões, M.; Borges, A.; Serra, S.; Abreu, A. C.; Saavedra, M. J. Evaluation of the Effects of Selected Phytochemicals on Quorum Sensing Inhibition and in Vitro Cytotoxicity. *Biofouling* **2014**, *30*, 183–195.

Borysowski, J.; Górski, A. Is Phage Therapy Acceptable in the Immunocompromised Host? *Int. J. Infect. Dis.* **2008**, *12*, 466–471.

Castilho, P. C.; Savluchinske-Feio, S.; Weinhold, T. S.; Gouveia, S. C. Evaluation of the Antimicrobial and Antioxidant Activities of Essential Oils, Extracts and Their Main Components from Oregano from Madeira Island, Portugal. *Food Control* **2012**, *23*, 552–558.

Ceri, H.; Olson, M. E.; Stremick, C.; Read, R. R.; Morck, D.; Buret, A. The Calgary Biofilm Device: New Technology for Rapid Determination of Antibiotic Susceptibilities of Bacterial Biofilms. *J. Clin. Microbiol.* **1999**, *37*, 1771–1776.

Chandra Sekhara Rao, G.; Satish Kumar, M.; Mathivanan, N.; Bhanoji Rao, M. E. Nanosuspensions as the Most Promising Approach in Nanoparticulate Drug Delivery Systems. *Pharmazie* **2004**, *59*, 5–9.

Chang, Y.; Shin, H.; Lee, J.-H.; Park, C. J.; Paik, S.-Y.; Ryu, S. Isolation and Genome Characterization of the Virulent Staphylococcus Aureus Bacteriophage SA97. *Viruses* **2015**, *7*, 5225–5242.

Chang, Y.; McLandsborough, L.; McClements, D. J. Physicochemical Properties and Antimicrobial Efficacy of Carvacrol Nanoemulsions Formed by Spontaneous Emulsification. *J. Agric. Food Chem.* **2013**, *61*, 8906–8913.

Chen, H.; Davidson, P. M.; Zhong, Q. Impacts of Sample Preparation Methods on Solubility and Antilisterial Characteristics of Essential Oil Components in Milk. *Appl. Environ. Microbiol.* **2013**, *80*, 907–916.

Cheng, R.; Feng, F.; Meng, F.; Deng, C.; Feijen, J.; Zhong, Z. Glutathione-Responsive Nano-Vehicles as a Promising Platform for Targeted Intracellular Drug and Gene Delivery. *J. Control. Release* **2011**, *152*, 2–12.

Cooper, R. A.; Bjarnsholt, T.; Alhede, M. Biofilms in Wounds: A Review of Present Knowledge. *J. Wound Care* **2014**, *23*, 570–582.

Costerton, J. W.; Montanaro, L.; Arciola, C. R. Biofilm in Implant Infections: Its Production and Regulation. *Int. J. Artif. Organs* **2005**, *28*, 1062–1068.

Courvalin, P. Transfer of Antibiotic Resistance Genes between Gram-Positive and Gram-Negative Bacteria. *Antimicrob. Agents Chemother.* **1994**, *38*, 1447–1451.

Cowan, M. M. Plant Products as Antimicrobial Agents. *Clin. Microbiol. Rev.* **1999**, *12*, 564–582.

Craig, W. A.; Welling, P. G. Protein Binding of Antimicrobials: Clinical Pharmacokinetic and Therapeutic Implications. *Clin. Pharmacokinet.* **1977**, *2*, 252–268.

Daddi Oubekka, S.; Briandet, R.; Fontaine-Aupart, M.-P.; Steenkeste, K. Correlative Time-Resolved Fluorescence Microscopy To Assess Antibiotic Diffusion-Reaction in Biofilms. *Antimicrob. Agents Chemother.* **2012**, *56*, 3349–3358.

Das, D.; Srinivasan, S.; Kelly, A. M.; Chiu, D. Y.; Daugherty, B. K.; Ratner, D. M.; Stayton, P. S.; Convertine, A. J. RAFT Polymerization of Ciprofloxacin Prodrug Monomers for the Controlled Intracellular Delivery of Antibiotics. *Polym. Chem.* **2016**, *7*, 826–837.

Das, K.; Tiwari, R. K. S.; Shrivastava, D. K. Techniques for Evaluation of Medicinal Plant Products as Antimicrobial Agent : Current Methods and Future Trends. *J. Med. Plants Res.* **2010**, *4*, 104–111.

Davies, J.; Spiegelman, G. B.; Yim, G. The World of Subinhibitory Antibiotic Concentrations. *Curr. Opin. Microbiol.* **2006**, *9*, 445–453.

del Pozo, J. L.; Patel, R. The Challenge of Treating Biofilm-Associated Bacterial Infections. *Clin. Pharmacol. Ther.* **2007**, *82*, 204–209.

DeLeon, S.; Clinton, A.; Fowler, H.; Everett, J.; Horswill, A. R.; Rumbaugh, K. P. Synergistic Interactions of Pseudomonas Aeruginosa and Staphylococcus Aureus in an In Vitro Wound Model. *Infect. Immun.* **2014**, *82*, 4718–4728.

Denou, E.; Bruttin, A.; Barretto, C.; Ngom-Bru, C.; Brüssow, H.; Zuber, S. T4 Phages against Escherichia Coli Diarrhea: Potential and Problems. *Virology* **2009**, *388*, 21–30.

Diaz, G.; Melis, M.; Batetta, B.; Angius, F.; Falchi, A. M. Hydrophobic Characterization of Intracellular Lipids in Situ by Nile Red Red/Yellow Emission Ratio. *Micron* **2008**, *39*, 819–824.

Dickinson, E. Hydrocolloids as Emulsifiers and Emulsion Stabilizers. *Food Hydrocoll.* **2009**, *23*, 1473–1482.

Djeussi, D. E.; Noumedem, J. A. K.; Seukep, J. A.; Fankam, A. G.; Voukeng, I. K.; Tankeo, S. B.; Nkuete, A. H. L.; Kuete, V. Antibacterial Activities of Selected Edible Plants Extracts against Multidrug-Resistant Gram-Negative Bacteria. *BMC Complement. Altern. Med.* **2013**, *13*, 164–171.

Donlan, R. Biofilms and Device-Associated Infections. *Emerg. Infect. Dis.* **2001**, *7*, 277–281.

Donsì, F.; Annunziata, M.; Vincensi, M.; Ferrari, G. Design of Nanoemulsion-Based Delivery Systems of Natural Antimicrobials: Effect of the Emulsifier. *J. Biotechnol.* **2012**, *159*, 342–350.

Dorman, H. J. D.; Deans, S. G. Antimicrobial Agents from Plants: Antibacterial Activity of Plant Volatile Oils. *J. Appl. Microbiol.* **2000**, *88*, 308–316.

Drenkard, E.; Ausubel, F. M. Pseudomonas Biofilm Formation and Antibiotic Resistance Are Linked to Phenotypic Variation. *Nature* **2002**, *416*, 740–743.

Duncan, B.; Li, X.; Landis, R. F.; Kim, S. T.; Gupta, A.; Wang, L.-S. S.; Ramanathan, R.; Tang, R.; Boerth, J. A.; Rotello, V. M. Nanoparticle-Stabilized Capsules for the Treatment of Bacterial Biofilms. *ACS Nano* **2015**, *9*, 7775–7782.

Eckert, R.; He, J.; Yarbrough, D. K.; Qi, F.; Anderson, M. H.; Shi, W. Targeted Killing of Streptococcus Mutans by a Pheromone-Guided "Smart" Antimicrobial Peptide. *Antimicrob. Agents Chemother.* **2006**, *50*, 3651–3657.

Elzoghby, A. O. Gelatin-Based Nanoparticles as Drug and Gene Delivery Systems: Reviewing Three Decades of Research. *J. Control. Release* **2013**, *172*, 1075–1091.

Etman, M.; Amin, M.; Nada, A. H.; Shams-Eldin, M.; Salama, O. Emulsions and Rectal Formulations Containing Myrrh Essential Oil for Better Patient Compliance. *Drug Discov. Ther.* **2011**, *5*, 150–156.

Farzaei, M. H.; Bahramsoltani, R.; Abbasabadi, Z.; Rahimi, R. A Comprehensive Review on Phytochemical and Pharmacological Aspects of Elaeagnus Angustifolia L. *J. Pharm. Pharmacol.* **2015**, *67*, 1467–1480.

Fazli, M.; Bjarnsholt, T.; Kirketerp-Møller, K.; Jørgensen, B.; Andersen, A. S.; Krogfelt, K. A.; Givskov, M.; Tolker-Nielsen, T. Nonrandom Distribution of Pseudomonas Aeruginosa and Staphylococcus Aureus in Chronic Wounds. *J. Clin. Microbiol.* **2009**, *47*, 4084–4089.

Flemming, H.; Wingender, J. The Biofilm Matrix. *Nat. Rev. Microbiol.* **2010**, *8*, 623–633.

Flemming, H.-C.; Wingender, J.; Szewzyk, U.; Steinberg, P.; Rice, S. A.; Kjelleberg, S. Biofilms: An Emergent Form of Bacterial Life. *Nat. Rev. Microbiol.* **2016**, *14*, 563–575.

Franks, P. J.; Moffatt, C. J. Quality of Life Issues in Chronic Wound Management. *Br. J. Community Nurs.* **1999**, *4*, 283–289.

Freire Rocha Caldas, G.; Araújo, A. V.; Albuquerque, G. S.; Silva-Neto, J. D. C.; Costa-Silva, J. H.; De Menezes, I. R. A.; Leite, A. C. L.; Da Costa, J. G. M.; Wanderley, A. G.; Caldas, G. F. R.; *et al.* Repeated-Doses Toxicity Study of the Essential Oil of Hyptis Martiusii Benth. (Lamiaceae) in Swiss Mice. *Evidence-Based Complement. Altern. Med.* **2013**, *2013*, No. 856168.

Fulaz, S.; Vitale, S.; Quinn, L.; Casey, E. Nanoparticle–Biofilm Interactions: The Role of the EPS Matrix. *Trends Microbiol.* **2019**, *27*, 915–926.

Gèze, A.; Putaux, J.-L.; Choisnard, L.; Jéhan, P.; Wouessidjewe, D. Long-Term Shelf Stability of Amphiphilicβ-Cyclodextrin Nanosphere Suspensions Monitored by Dynamic Light Scattering and Cryo-Transmission Electron Microscopy. *J. Microencapsul.* **2004**, *21*, 607–613.

Giacometti, A.; Cirioni, O.; Schimizzi, A. M.; Del Prete, M. S.; Barchiesi, F.; D'Errico, M. M.; Petrelli, E.; Scalise, G. Epidemiology and Microbiology of Surgical Wound Infections. *J. Clin. Microbiol.* **2000**, *38*, 918–922.

Golkar, Z.; Bagasra, O.; Pace, D. G. Bacteriophage Therapy: A Potential Solution for the Antibiotic Resistance Crisis. *J. Infect. Dev. Ctries.* **2014**, *8*, 129–136.

Gomes, C.; Moreira, R. G.; Castell-Perez, E. Poly (DL-Lactide-Co-Glycolide) (PLGA) Nanoparticles with Entrapped Trans-Cinnamaldehyde and Eugenol for Antimicrobial Delivery Applications. *J. Food Sci.* **2011**, *76*, 16–24.

Guarda, A.; Rubilar, J. F.; Miltz, J.; Galotto, M. J. The Antimicrobial Activity of Microencapsulated Thymol and Carvacrol. *Int. J. Food Microbiol.* **2011**, *146*, 144–150.

Gupta, A.; Landis, R. F.; Rotello, V. M. Nanoparticle-Based Antimicrobials: Surface Functionality Is Critical. *F1000Research* **2016**, *5*, 364.

Hall-stoodley, L.; Stoodley, P. Evolving Concepts in Biofilm Infections. *Cell. Microbiol.* **2009**, *11*, 1034–1043.

Hammer, K. A.; Carson, C. F.; Riley, T. V. Antimicrobial Activity of Essential Oils and Other Plant Extracts. *J. Appl. Microbiol.* **1999**, *86*, 985–990.

Harper, D. R.; Parracho, H. M. R. T.; Walker, J.; Sharp, R.; Hughes, G.; Werthén, M.; Lehman, S.; Morales, S. Bacteriophages and Biofilms. *Antibiotics*, **2014**, *3*, 270–284.

Harper, R. A.; Carpenter, G. H.; Proctor, G. B.; Harvey, R. D.; Gambogi, R. J.; Geonnotti, A. R.; Hider, R.; Jones, S. A. Diminishing Biofilm Resistance to Antimicrobial

Nanomaterials through Electrolyte Screening of Electrostatic Interactions. *Colloids Surfaces B Biointerfaces* **2019**, *173*, 392–399.

Harrison, J. J.; Stremick, C. A.; Turner, R. J.; Allan, N. D.; Olson, M. E.; Ceri, H. Microtiter Susceptibility Testing of Microbes Growing on Peg Lids: A Miniaturized Biofilm Model for High-Throughput Screening. *Nat. Protoc.* **2010**, *5*, 1236–1254.

Iannitelli, A.; Grande, R.; Di Stefano, A.; Di Giulio, M.; Sozio, P.; Bessa, L. J.; Laserra, S.; Paolini, C.; Protasi, F.; Cellini, L. Potential Antibacterial Activity of Carvacrol-Loaded Poly(DL-Lactide-Co-Glycolide) (PLGA) Nanoparticles against Microbial Biofilm. *Int. J. Mol. Sci.* **2011**, *12*, 5039–5051.

Ikuma, K.; Decho, A. W.; Lau, B. L. T. When Nanoparticles Meet Biofilms - Interactions Guiding the Environmental Fate and Accumulation of Nanoparticles. *Front. Microbiol.* **2015**, *6*, 1–6.

James, G. A.; Swogger, E.; Wolcott, R.; Pulcini, E. deLancey; Secor, P.; Sestrich, J.; Costerton, J. W.; Stewart, P. S. Biofilms in Chronic Wounds. *Wound Repair Regen.* **2008**, *16*, 37–44.

Järbrink, K.; Ni, G.; Sönnergren, H.; Schmidtchen, A.; Pang, C.; Bajpai, R.; Car, J. The Humanistic and Economic Burden of Chronic Wounds: A Protocol for a Systematic Review. *Syst. Rev.* **2017**, *6*, 1–7.

Jarvis, W. R.; Martone, W. J. Predominant Pathogens in Hospital Infections. *J. Antimicrob. Chemother.* **1992**, *29*, 19–24.

Kamaly, N.; Yameen, B.; Wu, J.; Farokhzad, O. C. Degradable Controlled-Release Polymers and Polymeric Nanoparticles: Mechanisms of Controlling Drug Release. *Chem. Rev.* **2016**, *116*, 2602–2663.

Karygianni, L.; Ren, Z.; Koo, H.; Thurnheer, T. Biofilm Matrixome: Extracellular Components in Structured Microbial Communities. *Trends Microbiol.* **2020**, *28*, 668–681.

Kataoka, K.; Harada, A.; Nagasaki, Y. Block Copolymer Micelles for Drug Delivery: Design, Characterization and Biological Significance. *Adv. Drug Deliv. Rev.* **2001**, *47*, 113–131.

Kim, C. K.; Karau, M. J.; Greenwood-Quaintance, K. E.; Tilahun, A. Y.; Krogman, A.; David, C. S.; Pritt, B. S.; Patel, R.; Rajagopalan, G. Superantigen-Producing Staphylococcus Aureus Elicits Systemic Immune Activation in a Murine Wound Colonization Model. *Toxins (Basel).* **2015**, *7*, 5308–5319.

Kim, K.-P.; Cha, J.-D.; Jang, E.-H.; Klumpp, J.; Hagens, S.; Hardt, W.-D.; Lee, K.-Y.; Loessner, M. J. PEGylation of Bacteriophages Increases Blood Circulation Time and Reduces T-Helper Type 1 Immune Response. *Microb. Biotechnol.* **2008**, *1*, 247–257.

Koser, S. A.; Chinn, B. D.; Saunders, F. Gelatin as a Source of Growth-Promoting Substances for Bacteria. *J. Bacteriol.* **1938**, *36*, 57–65.

Kreydiyyeh, S. I.; Usta, J.; Copti, R. Effect of Cinnamon, Clove and Some of Their Constituents on the Na+-K+-ATPase Activity and Alanine Absorption in the Rat Jejunum. *Food Chem. Toxicol.* **2000**, *38*, 755–762.

Kropinski, A. M.; Mazzocco, A.; Waddell, T. E.; Lingohr, E.; Johnson, R. P. Enumeration of Bacteriophages by Double Agar Overlay Plaque Assay BT - Bacteriophages: Methods and Protocols, Volume 1: Isolation, Characterization, and Interactions. In; Clokie, M. R. J.; Kropinski, A. M., Eds.; Humana Press: Totowa, NJ, 2009; pp. 69–76.

Lambert, R. J. W.; Skandamis, P. N.; Coote, P. J.; Nychas, G.-J. E. E. A Study of the Minimum Inhibitory Concentration and Mode of Action of Oregano Essential Oil, Thymol and Carvacrol. *J. Appl. Microbiol.* **2001**, *91*, 453–462.

Landis, R. F.; Gupta, A.; Lee, Y.-W.; Wang, L.-S.; Golba, B.; Couillaud, B.; Ridolfo, R.; Das, R.; Rotello, V. M. Cross-Linked Polymer-Stabilized Nanocomposites for the Treatment of Bacterial Biofilms. *ACS Nano* **2017**, *11*, 946–952.

Landis, R. F.; Li, C.-H.; Gupta, A.; Lee, Y.-W. W.; Yazdani, M.; Rotello, V. M.; Ngernyuang, N.; Altinbasak, I.; Mansoor, S.; Khichi, M. A. S. S.; *et al.* Biodegradable Nanocomposite Antimicrobials for the Eradication of Multidrug-Resistant Bacterial Biofilms without Accumulated Resistance. *J. Am. Chem. Soc.* **2018**, *140*, 6176–6182.

Lebeaux, D.; Chauhan, A.; Rendueles, O.; Beloin, C. From in Vitro to in Vivo Models of Bacterial Biofilm-Related Infections. *Pathogens* **2013**, *2*, 288–356.

Lebeaux, D.; Ghigo, J.-M.; Beloin, C. Biofilm-Related Infections: Bridging the Gap between Clinical Management and Fundamental Aspects of Recalcitrance toward Antibiotics. *Microbiol. Mol. Biol. Rev.* **2014**, *78*, 510–543.

Lee, Y.-W.; Luther, D. C.; Goswami, R.; Jeon, T.; Clark, V.; Elia, J.; Gopalakrishnan, S.; Rotello, V. M. Direct Cytosolic Delivery of Proteins through Coengineering of Proteins and Polymeric Delivery Vehicles. *J. Am. Chem. Soc.* **2020**, *142*, 4349–4355.

Leite, A. M.; Lima, E. D. O.; Souza, E. L. De; De, M. Inhibitory Effect of β -Pinene , α -Pinene and Eugenol on the Growth of Potential Infectious Endocarditis Causing Gram-Positive Bacteria. *Rev. Bras. Cienc. Farm.* **2007**, *43*, 121–126.

Levic, J.; Cabarkapa, I.; Todorovic, G.; Pavkoc, S.; Sredanovic, S.; Coghill-Galonja, T.; Kostadinovic, L. In Vitro Antibacterial Activity of Essential Oils from Plant Family Lamiaceae. *Rom. Biotechnol. Lett.* **2011**, *16*, 6034–6041.

Levy, S. B. Active Efflux, a Common Mechanism for Biocide and Antibiotic Resistance. *J. Appl. Microbiol.* **2002**, *92*, 65S-71S.

Lewis, K. Multidrug Tolerance of Biofilms and Persister Cells BT - Bacterial Biofilms. In; Romeo, T., Ed.; Springer Berlin Heidelberg: Berlin, Heidelberg, 2008; pp. 107–131.

Li, X.; Yeh, Y. C.; Giri, K.; Mout, R.; Landis, R. F.; Prakash, Y. S.; Rotello, V. M. Control of Nanoparticle Penetration into Biofilms through Surface Design. *Chem. Commun.* **2015**, *51*, 282–285.

Lin, L.; Cui, H.; Zhou, H.; Zhang, X.; Bortolini, C. Nanoliposomes Containing Eucalyptus Citriodora as Antibiotic with Specific Antimicrobial Activity. *Chem. Commun.* **2015**, *51*, 2653–2655.

Ling, L. L.; Schneider, T.; Peoples, A. J.; Spoering, A. L.; Engels, I.; Conlon, B. P.; Mueller, A.; Schaberle, T. F.; Hughes, D. E.; Epstein, S.; *et al.* A New Antibiotic Kills Pathogens without Detectable Resistance. *Nature* **2015**, *517*, 455–459.

Liu, L.; Xu, K.; Wang, H.; Jeremy Tan, P. K.; Fan, W.; Venkatraman, S. S.; Li, L.; Yang, Y.-Y. Self-Assembled Cationic Peptide Nanoparticles as an Efficient Antimicrobial Agent. *Nat. Nanotechnol.* **2009**, *4*, 457–463.

Liu, X.; Wang, Z.; Feng, X.; Bai, E.; Xiong, Y.; Zhu, X.; Shen, B.; Duan, Y.; Huang, Y. Platensimycin-Encapsulated Poly(Lactic-Co-Glycolic Acid) and Poly(Amidoamine) Dendrimers Nanoparticles with Enhanced Anti-Staphylococcal Activity in Vivo. *Bioconjug. Chem.* **2020**, *31*, 1425–1437.

Liu, Y.; Shi, L.; Su, L.; Van der Mei, H. C.; Jutte, P. C.; Ren, Y.; Busscher, H. J. Nanotechnology-Based Antimicrobials and Delivery Systems for Biofilm-Infection Control. *Chem. Soc. Rev.* **2019**, *48*, 428–446.

Lu, T. K.; Collins, J. J. Dispersing Biofilms with Engineered Enzymatic Bacteriophage. *Proc. Natl. Acad. Sci.* **2007**, *104*, 11197–11202.

Lu, T. K.; Koeris, M. S. The Next Generation of Bacteriophage Therapy. *Curr. Opin. Microbiol.* **2011**, *14*, 524–531.

Madsen, J. S.; Burmølle, M.; Hansen, L. H.; Sørensen, S. J. The Interconnection between Biofilm Formation and Horizontal Gene Transfer. *FEMS Immunol. Med. Microbiol.* **2012**, *65*, 183–195.

Mah, T. C.; Toole, G. A. O. Mechanisms of Biofilm Resistance to Antimicrobial Agents. *Trends Microbiol* **2001**, *9*, 34–39.

Maia, M. F.; Moore, S. J. Plant-Based Insect Repellents: A Review of Their Efficacy, Development and Testing. *Malar. J.* **2011**, *10*, S11.

Makabenta, J. M. V.; Nabawy, A.; Li, C.-H. H.; Schmidt-Malan, S.; Patel, R.; Rotello, V. M. Nanomaterial-Based Therapeutics for Antibiotic-Resistant Bacterial Infections. *Nat. Rev. Microbiol.* **2021**, *19*, 23–36.

McCall, A. S.; Kraft, S.; Edelhauser, H. F.; Kidder, G. W.; Lundquist, R. R.; Bradshaw, H. E.; Dedeic, Z.; Dionne, M. J. C.; Clement, E. M.; Conrad, G. W. Mechanisms of Corneal Tissue Cross-Linking in Response to Treatment with Topical Riboflavin and Long-Wavelength Ultraviolet Radiation (UVA). *Invest. Ophthalmol. Vis. Sci.* **2010**, *51*, 129–138.

Michael, C. A.; Dominey-Howes, D.; Labbate, M. The Antimicrobial Resistance Crisis: Causes, Consequences, and Management. *Frontiers in Public Health*, **2014**, *2*, 145.

Miller, L. S.; Cho, J. S. Immunity against Staphylococcus Aureus Cutaneous Infections. *Nat. Rev. Immunol.* **2011**, *11*, 505–518.

Mitzel, M. R.; Sand, S.; Whalen, J. K.; Tufenkji, N. Hydrophobicity of Biofilm Coatings Influences the Transport Dynamics of Polystyrene Nanoparticles in Biofilm-Coated Sand. *Water Res.* **2016**, *92*, 113–120.

Monte, J.; Abreu, C. A.; Borges, A.; Simões, C. L.; Simões, M. Antimicrobial Activity of Selected Phytochemicals against Escherichia Coli and Staphylococcus Aureus and Their Biofilms. *Pathogens* **2014**, *3*, 473–498.

Morales, E.; Cots, F.; Sala, M.; Comas, M.; Belvis, F.; Riu, M.; Salvadó, M.; Grau, S.; Horcajada, J. P.; Montero, M. M.; *et al.* Hospital Costs of Nosocomial Multi-Drug Resistant Pseudomonas Aeruginosa Acquisition. *BMC Health Serv. Res.* **2012**, *12*, 122–129.

Moreau-Marquis, S.; Stanton, B. A.; O'Toole, G. A. Pseudomonas Aeruginosa Biofilm Formation in the Cystic Fibrosis Airway. *Pulm. Pharmacol. Ther.* **2008**, *21*, 595–599.

Mukherjee, S.; Raghuraman, H.; Chattopadhyay, A. Membrane Localization and Dynamics of Nile Red: Effect of Cholesterol. *Biochim. Biophys. Acta - Biomembr.* **2007**, *1768*, 59–66.

Nananda F. Col, R. W. O.; Col, N. F.; O'Connor, R. W. Estimating Worldwide Current Antibiotic Usage: Report of Task Force 1. *Rev. Infect. Dis.* **1987**, *9*, S232–S243.

Nathwani, D.; Raman, G.; Sulham, K.; Gavaghan, M.; Menon, V. Clinical and Economic Consequences of Hospital-Acquired Resistant and Multidrug-Resistant Pseudomonas Aeruginosa Infections: A Systematic Review and Meta-Analysis. *Antimicrob. Resist. Infect. Control* **2014**, *3*, 32–47.

Naylor, N. R.; Atun, R.; Zhu, N.; Kulasabanathan, K.; Silva, S.; Chatterjee, A.; Knight, G. M.; Robotham, J. V. Estimating the Burden of Antimicrobial Resistance: A Systematic Literature Review. *Antimicrob. Resist. Infect. Control* **2018**, *7*, 58.

Nazzaro, F.; Fratianni, F.; De Martino, L.; Coppola, R.; De Feo, V. Effect of Essential Oils on Pathogenic Bacteria. *Pharmaceuticals* **2013**, *6*, 1451–1474.

Nomura, K.; Abdellatif, M. M. Precise Synthesis of Polymers Containing Functional End Groups by Living Ring-Opening Metathesis Polymerization (ROMP): Efficient Tools for Synthesis of Block/Graft Copolymers. *Polymer (Guildf).* **2010**, *51*, 1861–1881.

Nostro, A.; Blanco, A. R.; Cannatelli, M. A.; Enea, V.; Flamini, G.; Morelli, I.; Sudano Roccaro, A.; Alonzo, V.; Roccaro, A. S.; Alonzo, V. Susceptibility of Methicillin-Resistant Staphylococci to Oregano Essential Oil, Carvacrol and Thymol. *FEMS Microbiol. Lett.* **2004**, *230*, 191–195.

O'Connell, K. M. G.; Hodgkinson, J. T.; Sore, H. F.; Welch, M.; Salmond, G. P. C.; Spring, D. R. Combating Multidrug-Resistant Bacteria: Current Strategies for the Discovery of Novel Antibacterials. *Angew. Chemie Int. Ed.* **2013**, *52*, 10706–10733.

O'Toole, G. A. Microtiter Dish Biofilm Formation Assay. *J. Vis. Exp.* **2011**, 2437.

Olsen, I. Biofilm-Specific Antibiotic Tolerance and Resistance. *Eur. J. Clin. Microbiol. Infect. Dis.* **2015**, *34*, 877–886.

Ommen, P.; Zobek, N.; Meyer, R. L. Quantification of Biofilm Biomass by Staining: Non-Toxic Safranin Can Replace the Popular Crystal Violet. *J. Microbiol. Methods* **2017**, *141*, 87–89.

Palermo, E. F.; Kuroda, K. Structural Determinants of Antimicrobial Activity in Polymers Which Mimic Host Defense Peptides. *Appl. Microbiol. Biotechnol.* **2010**, *87*, 1605–1615.

Parasion, S.; Kwiatek, M.; Gryko, R.; Mizak, L.; Malm, A. Bacteriophages as an Alternative Strategy for Fighting Biofilm Development. *Polish J. Microbiol.* **2014**, *63*, 137–145.

Park, S.; Kyong, Y.; Oliveira, M.; Cho, E.; Jin, D.; Kook, J. Anaerobe Antimicrobial Effect of Linalool and a -Terpineol against Periodontopathic and Cariogenic Bacteria. *Anaerobe* **2012**, *18*, 369–372.

Pastar, I.; Nusbaum, A. G.; Gil, J.; Patel, S. B.; Chen, J.; Valdes, J.; Stojadinovic, O.; Plano, L. R.; Tomic-Canic, M.; Davis, S. C. Interactions of Methicillin Resistant Staphylococcus Aureus USA300 and Pseudomonas Aeruginosa in Polymicrobial Wound Infection. *PLoS One* **2013**, *8*, 1–11.

Pelgrift, R. Y.; Friedman, A. J. Nanotechnology as a Therapeutic Tool to Combat Microbial Resistance. *Adv. Drug Deliv. Rev.* **2013**, *65*, 1803–1815.

Percival, S. L.; McCarty, S. M.; Lipsky, B. Biofilms and Wounds: An Overview of the Evidence. *Adv. Wound Care* **2014**, *4*, 373–381.

Pettit, R. K.; Weber, C. A.; Pettit, G. R. Application of a High Throughput Alamar Blue Biofilm Susceptibility Assay to Staphylococcus Aureus Biofilms. *Ann. Clin. Microbiol. Antimicrob.* **2009**, *8*, 28.

Peulen, T.; Wilkinson, K. J. Diffusion of Nanoparticles in a Biofilm. *Environ. Sci. Technol.* **2011**, *45*, 3367–3373.

Potera, C. Forging a Link Between Biofilms and Disease. *Science.* **1999**, *283*, 1837–1839.

Pounder, R. J.; Stanford, M. J.; Brooks, P.; Richards, S. P.; Dove, A. P. Metal Free Thiol–Maleimide 'Click' Reaction as a Mild Functionalisation Strategy for Degradable Polymers. *Chem. Commun.* **2008**, 5158–5160.

Prashar, A.; Locke, I. C.; Evans, C. S. Cytotoxicity of Clove (Syzygium Aromaticum) Oil and Its Major Components to Human Skin Cells. *Cell Prolif.* **2006**, *39*, 241–248.

Rajamani, S.; Bauer, W. D.; Robinson, J. B.; Farrow, J. M.; Pesci, E. C.; Teplitski, M.; Gao, M.; Sayre, R. T.; Phillips, D. A. The Vitamin Riboflavin and Its Derivative Lumichrome Activate the LasR Bacterial Quorum-Sensing Receptor. *Mol. Plant-Microbe Interact.* **2008**, *21*, 1184–1192.

Ramalingam, K.; Amaechi, B. T.; Ralph, R. H.; Lee, V. A. Antimicrobial Activity of Nanoemulsion on Cariogenic Planktonic and Biofilm Organisms. *Arch. Oral Biol.* **2012**, *57*, 15–22.

Reichling, J.; Suschke, U. Essential Oils of Aromatic Plants with Antibacterial , Antifungal , Antiviral , and Cytotoxic Properties – an Overview. *Complement. Med. Res.* **2009**, 79–90.

Ribes, J.; Beztsinna, N.; Bailly, R.; Castano, S.; Rascol, E.; Taib-Maamar, N.; Badarau, E.; Bestel, I. Flavin-Conjugated Nanobombs: Key Structural Requirements Governing Their Self-Assemblies' Morphologies. *Bioconjug. Chem.* **2021**, *32*, 553–562.

Richards, M. J.; Edwards, J. R.; Culver, D. H.; Gaynes, R. P. Nosocomial Infections in Combined Medical-Surgical Intensive Care Units in the United States. *Infect Control Hosp Epidemiol* **2000**, *21*, 510–515.

Roberts, M. E.; Stewart, P. S. Modelling Protection from Antimicrobial Agents in Biofilms through the Formation of Persister Cells. *Microbiology* **2005**, *151*, 75–80.

Samperio, C.; Boyer, R.; Eigel, W. N.; Holland, K. W.; McKinney, J. S.; O'Keefe, S. F.; Smith, R.; Marcy, J. E. Enhancement of Plant Essential Oils' Aqueous Solubility and Stability Using Alpha and Beta Cyclodextrin. *J. Agric. Food Chem.* **2010**, *58*, 12950–12956.

Sanchez, C. J.; Mende, K.; Beckius, M. L.; Akers, K. S.; Romano, D. R.; Wenke, J. C.; Murray, C. K. Biofilm Formation by Clinical Isolates and the Implications in Chronic Infections. *BMC Infect. Dis.* **2013**, *13*, 47–58.

Sanson, C.; Schatz, C.; Le Meins, J.-F.; Brûlet, A.; Soum, A.; Lecommandoux, S. Biocompatible and Biodegradable Poly(Trimethylene Carbonate)-b-Poly(l-Glutamic Acid) Polymersomes: Size Control and Stability. *Langmuir* **2010**, *26*, 2751–2760.

Schierle, C. F.; De la Garza, M.; Mustoe, T. A.; Galiano, R. D. Staphylococcal Biofilms Impair Wound Healing by Delaying Reepithelialization in a Murine Cutaneous Wound Model. *Wound Repair Regen.* **2009**, *17*, 354–359.

Sen, C. K.; Gordillo, G. M.; Roy, S.; Kirsner, R.; Lambert, L.; Hunt, T. K.; Gottrup, F.; Gurtner, G. C.; Longaker, M. T. Human Skin Wounds: A Major and Snowballing Threat to Public Health and the Economy. *Wound Repair Regen.* **2009**, *17*, 763–771.

Serra, R.; Grande, R.; Butrico, L.; Rossi, A.; Settimio, U. F.; Caroleo, B.; Amato, B.; Gallelli, L.; de Franciscis, S. Chronic Wound Infections: The Role of Pseudomonas Aeruginosa and Staphylococcus Aureus. *Expert Rev. Anti. Infect. Ther.* **2015**, *13*, 605–613.

Simmons, M.; Drescher, K.; Nadell, C. D.; Bucci, V. Phage Mobility Is a Core Determinant of Phage-Bacteria Coexistence in Biofilms. *ISME J.* **2018**, *12*, 531–543.

Simões, M.; Bennett, R. N.; Rosa, E. A. S. Understanding Antimicrobial Activities of Phytochemicals against Multidrug Resistant Bacteria and Biofilms. *Nat. Prod. Rep.* **2009**, *26*, 746–757.

Simone, E. A.; Dziubla, T. D.; Muzykantov, V. R. Polymeric Carriers: Role of Geometry in Drug Delivery. *Expert Opin. Drug Deliv.* **2008**, *5*, 1283–1300.

Singer, A. J.; Clark, R. A. F. Cutaneous Wound Healing. *N. Engl. J. Med.* **1999**, *341*, 738–746.

Singh, R.; Ray, P.; Das, A.; Sharma, M. Penetration of Antibiotics through Staphylococcus Aureus and Staphylococcus Epidermidis Biofilms. *J. Antimicrob. Chemother.* **2010**, *65*, 1955–1958.

Song, J.; Jang, J. Antimicrobial Polymer Nanostructures: Synthetic Route, Mechanism of Action and Perspective. *Adv. Colloid Interface Sci.* **2014**, *203*, 37–50.

Stewart, P. S.; William Costerton, J. Antibiotic Resistance of Bacteria in Biofilms. *Lancet* **2001**, *358*, 135–138.

Sukegawa, T.; Masuko, I.; Oyaizu, K.; Nishide, H. Expanding the Dimensionality of Polymers Populated with Organic Robust Radicals toward Flow Cell Application:

Synthesis of TEMPO-Crowded Bottlebrush Polymers Using Anionic Polymerization and ROMP. *Macromolecules* **2014**, *47*, 8611–8617.

Sun, B. K.; Siprashvili, Z.; Khavari, P. A. Advances in Skin Grafting and Treatment of Cutaneous Wounds. *Science.* **2014**, *346*, 941 LP – 945.

Sybiya Vasantha Packiavathy, I. A.; Agilandeswari, P.; Musthafa, K. S.; Karutha Pandian, S.; Veera Ravi, A. Antibiofilm and Quorum Sensing Inhibitory Potential of Cuminum Cyminum and Its Secondary Metabolite Methyl Eugenol against Gram Negative Bacterial Pathogens. *Food Res. Int.* **2012**, *45*, 85–92.

Szomolay, B.; Klapper, I.; Dockery, J.; Stewart, P. S. Adaptive Responses to Antimicrobial Agents in Biofilms. *Environ. Microbiol.* **2005**, *7*, 1186–1191.

Tait, K.; Skillman, L. C.; Sutherland, I. W. The Efficacy of Bacteriophage as a Method of Biofilm Eradication. *Biofouling* **2002**, *18*, 305–311.

Tam, V. H.; Rogers, C. A.; Chang, K.-T.; Weston, J. S.; Caeiro, J.-P.; Garey, K. W. Impact of Multidrug-Resistant Pseudomonas Aeruginosa Bacteremia on Patient Outcomes. *Antimicrob. Agents Chemother.* **2010**, *54*, 3717–3722.

Terjung, N.; Löffler, M.; Gibis, M.; Hinrichs, J.; Weiss, J. Influence of Droplet Size on the Efficacy of Oil-in-Water Emulsions Loaded with Phenolic Antimicrobials. *Food Funct.* **2012**, *3*, 290–301.

Tiwari, B. K.; Valdramidis, V. P.; O' Donnell, C. P.; Muthukumarappan, K.; Bourke, P.; Cullen, P. J. Application of Natural Antimicrobials for Food Preservation. *J. Agric. Food Chem.* **2009**, *57*, 5987–6000.

Tseng, B. S.; Zhang, W.; Harrison, J. J.; Quach, T. P.; Song, J. L.; Penterman, J.; Singh, P. K.; Chopp, D. L.; Packman, A. I.; Parsek, M. R. The Extracellular Matrix Protects Pseudomonas Aeruginosa Biofilms by Limiting the Penetration of Tobramycin. *Environ. Microbiol.* **2013**, *15*, 2865–2878.

Ultee, A.; Bennik, M. H. J.; Moezelaar, R. The Phenolic Hydroxyl Group of Carvacrol Is Essential for Action against the Food-Borne Pathogen Bacillus Cereus. *Appl. Environ. Microbiol.* **2002**, *68*, 1561–1568.

Van Acker, H.; Van Dijck, P.; Coenye, T. Molecular Mechanisms of Antimicrobial Tolerance and Resistance in Bacterial and Fungal Biofilms. *Trends Microbiol.* **2014**, *22*, 326–333.

Ventola, C. L. The Antibiotic Resistance Crisis Part 1 : Causes and Threats. *Pharm. Ther.* **2015**, *40*, 277–283.

Ventola, C. L. The Antibiotic Resistance Crisis Part 2 : Management Strategies and New Agents. *Pharm. Ther.* **2015**, *40*, 344–352.

Vroom, J. M.; De Grauw, K. J.; Gerritsen, H. C.; Bradshaw, D. J.; Marsh, P. D.; Watson, G. K.; Birmingham, J. J.; Allison, C. Depth Penetration and Detection of PH Gradients in Biofilms by Two-Photon Excitation Microscopy. *Appl. Environ. Microbiol.* **1999**, *65*, 3502–3511.

Walters, M. C.; Roe, F.; Bugnicourt, A.; Franklin, M. J.; Stewart, P. S. Contributions of Antibiotic Penetration, Oxygen Limitation, and Low Metabolic Activity to Tolerance of Pseudomonas Aeruginosa Biofilms to Ciprofloxacin and Tobramycin. *Antimicrob. Agents Chemother.* **2003**, *47*, 317–323.

Wang, L. S.; Gupta, A.; Rotello, V. M. Nanomaterials for the Treatment of Bacterial Biofilms. *ACS Infect. Dis.* **2016**, *2*, 3–4.

Werthén, M.; LINA, H.; Jensen, P. Ø.; Sternberg, C.; M. Givskov, M.; Bjarnsholt, T. An in Vitro Model of Bacterial Infections in Wounds and Other Soft Tissues. *APMIS* **2010**, *118*, 156–164.

Willyard, C. The Drug-Resistant Bacteria That Pose the Greatest Health Threats. *Nature* **2017**, *543*, 15.

Wolcott, R. D.; Rhoads, D. D.; Bennett, M. E.; Wolcott, B. M.; Gogokhia, L.; Costerton, J. W.; Dowd, S. E. Chronic Wounds and the Medical Biofilm Paradigm. *J. Wound Care* **2010**, *19*, 45–53.

Wolcott, R. D.; Rhoads, D. D.; Dowd, S. E. Biofilms and Chronic Wound Inflammation. *J. Wound Care* **2008**, *17*, 333–341.

Wollensak, G.; Spoerl, E.; Seiler, T. Riboflavin/Ultraviolet-a–Induced Collagen Crosslinking for the Treatment of Keratoconus. *Am. J. Ophthalmol.* **2003**, *135*, 620–627.

Wu, H.; Moser, C.; Wang, H.-Z.; Hoiby, N.; Song, Z.-J. Strategies for Combating Bacterial Biofilm Infections. *J. Oral. Sci.* **2015**, *7*, 1–7.

Wu, Y.-K.; Cheng, N.-C.; Cheng, C.-M. Biofilms in Chronic Wounds: Pathogenesis and Diagnosis. *Trends Biotechnol.* **2019**, *37*, 505–517.

Xia, G.; Wolz, C. Phages of Staphylococcus Aureus and Their Impact on Host Evolution. *Infect. Genet. Evol.* **2014**, *21*, 593–601.

Xiong, M. H.; Bao, Y.; Yang, X. Z.; Zhu, Y. H.; Wang, J. Delivery of Antibiotics with Polymeric Particles. *Adv. Drug Deliv. Rev.* **2014**, *78*, 63–76.

Xu, C.; Akakuru, O. U.; Ma, X.; Zheng, J.; Zheng, J.; Wu, A. Nanoparticle-Based Wound Dressing: Recent Progress in the Detection and Therapy of Bacterial Infections. *Bioconjug. Chem.* **2020**, *31*, 1708–1723.

Yang, J.; Liu, F.; Yang, L.; Li, S. Hydrolytic and Enzymatic Degradation of Poly(Trimethylene Carbonate-Co-d,l-Lactide) Random Copolymers with Shape Memory Behavior. *Eur. Polym. J.* **2010**, *46*, 783–791.

Yata, T.; Lee, K.-Y.; Dharakul, T.; Songsivilai, S.; Bismarck, A.; Mintz, P. J.; Hajitou, A. Hybrid Nanomaterial Complexes for Advanced Phage-Guided Gene Delivery. *Mol. Ther. Nucleic Acids* **2014**, *3*, e185–e185.

Yoo, C.; Han, K.; Cho, K.-S.; Ha, J.; Park, H.-J.; Nam, J.-H.; Kil, U.-H.; Lee, K.-T. Eugenol Isolated from the Essential Oil of Eugenia Caryophyllata Induces a Reactive Oxygen Species-Mediated Apoptosis in HL-60 Human Promyelocytic Leukemia Cells. *Cancer Lett.* **2005**, *225*, 41–52.

Zhou, Z.; Zheng, A.; Zhong, J. Interactions of Biocidal Guanidine Hydrochloride Polymer Analogs with Model Membranes: A Comparative Biophysical Study. *Acta Biochim. Biophys. Sin. (Shanghai).* **2011**, *43*, 729–737.